UNIVERSITÉ DE MONTRÉAL

EFFECT OF PREFERENTIAL FLEXIBILITY ANGLE ON FLUIDELASTIC INSTABILITY OF A ROTATED TRIANGULAR TUBE BUNDLE

AFSHIN KHALVATTI
DÉPARTEMENT DE GÉNIE MÉCANIQUE
ÉCOLE POLYTECHNIQUE DE MONTRÉAL

MÉMOIRE PRÉSENTÉ EN VUE DE L'OBTENTION
DU DIPLÔME DE MAÎTRISE ÈS SCIENCES APPLIQUÉES
(GÉNIE MÉCANIQUE)
NOVEMBER 2007

© Afshin Khalvatti, 2007.

Library and Archives Canada

Published Heritage Branch

395 Wellington Street
Ottawa ON K1A 0N4
Canada

Bibliothèque et Archives Canada

Direction du Patrimoine de l'édition

395, rue Wellington
Ottawa ON K1A 0N4
Canada

Your file Votre référence
ISBN: 978-0-494-36918-0
Our file Notre référence
ISBN: 978-0-494-36918-0

NOTICE:
The author has granted a non-exclusive license allowing Library and Archives Canada to reproduce, publish, archive, preserve, conserve, communicate to the public by telecommunication or on the Internet, loan, distribute and sell theses worldwide, for commercial or non-commercial purposes, in microform, paper, electronic and/or any other formats.

The author retains copyright ownership and moral rights in this thesis. Neither the thesis nor substantial extracts from it may be printed or otherwise reproduced without the author's permission.

AVIS:
L'auteur a accordé une licence non exclusive permettant à la Bibliothèque et Archives Canada de reproduire, publier, archiver, sauvegarder, conserver, transmettre au public par télécommunication ou par l'Internet, prêter, distribuer et vendre des thèses partout dans le monde, à des fins commerciales ou autres, sur support microforme, papier, électronique et/ou autres formats.

L'auteur conserve la propriété du droit d'auteur et des droits moraux qui protège cette thèse. Ni la thèse ni des extraits substantiels de celle-ci ne doivent être imprimés ou autrement reproduits sans son autorisation.

In compliance with the Canadian Privacy Act some supporting forms may have been removed from this thesis.

While these forms may be included in the document page count, their removal does not represent any loss of content from the thesis.

Conformément à la loi canadienne sur la protection de la vie privée, quelques formulaires secondaires ont été enlevés de cette thèse.

Bien que ces formulaires aient inclus dans la pagination, il n'y aura aucun contenu manquant.

Canada

UNIVERSITÉ DE MONTRÉAL

ÉCOLE POLYTECHNIQUE DE MONTRÉAL

Ce mémoire intitulé :

EFFECT OF PREFERENTIAL FLEXIBILITY ANGLE ON FLUIDELASTIC INSTABILITY OF A ROTATED TRIANGULAR TUBE BUNDLE

présenté par : KHALVATTI Afshin

en vue de l'obtention du diplôme de : Maîtrise ès sciences appliquées

a été dûment accepté par le jury d'examen constitué de :

M. KAHAWITA René, Ph.D, président

M. MUREITHI Njuki W., Ph.D., membre et directeur de recherche

M. PETTIGREW Michel J., Post.Grad.Dipl., membre et codirecteur de recherche

M. GORMAN, Daniel J., Ph.D, membre

ACKNOWLEDGMENTS

I express my warmest thanks to those who contributed during these two years in the industrial chair of research BWC/AECL/NSERC Chair of Fluid-Structure Interaction.

I would like to thank Prof. N. Mureithi and Prof. M. Pettigrew for their valuable leadership and supervision throughout this research study. Work with them to me was a great privilege and incredible experiences both in my life and carrier.

I would like also to express my gratitude toward T. Lafrance, B. Besner for their assistance in the technical aspects of this project. Thanks to N. Aimène for his expertise on the strain gauges and for his good mood.

Also thanks to M. Ruël and M. Antoine for the design of test section used in this project as well as chair students for their sympathy and helpful ideas.

I would like to appreciate Dr. J. Ghata for his valuable effort during writing process of the texts. Also many thanks to Prof. E. Mir, who was the firs, showed me the meaning of engineering.

My parents have been most involved to encourage me until this level of education and I would like to express my deepest gratitude toward them. Finally, this whole endeavor would not have been possible without the patience, support and encouragement of my best friend and lovely wife Dr. Zohreh Emad.

Résumé

L'instabilité fluidelastique est le mécanisme d'excitation vibration le plus important pour les faisceaux de tubes dans un échangeur de chaleur et pouvant pousser des dommages irréversibles. Dans des générateurs de vapeur de centrale nucléaire, l'écoulement diphasique à haute vitesse peut causer cette instabilité.

Ainsi la région du souci dans les générateurs de vapeur (GV) est la région où l'écoulement croise un grand nombre de tubes ce qui peuvent causer une résistance hydraulique significative. Cette résistance hydraulique force l'écoulement à changer de direction. En conséquence l'écoulement traverse le faisceau de tubes à différents angles d'attaque de 0° à 90°. Le faisceau de tubes est alors excité par écoulement oblique.

Le but de ce travail est d'examiner les phénomènes d'instabilité dans un faisceau de tubes en configuration triangulaire tourné soumis an écoulement oblique monophasique. Une étude en soufflerie a donc été entreprise pour déterminer l'effet de l'angle d'attaque de l'écoulement sur l'instabilité fluidelastique sur un faisceau de tubes triangulaire tourné.

Le faisceau se compose de tubes flexibles dans une seule direction. Les fixations des tubes sont conçues avec des possibilités de rotation afin de fournir différents angles d'attaque de 0°, 30°, 60° et 90 degrés.

Les résultats sont en accord avec les prédictions. Ils prouvent que l'instabilité fluidelastique dépend fortement de l'angle d'attaque.

Les résultats prouvent également que, généralement, l'élimination de la flexibilité dans la direction normale à l'écoulement, affecte considérablement le comportement de stabilité de faisceau de tubes.

Toutefois dans certains cas, changer l'angle d'attaque n'affecte pas la vitesse critique pour l'instabilité, parce que malgré la réduction de flexibilité des tubes, le nombre efficace de tubes flexibles reste constant dans le faisceau de tubes.

La théorie quasi-statique présentée par Price et Païdoussis (1986 et 1987) est utilisé comme base pour le développement d'un modèle de stabilité pour un cylindre flexible simple entouré par des cylindres rigides soumis an écoulement oblique monophasique.

Les résultats obtenus, pour la vitesse critique d'écoulement avec le modèle quasi-statique sont raisonnables.

Les résultats expérimentaux sont utilisés pour valider l'application des modèles théoriques.

ABSTRACT

Fluidelastic instability is the most important vibration excitation mechanism for heat exchanger, or nuclear steam generator tube bundles. It leads to very high vibration amplitudes and may cause short term failure by fatigue or wear. In nuclear power plants, steam generator U-tubes are susceptible to fluidelastic instability because of the high velocity two-phase flow in the U-tube region. Thus the region of concern in Steam Generators (SG) is the upper most U-bend region where the flow crosses a large number of tubes which can cause significant hydraulic resistance. This hydraulic resistance forces the flow to change direction. As a result the flow leaves the tube bundle at different angles of attack varying from 0° to 90°. From a fluidelastic instability point of view, the tube bundle is excited by oblique cross flow. The purpose of this work is to examine the instability phenomena in a rotated triangle tube bundle subjected to oblique single phase cross flow.

A wind tunnel study was conducted to determine the effect of the flexibility angle on the cross-flow induced fluidelastic instability on a rotated triangular tube bundle. The array consists of unidirectionally flexible tubes. The tubes supports in the bundle are designed with capability of rotation in order to provide different angles of attack in four steps, from 0 to 90 degrees. Fluidelastic instability results are in agreement with what was expected. The results show that fluidelastic instability is strongly dependent on the angle of attack. The results also show that, generally, the elimination of bundle flexibility in the direction transverse to the flow, greatly affects the stability behavior of the array. However in a few cases, changing the angle of the attack does not affect the critical velocity for instability, because the effective number of flexible tubes remains constant, in spite of the reduction of tube bundle flexibility.

The quasi-static theory presented by Price & Païdoussis (1986 & 87) is used as the basis for the development of a stability model for a single flexible cylinder surrounded by rigid cylinders and subject to oblique cross-flow. A reasonable degree of

success has been achieved with this quasi-static type analyses to predict fluidelastic instability critical flow velocity. Experimental results are used to validate theoretical model applications.

Condensé en français

L'instabilité fluidelastique est le mécanisme d'excitation de vibration le plus important pour les faisceaux de tubes que l'on retrouve à l'intérieur des générateurs de vapeur et des échangeurs de chaleur. Il en est ainsi à cause des vibrations de très large amplitude subies par un faisceau instable. Ces dernières peuvent conduire rapidement à des bris par fatigue ou par usure par frottement. La région des tubes en U constitue sans aucun doute l'endroit le plus propice à l'intérieur des générateurs de vapeur pour le développement de ce phénomène à cause des hautes vitesses d'écoulement qu'on y trouve et des faibles fréquences naturelles des tubes en U dans la direction hors plan. À l'intérieur des générateurs de vapeur de centrale nucléaire, des supports AVB (Anti Vibration Bar) ont été introduits afin de soutenir les tubes en U dans cette direction. Bien que les supports AVB supportent convenablement les tubes dans la direction hors plan, ces derniers ne sont pas aussi efficaces pour restreindre les vibrations dans le plan des tubes.

Dans ce travail, des études expérimentales et théoriques sont effectuées afin d'étudier l'instabilité fluidelastique dans un faisceau de tubes spécifique. Ces efforts ont été entrepris dans le cadre d'un projet de maîtrise recherche en génie mécanique à l'École Polytechnique de Montréal.

Cette étude se concentre sur la région les tubes en U, dans laquelle l'écoulement croise un grand nombre de tubes causant une résistance hydraulique significative. Cette résistance hydraulique force l'écoulement à changer de direction. En conséquence, l'écoulement sort du faisceau de tubes à différents angles d'attaques s'étendant de 0° à 90°. Le faisceau de tubes est alors excité par écoulement oblique.

Le travail de recherche sur l'instabilité fluidelastique est divisé en deux catégories. La premier vise à obtenir une compréhension de base de l'instabilité fluidelastique.

La deuxième catégorie, d'autre part, vise à produire des informations pour la conception de générateur de vapeur. Pettigrew et Taylor (1991) ont constaté que seules

les données des expérimentales où tous les tubes étaient libres du vibrer sont valides du point de vue de la conception. Ce type de travail est habituellement effectué sur des faisceaux de tubes réalistes d'échangeurs de chaleur qui sont souvent étudiés avec un écoulement liquide. Pour l'écoulement diphasique, cette méthode a été employée seulement pour quelques cas, en raison de son coût élevé et d'autres restrictions pratiques. Cependant, cette méthode fournit souvent des informations beaucoup plus réalistes pour de vrais échangeurs de chaleur.

Les essais courants ont été réalisés dans une soufflerie avec une rangée de tube soumise à un écoulement transversal monophasique. Bien que les essais avec écoulement monophasique ne représente pas les écoulements diphasique, dans beaucoup d'études la méthode de circulation d'air est utilisé à cause de sa simplicité et équipement moins cher.

Un modèle approximatif a été employé pour simuler la région supérieure des tubes en U dans le générateur nucléaire de vapeur. L'essai a été effectué dans une soufflerie avec une section d'essai de 305mm ×305mm, dans laquelle la vitesse maximum d'écoulement est 48.8m/s dans la section vide d'essai, et de 8m/s avec le faisceau en place. Le faisceau de tubes représenté sur la Figure 2.2 se compose d'une rangée de tubes légers avec un diamètre extérieur de 40.4mm, et de longueur de 288.9mm, placé dans une configuration triangulaire tourné avec un rapport pas sur diamètre de $P/D = 1.37$. La section d'essais se compose de quatre rangées et cinq colonnes de tube.

Chaque cylindre se comprend d'un tube avec une lamelle d'acier doux fixé au milieu du tube par l'intermédiaire d'une bride en bois comme représenté sur la figure 2.3. Le méplat possède une section transversale rectangulaire de 1.5mm ×15mm ce qui donne un faisceau de tubes de flexibilité unidirectionnelle.

La fréquence naturelle de l'assemblage est de 188 Hz dans la direction transversale, et de 19.44 Hz dans l'autre direction, ce qui rendre le tube essentiellement rigide dans la direction traversale.

Un mécanisme simple a été conçu pour tourner les tubes axialement pour fournir différentes orientations de flexibilité, s'étendant de 0° à 90° (Figure 2.4). Afin de couvrir une gamme de configurations de faisceau de tubes, chacun des tubes a pu être indépendamment retenu de vibrer, à l'aide d'une bride en aluminium montée à l'extrémité libre. La vitesse d'écoulement est mesurée à l'entrée de la section d'essai à l'aide d'un tube de Pitot. Avant que le faisceau de tubes ait été inséré dans la section d'essais de le soufflerie, un calibrage soigneux est nécessaire pour déterminer la relation statique entre déplacement et contrainte appliquée.

Dans la littérature la vitesse critique pour l'instabilité fluidelastique, est définie par différents critères proposés par différents chercheurs. Par exemple Heilker et Vincent (1981) ont employé la vitesse à laquelle les tubes rentrent en contact comme critère, alors que Soper (1983) employait le point auquel la tangente à la réponse a intersecté l'axe de vitesse.

Teh et Goyder (1988) ont pris la vitesse à laquelle l'amortissement semble être zéro. Ici nous avons adopté une approche très pratique comme présenté par Pettigrew et Taylor (1991). Quand le seuil d'instabilité est bien défini, nous avons simplement pris la vitesse d'écoulement à laquelle se produit l'instabilité, Figure 2.10. Quand il n'est pas bien défini, on prendre la vitesse auquel on remarque une amplitude excessive de vibration, Figure 2.11.

Des essais ont été réalisés sur trois configurations différentes de faisceau de tubes. Tous les tubes ont été à l'origine conçue en tant que tubes en porte-à-faux. A la fin de cette étude, chaque tube a pu être indépendamment retenu de vibrer au moyen d'un appui inséré dans l'espace entre le tube et la fenêtre supérieure de la section d'essai, par conséquent simulant un tube rigidement fixé. Chaque tube a pu être tourné axialement, en utilisant un mécanisme simple décrit dans la section 2.1.1. Ce mécanisme fournit les différentes orientations de flexibilité, qui créent divers angles d'attaques de 0°, 30°, 60° et 90° pour chaque configuration de faisceau de tubes.

Pour chaque essai, une durée suffisante a été accordée pour qu'un état d'équilibre soit atteint (habituellement plusieurs minutes). Les vitesses d'écoulements ont été

enregistrés et les déplacements r.m.s mesurés. La vitesse d'écoulement a été augmentée graduellement et le processus fut répété jusqu'à ce que le faisceaux de tubes ait bien atteint l'instabilité. Pour la configuration d'un seul tube flexible, le tube #2 est laissé flexible dans le faisceau. Les Figures 2.12 et 2.13 montrent les trois configurations principales de faisceau de tubes et les quatre orientations principales de flexibilité de tube.

Dans le deuxième chapitre, les équipements d'essais et les méthodes expérimentales utilisés dans ce travail ont été décrits en détails. Dans le troisième chapitre, les résultats expérimentaux sont examinés.

Huit tubes instrumentés (marqués 1-8 Figure.2.12 (a)) ont été suivis dans le faisceau de tubes entièrement flexible. La réponse de vibration pour le tube No.7 est donnée sur Figure 3.1. Les spectres de réponse montrent que l'excitation est minimale cette excitation est due à la turbulence pour de basses vitesses d'écoulement. À la vitesse critique $U_p = 4.75 m/s$, une instabilité forte s'est développée. La variation d'amplitude de réponse r.m.s par rapport à la vitesse d'écoulement est montrée sur la Figure 3.2. L'augmentation de la vitesse d'écoulement à $U_p = 5.3 m/s$ a pour conséquence des amplitudes maximales accrues. Par coïncidence avec une grande augmentation de l'amplitude de vibration, on a observé une coalescence des différentes fréquences du tube à une seule fréquence modale comme représenté sur le Figure 3.3, confirmant encore le début de l'instabilité fluidelastique.

Les essais de la première série, sont effectués dans un faisceau de tubes entièrement flexible. La direction de flexibilité de tube a été changée dans quatre étapes. Les essais ont commencé par un angle d'attaque de 90° qui tient compte du mouvement du tube dans la direction de portance. Dans les étape suivantes, les tubes ont été tournés de 30 degrés pour obtenir un angle d'attaque différent jusqu a à 0° (flexibilité dans le sens d'écoulement). Les données rassemblées montrent comment la vitesse critique d'instabilité fluidelastique augmente avec l'angle d'attaque décroissant de 90° à 0°.

La vitesse critique d'écoulement pour un angle d'attaque de 90° est $U_{pc} = 4.75 m/s$ pour un angle d'attaque 60° la vitesse critique augmente de 61% à $U_{pc} = 7.65 m/s$. Le passage d'un angle d'attaque à 30° à 0° augmente la vitesse critique d'écoulement respectivement de $U_{pc} = 8.0 m/s$ à $U_{pc} = 8.75 m/s$. La figure 4.1 montre comment la vitesse critique d'écoulement d'instabilité fluidelastique change avec une diminution de l'angle d'attaque.

Dans la deuxième série d'essais, qui a été réalisée avec un faisceau de trois-colonne de tubes flexibles, le procédé précédent a été répété et la vitesse critique d'écoulement pour l'instabilité fluidelastique a été mesurée. Les résultats présentés au chapitre 3 prouvent que pour un angle d'attaque de 90° la vitesse critique de d'instabilités passe de $U_{pc} = 5.3 m/s$. À $U_{pc} = 8.0 m/s$ pour 60°.

Réduire l'angle d'attaque à 30° entraîne une augmentation de la vitesse d'écoulement jusqu'à $U_{pc} = 8.4 m/s$. Pour un angle d'attaque de 0° (direction trainée) la vitesse critique pour l'instabilité fluidelastique obtenue est $U_{pc} = 9.15 m/s$. La variation de la vitesse critique par rapport à l'angle d'attaque est illustrée sur Figure 4.2.

Les dernières séries d'essais ont été effectuées avec un faisceau de sept tubes flexibles. Les données rassemblées dans le troisième chapitre montrent comment la vitesse critique d'écoulement change avec l'angle d'attaque. Pour un angle d'attaque de 90° (mouvement normale à l'écoulement), la vitesse critique d'écoulement est $U_{pc} = 5.85 m/s$. Elle augmente de 36% à $U_{pc} = 8.0 m/s$ pour un angle d'attaque 60°. Pour un angle d'attaque 30° la vitesse critique est $U_{pc} = 9.5 m/s$. Enfin pour la direction de la traînée (angle d'attaque 0°) elle est de $U_{pc} = 9.85 m/s$. Le cas d'un nombre réduit de tubes flexibles est discuté plus tard. Les résultats donnés dans la section 3.4, prouvent que le comportement de la stabilité change de manière significative dans le cas extrême de seulement deux cylindres flexibles. L'instabilité fluidelastique se produit toujours pour deux cylindres flexibles. Deux configurations différentes avec des tubes flexibles seulement dans le sens de la portance ont été examinées. D'abord les deux tubes flexibles

ont été placés dans la même colonne (les tubes # 2, 3 Figure 2.14a). En second lieu, les deux tubes flexibles ont été placé dans les colonnes voisines (les tubes # 3, 7 Figure 2.14a).

La vitesse critique à $U_{pc} = 13.2\,m/s$ est plus du double de la vitesse critique pour la rangée entièrement flexible ($U_{pc} = 5.3\,m/s$). Les résultats prouvent que dans le cas de deux cylindres flexibles, la position relative des tubes est très importante. La Figure 3.37 montre la réponse vibratoire quand les deux tubes flexibles sont dans les colonnes voisines ; dans ce cas-ci, les tubes No.3 et 7 ont été examinés. La vitesse d'instabilité est plus haute que celle pour deux tubes dans la même colonne. Pour le cas de la flexibilité dans le sens d'écoulement, Mureithi et al. (2005), ont expérimentalement prouvé que pour deux cylindres flexibles, les positions relatives des tubes est importante. Ils ont signalé que la vitesse d'instabilité pour deux tubes dans les colonnes voisines est plus haute que pour le cas de deux tubes flexibles dans la même colonne. C'est en accord avec ce que nous avons trouvé dans ce travail. Ce n'est pas le cas pour l'écoulement diphasique. Violette et al. (2006), ont expérimentalement montré que pour l'instabilité fluidelastique se produise dans un faisceau de tubes flexibles seulement dans la direction de la traînée, les tubes flexibles doivent être situés dans deux colonnes adjacentes.

Païdoussis et Price (1988) ont démontré que pour qu'une instabilité par mécanisme contrôlé par l'amortissement survienne dans la direction de la portance, la dérivée du coefficient de portance du tube en fonction de son mouvement dans cette même direction (y) doit être négative et avoir une valeur absolue suffisamment élevée ($\partial C_L/\partial y < 0$). La même logique s'applique pour l'instabilité dans la direction de la traînée ($\partial C_D/\partial x < 0$). Païdoussis et al. ont mesurés la valeur du coefficient de portance et du coefficient de traînée en fonction du déplacement statique d'un tube de 25,4 millimètres à l'intérieur d'un faisceau de tubes triangulaire tourné de ratio pas sur diamètre (P/D) de 1,375 et soumis à un écoulement d'air. Ils ont clairement montés que la condition d'instabilité est respectée pour la direction de la portance (i.e. $\partial C_L/\partial y << 0$). Par contre, ce n'est pas le cas pour la direction de la traînée. Ces données montrent qu'une instabilité fluidelastique ne se produira pas pour un tube flexible dans la direction

de l'écoulement soumis à un écoulement d'air. Ces résultats, bien qu'obtenus en air, confirment la tendance observée en diphasique. On déduit donc que les instabilités fluidelastique obtenues dans le cas de plusieurs tubes flexibles seulement dans la direction de l'écoulement sont seulement le fruit du mécanisme contrôlé par la rigidité.

On confirme maintenant que l'instabilité fluidelastique peut se produire dans un faisceau de tubes triangulaire tourné soumis à un écoulement traverse d'air avec l'orientation de flexibilité de tube dans le sens d'écoulement (0°), 30°, 60° et 90° d'angle d'attaque. Les résultats d'essais fluidelastique dans le chapitre trois sont maintenant comparés aux données existantes pour la configuration de triangle tournée sur la carte d'instabilité donnée sur la Figure 4.4, présenté par Pettigrew et al. (1989). Sur cette carte, l'axe horizontal est le paramètre masse amortissement et l'axe vertical est la vitesse réduite. Les données expérimentales pour les tubes qui sont flexible dans la direction de traînée et soumis à un écoulement transverse monophasique dans une soufflerie s'avèrent en bon accord avec ce que Violette et al. ont rapporté en 2006 pour le même faisceau de tubes soumis à l'écoulement transverse diphasique $K \cong 8$. Apparaît également dans cette figure les résultats obtenus par Mureithi et al. 2005, dans une soufflerie pour un faisceau de tubes semblable à celui utilisé dans cette étude pour deux configurations, le faisceau central (Cluster) et la colonne flexible simple. Les deux configurations utilisent les tubes qui sont flexibles dans le sens de l'écoulement. Comme montré sur la Figure 4.4, les résultats sont en bon accord avec ceux obtenus dans cette étude pour les tubes flexibles dans le sens de l'écoulement. D'autre part, Mureithi et al. (2005) ont rapporté une constante d'instabilité, $K = 5$ pour un faisceau de tubes entièrement flexibles.

En utilisant l'équation 4.10, le comportement d'instabilité fluidelastique pour la rangée triangulaire tournée peut être facilement expliqué. Puisque l'instabilité fluidelastique est possible quand l'énergie absorbée du fluide par les tubes excède l'énergie absorbée par amortissement, l'amortissement par rapport à l'angle de flexibilité sera discuté. Il est bien connu que l'amortissement visqueux dans le sens d'écoulement soit plus grand que l'amortissement visqueux dans le sens de la portance, souvent presque deux fois (Price et Païdoussis 1986 et 1988). La partie imaginaire de l'équation

4.10 représente amortissement total. Ces limites sont également fonction de l'angle d'attaque θ.

La valeur maximum de ces termes se produit lorsque $\theta = 0^{\circ}$ (direction de traînée) donc une augmentation de l'amortissement total entraîne une hausse de la vitesse critique d'instabilité fluidelastique.

Pour la même raison, pour un l'angle d'attaque de 90° ($\theta = 90^{\circ}$) le terme d'amortissement total est minimum, ce qui signifie que le faisceau de tubes devient très instable à la plus basse vitesse critique.

Pour les cas $\theta = 30^{\circ}$ and 60° d'angle d'attaque on suit vu que les valeurs des $\cos^2 30^{\circ} \succ \cos^2 60^{\circ}$ à la suite l'amortissement total diminutions forment 30° à 60° et en conséquence la vitesse critique d'instabilité fluidelastique diminue de 30° à 60°.

La Figure 4.6 montre que, pour les données disponibles, les résultats expérimentaux sont en accord qualitatif avec ceux du modèle théorique. Comme mentionné au tableau 4.1, les vitesses critiques pour l'instabilité fluidelastique ont moqué pour 0° et pour 30°, parce que la vitesse maximum d'écoulement de la soufflerie était de 8m/s avec les tubes en place. Les résultats expérimentaux disponibles pour l'instabilité fluidelastique pour un faisceau de tubes entièrement flexible, trois-colonnes flexibles, et faisceau central (Cluster) peuvent être comparés aux résultats du modèle flexible simple d'un cylindre. On voit sur les Figures 4.6 et 4.7 que la courbe théorique donne une limite légèrement inférieure pour l'instabilité fluidelastique. Cependant l'accord entre le modèle théorique pour un seul cylindre flexible et les données expérimentales pour différentes configurations de faisceau de tubes avec différente orientation de flexibilité, est généralement acceptable.

L'objectif principal de ce travail était de déterminer expérimentalement comment le comportement fluidelastique d'instabilité d'un faisceau de tubes triangulaire tourné change avec l'angle de flexibilité de tube. Les conclusions principales obtenues de ce travail sont les suivantes :

- L'instabilité fluidelastique peut prendre place dans un faisceau de tubes triangulaire tourné qui est flexible dans le sens de l'écoulement ou dans la direction normale à l'écoulement.

- L'instabilité fluidelastique dépend fortement de l'angle entre le sens de l'écoulement et la direction de flexibilité du faisceau de tubes que nous appelons "angle d'attaque".

- L'augmentation de l'angle d'attaque a comme conséquence une diminution de la vitesse critique d'instabilité fluidelastique.

- L'augmentation du nombre de tubes flexibles dans une rangée a comme conséquence une vitesse critique d'instabilité fluidelastique réduite pour tous les angles d'attaques.

- Une gamme de la constante d'instabilité fluidelastique (K) entre "3.8 et 8" ont été trouvées respectivement pour une gamme d'angles d'attaque de 90 à 0 degrés.

- L'instabilité fluidelastique peut se produire dans une simple colonne flexible (même avec seulement deux tubes flexibles) dans un faisceau de tubes triangulaire tourné flexible dans le sens d'écoulement.

- Les résultats obtenus en écoulement monophasique se sont avérés en bon accord avec celle rapporté par Violette (2006) pour l'écoulement diphasique, excepté pour la configuration flexible simple d'une colonne dans laquelle les tubes étaient flexibles seulement dans le sens d'écoulement.

Les essais en soufflerie présentée ici sont des essais préliminaires pour étudier l'instabilité fluidelastique dans un écoulement transverse oblique. Pour arriver aux

conclusions finales concernant le comportement de stabilité dans des générateurs de vapeur, des essais en écoulement diphasique est nécessaire.

Dans la dernière étape de la présente étude, une section d'essais en écoulement diphasique a été modifiée par un mécanisme simple pour orienter les tubes axialement. Ainsi l'orientation de flexibilité du faisceau de tubes peut être changée de 0° à 90° à tout les 30 degrés. Ceci permettra des essais à différents angles d'attaque en l'écoulement diphasique. Des dessin techniques appropriés sont donnés dans l'annexe CC.

Table of contents

Acknowledgment.....iv

Résumé.....v

Abstract.....vii

Condensé en français.....ix

Table of contents.....xix

List of figures.....xxii

List of tables.....xxvi

List of symbols.....xxvii

List of appendixes.....xxix

Chapter 1 Introduction.....1

1.1 Background.....1

1.2 Tube bundle vibratory excitation mechanisms.....2

1.2.2 Periodic Shedding.....2

1.2.2 Random excitation caused by turbulent flow.....4

1.2.3 Fluidelastic instability.....4

1.2.4 Acoustic resonance in tube bundles.....6

1.3 A review of fluidelastic instability for external cross flows.....8

1.3.1 Development of a criterion.....8

1.3.2 Development of the theory.....10

1.3.3 Fluidelastic instabilities in two-phase flow.....12

1.4 Motivation for the present work.....12

1.5 Objective.....14

1.6 Thesis layout.....14

Chapter 2 Test Apparatus and Experimental Procedure.....15

2.1 Experimental assembly structure.....15

2.1.1 Test section components.....15

2.1.2 Wind tunnel specifications....18
2.2 Measuring equipments....19
2.2.1 Flow velocity measurement....19
2.2.2 Instrumented tube calibration....21
2.2.2 Tube structural damping and natural frequency measurement....23
2.3 Experimental methods and procedure....24
2.3.1 More frequently used definitions....24
2.3.2 Tests procedure....26

Chapter 3 Experimental Results....29
3.1 Fully flexible tube bundle....29
3.1.1 Stability behavior of the fully flexible bundle with tube motion in cross flow (Angle of attack 90°)....29
3.1.2 Stability behavior of the fully flexible bundle with tube motion at 60° to the flow direction (Angle of attack 60°)....32
3.1.3 Stability behavior of the fully flexible bundle with tube motion at 30° to the flow direction (Angle of attack 30°)....35
3.1.4 Stability behavior of the fully flexible bundle with tube motion in-line with the flow direction (Angle of attack 0°)....37
3.2 Stability behavior of the three-column flexible tube bundle (two fixed adjacent columns)....38
3.2.1 Stability behavior of three-column flexible bundle with tube motion in cross flow direction (Angle of attack 90°)....39
3.2.2 Stability behavior of three-column flexible bundle with tube motion at 60° to the flow direction (Angle of attack 60°)....41
3.2.3 Stability behavior of three-column flexible bundle with tube motion at 30° to the flow direction (Angle of attack 30°)....43
3.2.4 Stability behavior of the three-column flexible bundle with tube motion in-line with the flow direction (Angle of attack 0°)....45

3.3 Stability behavior of the cluster tube bundle configuration.....47
3.3.1 Stability behavior of cluster bundle configuration with tube motion in cross flow direction (Angle of attack 90°).....47
3.3.2 Stability behavior of cluster bundle configuration with tube motion at 60° to the flow direction (Angle of attack 60°).....49
3.3.3 Stability behavior of cluster bundle configuration with tube motion at 30° to the flow direction (Angle of attack 30°).....51
3.3.4 Stability behavior of cluster tube bundle configuration with tube motion in-line with the flow direction (Angle of attack 0°).....53
3.4 Stability behavior of two flexible cylinders.....55
3.4.1 Stability behavior of two flexible cylinders with tubes motion in cross flow (Angle of attack 90°).....55
3.4.2 Stability behavior of two flexible cylinders with motion at 60° to the flow direction (Angle of attack 60°).....57

Chapter 4 Data Analysis.....60
4.1 Experimental data.....60
4.1.1 Fully flexible tube bundle.....60
4.1.2 Three-columns flexible tube bundle.....61
4.1.3 Cluster tube bundle configuration.....62
4.1.4 Stability behavior for two flexible cylinders.....63
4.2 On instability mechanisms.....64
4.3 Fluidelastic instability result comparison.....66
4.4 Modified quasi-steady theory.....67
4.5 Comparison with experimental data.....73

Chapter 5 Conclusions.....76
Future work.....77
References.....79

Appendixes.....**86**

List of figures

Figure 1.1 Fluid flows past a cylinder.....3

Figure 1.2 Vibration amplitude of a cylinder versus flow rate (Pettigrew et. al 1991).....5

Figure 1.3 Flow stream alterations due to hydraulic resistance.....13

Figure 2.1 U-tube area of the steam generator and approximated experimental model..15

Figure 2.2 Test section and air flow direction.....16

Figure 2.3(a) Exploded view of the flexible tube assembly.....17

Figure 2.3(b) Assembled view of the flexible tube.....17

Figure 2.4 Positioning mechanism for the flexibility orientation.....18

Figure 2.5 Open-loop ELD wind tunnel Model 402.....19

Figure 2.6 Flow velocity measurement chain.....19

Figure 2.7 Typical transducer cross-section.....20

Figure 2.8 Tube displacement and relative deflection factor.....22

Figure 2.9 Natural frequency measurement 24

Figure 2.10 Well-defined fluidelastic instability.....25

Figure 2.11 Less well-defined fluidelastic instability.....25

Figure 2.12 Three main tube bundle configurations (a)Fully flexible tube bundle, (b) Three-column flexible tube bundle, (c) Cluster tube bundle configuration..27

Figure 2.13 The main four tube flexibility orientations, a) 90° to flow direction (cross flow), b) 0° to flow direction (in flow direction), c) 30° to flow direction, d) 60° to flow direction.....27

Figure 3.1 Response spectra variation with flow velocity for Tube No.7 in a fully flexible bundle, at a 90°angle of attack 30

Figure 3.2 R.M.S vibration response for the fully-flexible tube bundle, at an angle of attack 90°.....31
Figure 3.3 Response frequency versus flow pitch velocity for the flexible tube bundle, at a 90° angle of attack.....32
Figure 3.4 Response spectra variation with flow velocity for Tube No.7 in a fully flexible bundle, at a 60° angle of attack.....33
Figure 3.5 R.M.S vibration response for the fully flexible tube bundle, at a 60° angle of attack.....34
Figure 3.6 Response frequency versus flow pitch velocity for the flexible tube bundle, at a 60° angle of attack.....34
Figure 3.7 Response spectra variation with flow velocity for Tube No.4 in a fully flexible bundle, at an angle of attack 30°.....35
Figure 3.8 R.M.S vibration response for the fully flexible tube bundle, at a 30° angle of attack.....36
Figure 3.9 Response frequency versus flow pitch velocity for the flexible tube bundle, at a 30° angle of attack.....36
Figure 3.10 R.M.S vibration response for the fully flexible tube bundle, at a 0° angle of attack 37
Figure 3.11 Response frequency versus flow pitch velocity for the flexible tube bundle, at a 0° angle of attack.....38
Figure 3.12 R.M.S vibration response for the three-column flexible tube bundle, at an angle of attack 90°.....39
Figure 3.13 Response frequency versus flow pitch velocity for three-column flexible tube bundle, at a 90° angle of attack.....40
Figure 3.14 Response spectra variation with flow velocity for Tube No.4 in a three-column flexible bundle, at a 90° angle of attack 40
Figure 3.15 R.M.S vibration response for the three-column flexible tube bundle, at a 60° angle of attack.....41

Figure 3.16 Response frequency versus flow pitch velocity for three-column flexible tube bundle, at a 60° angle of attack....42
Figure 3.17 Response spectra variation with flow velocity for Tube No.4 in a three-column flexible bundle, at a 60° angle of attack 42
Figure 3.18 R.M.S vibration response for the three-column flexible tube bundle, at a 30° angle of attack 43
Figure 3.19 Response frequency versus flow pitch velocity for three-column flexible tube bundle, at a 30° angle of attack....44
Figure 3.20 Response spectra variation with flow velocity for Tube No.4 in a three-column flexible bundle, at a 30° angle of attack 44
Figure 3.21 R.M.S vibration response for the three-column flexible tube bundle, at a 0° angle of attack....45
Figure 3.22 Response frequency versus flow pitch velocity for three-column flexible tube bundle, at a 0° angle of attack....46
Figure 3.23 Response spectra variation with flow velocity for Tube No.7 in a three-column flexible bundle, at a 0° angle of attack....46
Figure 3.24 R.M.S vibration response for the cluster tube bundle configuration, at a 90° angle of attack....47
Figure 3.25 Response frequency versus flow pitch velocity for cluster tube bundle configuration, at a 90° angle of attack....48
Figure 3.26 Response spectra variation with flow velocity for Tube No.7 in a cluster bundle configuration, at a 90° angle of attack 48
Figure 3.27 R.M.S vibration response for the cluster tube bundle configuration, at a 60° angle of attack....49
Figure 3.28 Response frequency versus flow pitch velocity for cluster tube bundle configuration, at a 60° angle of attack....50
Figure 3.29 Response spectra variation with flow velocity for Tube No.2 in a cluster bundle configuration, at a 60° angle of attack....50

Figure 3.30 R.M.S vibration response for the cluster tube bundle configuration, at a 30° angle of attack....51
Figure 3.31 Response frequency versus flow pitch velocity for cluster tube bundle configuration, at a 30° angle of attack....52
Figure 3.32 Response spectra variation with flow velocity for Tube No.2 in a cluster bundle configuration, at a 30° angle of attack....52
Figure 3.33 R.M.S vibration response for the cluster tube bundle configuration, at a 0° angle of attack....53
Figure 3.34 Response frequency versus flow pitch velocity for cluster tube bundle configuration, at a 0° angle of attack....54
Figure 3.35 Response spectra variation with flow velocity for Tube No.2 in a cluster bundle configuration, at a 0° angle of attack....54
Figure 3.36 Response spectra variation with flow velocity for Tube No.2 in two flexible tube bundle configuration, at an angle of attack 90°....55
Figure 3.37 R.M.S vibration response for the two flexible tube bundle configuration, at a 90° angle of attack, tube #2,3(inline)....56
Figure 3.38 Response frequency versus flow pitch velocity for the two flexible tube bundle configuration, at a 90° angle of attack, tube #2,3(inline)....56
Figure 3.39 R.M.S vibration response for the two flexible tube bundle configuration, at a 90° angle of attack, tube #3,7 (neighbor columns)....57
Figure 3.40 R.M.S vibration response for the two flexible tube bundle configuration, at a 60° angle of attack, tube #2,3 (inline)....58
Figure 3.41 Response frequency versus flow pitch velocity for the two flexible tube bundle configuration, at a 60° angle of attack, tube #2,3(inline)....59
Figure 3.42 R.M.S vibration response for the two flexible tube bundle configuration, at a 60° angle of attack, tube #3,7 (neighbor columns)....59

Figure 3.43 Response frequency versus flow pitch velocity for the two flexible tube bundle configuration, at a 60° angle of attack, tube #3,7(neighbor columns).....60
Figure 4.1 Critical pitch velocity versus flexibility orientation (angle of attack) for fully flexible tube bundle.....56
Figure 4.2 Critical pitch velocity versus flexibility orientation (angle of attack) for three-column flexible tube bundle.....57
Figure 4.3 Critical pitch velocity versus flexibility orientation (angle of attack) for cluster tube bundle configuration.....58
Figure 4.4 Stability map.....61
Figure 4.5a Cross-section of a small part of an array of cylinders in cross flow and velocity vector diagram.....62
Figure 4.5b Displacement vectors for rotated flexibility angle by θ°.....63
Figure 4.6 Upstream velocity variations with angle of attack comparison 69
Figure 4.7 Upstream velocity variations with angle of attack for three configurations...69

List of tables

Table 2.1 Instrumented tubes calibration.....22
Table 2.2 Natural frequency and damping for eight instrumented tubes.....23
Table 4.1 summary of experimental and numerical results.....68
Table 4.2 summary of experimental results and instability constant K.....70

List of symbols

Re	Reynolds number
S	Strouhal number
f_s	vortex shedding frequency correspond to Strouhal number (S)
V	flow velocity(m/s)
D	Diameter (m)
f_i	The acoustic natural frequency(Hz)
c	sound speed(m/s) (otherwise specified)
W	duct width(m)
i	order of acoustic mode
U_{Pc}	pitch flow velocity(m/s)
K	fluidelastic constant
ζ	damping ratio
ρ	fluid density(kg/m^3)
P	tube pitch(m)
U_∞	upstream flow velocity(m/s)
ΔP	differential pressure (N/m^2)
h	the reading on the digital transducer indicator
C_L	lift coefficient
C_D	drag coefficient
m	mass of the tube(kg) (otherwise specified)
l	length of the tube(m)
k	effective mechanical stiffness
F_x	fluid-dynamic force
U_r	tube displacement velocity

$\dot{x}$	tube displacement velocity in x direction(m/s)
$\dot{x}'$	tube displacement velocity in the x' direction(m/s)
θ	angle of attack(°)
τ	dimensionless time, ωt

List of appendixes

Appendix A 86
Appendix B 93
Appendix C 103

CHAPTER 1

INTRODUCTION

1.1 Background

To increase electrical power production, the nuclear energy operators aim to generate electrical power in great quantity, low cost with high safety features for both the population and the environment. A large majority of the existing companies have encountered unfavorable events regarding safety factors which have since raised concerns about the security of energy production. To address these issues, a number of important technological projects have been carried out to improve the design, maintenance and operation of these generators.

Despite great progress in the improvement of energy production, some specific problems occurred due to failures of heat exchanger tube bundles. Such failures were mainly caused by undesirable vibrations with large amplitudes. Three important mechanisms were found to be responsible for these vibrations in nuclear steam generator tubes: i) vibration induced by internal axial flow, ii) vibration induced by external axial flow, iii) vibration induced by external cross flow (Païdoussis 1983). The latter mechanism is the most crucial of the three since it causes fluidelastic instability; a vibratory phenomenon of particularly dangerous intensity. This instability can occur inside a typical tube array of steam generators or heat exchangers. Quick failure due to fatigue or abrasive wear/impact inside an unstable tube bundle makes understanding of fluidelastic instability important for the prediction and the identification of components at risk. The U-tube region of steam generators is undoubtedly one of these components. Indeed, low rigidity of these tubes, high flow rates of steam-water, two-phase cause flow adversely affect stabilities.

In the present work, experimental and theoretical studies are carried out in order to investigate fluidelastic instability in a typical tube bundle. This is done within the framework of the BWC/AECL/NSERC Chair of Fluid-Structure Interaction in the Mechanical engineering department at the École Polytechnique de Montréal. This chapter presents an introduction to the various vibration mechanisms of cylinders subjected to the external cross flow, a review of the scientific literature concerning the phenomenon of the fluidelastic instability, and the methodology of the present study. Finally the introduction is concluded with a summary of the project objectives and the contents of the ensuing chapters.

Since vibration of tube bundles is a critical problem, it is necessary to assess the probable sources of such vibrations. In this section we discuss various excitation mechanisms which can possibly take place with an isolated tube or tubes inside a bundle. As mentioned before, there are three possible situations in which a cylinder can be dynamically excited by the flow of a fluid: as fluid flows inside the tube, as fluid flows out in the axial direction on its external wall, and as flow is in the transverse direction to a cylinder external wall. In this study, we focus on the case of the transverse external flow excitation mechanisms. A review of the possible vibratory mechanisms for this case follows.

1.2 Tube bundle vibratory excitation mechanisms

1.2.1 Periodic Shedding

As fluid flow passes a smooth cylinder, under certain conditions which are given below, a regular pattern of alternating vortices (Karman vortices) form on the downstream part of the tube as shown in figure 1.1.

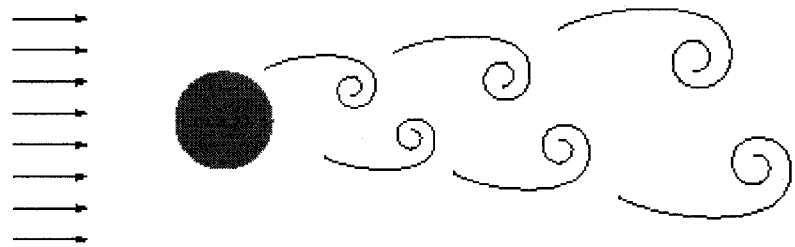

Figure 1.1 Fluid flows past a cylinder

The Karman vortices are shed alternately clockwise and counterclockwise and thus cause harmonically varying lift forces on the cylinder perpendicular to the velocity of the fluid. Experimental data show that regular vortex shedding occurs strongly in a range of Reynolds number (Re) from about 60 to 5000. The dimensionless frequency of vortex shedding is expressed as a Strouhal number (S) defined by equation (1.1). The Strouhal number is approximately equal to $S = 0.21$ for a smooth cylinder while, for a tube bundle, the St number is $S \cong 0.4 - 0.6$. Thus the frequency, f_s for these fluctuations is determined by the following relation:

$$S = \frac{fD}{V} \tag{1.1}$$

where V is the flow velocity and D is the outside diameter of the tube. If the shedding frequency corresponds to one of the natural frequencies of the structure, resonance occurs, and thereby the cylinder will start to vibrate in an excessive way. One can note that this resonance, however, occurs only for a small range of flow rate, the lock-in range. The amplitude of vibration decreases to an acceptable value as the flow rate becomes greater than the lock-in flow velocity limits.

Concerning vortex shedding effect in tube bundles subjected to two-phase cross flow, Taylor et al. (1989) suggest that any addition of the gas phase inhibits the

formation of vortices. It should be noted that beyond a void fraction of 15%, no evidence of periodic wake shedding has been found. In general, the effect of periodic wake shedding can be a significant contribution to tube vibration in two-phase flows up to a void fraction of about 15%. Pettigrew et al. (2004) have clarified that for a rotated triangular tube bundle subjected to a two-phase flow, no periodic wake shedding can be found even at very high void fractions (80%-95%). In general periodic wake shedding, or vortex shedding, may be a problem when the shedding frequency coincides with a tube natural frequency. This may lead to resonance and large vibration amplitudes. The calculated St number for the present work $S = 0.15$ which corresponds to the St number for tube bundles, shows that for the tube natural frequency, tube diameter and minimum flow velocity measured in the test section in which the large amplitude were observed, no periodic wake shedding could occur.

1.2.2 Random excitation caused by turbulent flow

Random pressure fluctuations on the external surface of tubes caused by turbulence causes the cylinder to vibrate. Pettigrew and Taylor (1995) noticed that turbulence is more important in two-phase flow as compared to single-phase flow. Turbulence in single-phase flow causes minimal excitation in tube bundles. Corresponding experimental data are discussed in Chapter 3. In fact, turbulence induces minimal excitation as compared to vibration caused by vortex shedding or fluidelastic instability mechanisms. Turbulence-induced vibrations do not cause significant damage to the component in the short term. However, considerable wear can result from friction between tubes and supports in the long term.

1.2.3 Fluidelastic instability

According to the experimental data reported by several authors in the available literature, fluidelastic instability in cross flow is the principal cause of many tube

vibration problems in heat exchangers and nuclear steam generators. As far as a tube bundle subjected to single-phase or two-phase cross flow is concerned, fluidelastic instability is the most important excitation mechanism, while other vibratory excitation mechanisms are less significant. Dynamic excitation forces for this mechanism are functions of the motion (i.e. position, velocity, and acceleration) of the tube itself and other surrounding tubes. As the motion, during an oscillation cycle, absorbs more energy than it dissipates by damping, its amplitude increases drastically leading the system to instability. Contrary to the wake shedding phenomenon, an increased flow velocity following the instability point does not decrease the vibration amplitude level. Indeed, such increase in flow velocity increases the vibration amplitude which leads to the failure of the system. Figure 1.2 clearly illustrates the difference between the three excitation mechanisms presented above.

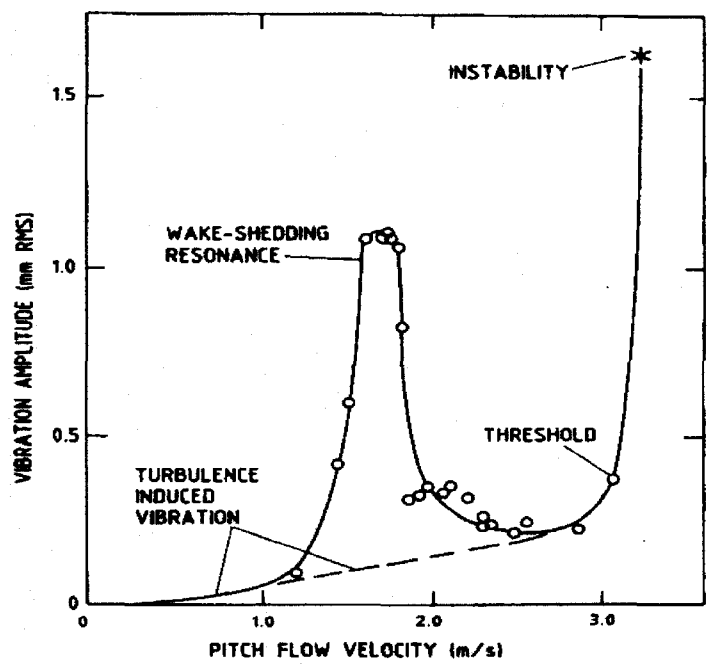

Figure 1.2 Vibration amplitude of a cylinder versus flow rate (Pettigrew et. al 1991)

Tube bundle instability results in contact between adjacent tubes or between tubes and anti-vibration beams (AVBs). This in turn limits the amplitude of tube vibrations. Such contacts remain the principal cause of serious and very quickly deteriorating damage to the tube bundle, hence significant reduction in the system life-cycle. A single tube (single-degree-of freedom) within a rotated triangular array cannot undergo fluidelastic instability in the flow direction as showed by Mureithi et al., (2004). It should be noted that the same array is highly unstable in cross-flow (Weaver and Fitzpatrik, 1988; Mureithi et al., 1994). Cross-flow instability is less of a concern for an actual steam generator due to the fact that the tubes are supported in cross-flow by AVBs. However, due to clearance and fabrication tolerances the AVBs do not hold the tubes entirely.

1.2.4 Acoustic resonance in tube bundles

An acoustic resonance phenomenon may occur in heat exchangers such as gas heaters or boilers that contain tube bundles. This phenomenon depends on three factors: tube bundle geometry, gas flow normal to tube axis, and the acoustic space limited by the duct walls. High level of noise generated by acoustic resonance has been a great concern for heat exchanger designers. As the gas flow rate inside a duct surpasses a critical level, generation of high level noise by the acoustic resonance phenomenon may occur. In the extreme case, this phenomenon may make it impossible to operate a plant or may cause structural damage. As the gas flow rate increases, the Karman vortex shedding frequency increases considerably, reaching the natural frequency of an acoustic mode inside a duct. The acoustic natural frequency f_i inside the duct is estimated by (Blevins, 1979):

$$f_i = \frac{ic}{2W} \quad ; i = 1,2,3,... \tag{1.2}$$

where *c, W,* and *i* are sound speed, duct width, and order of acoustic mode, respectively. As discussed in the previous section, the vortex shedding frequency f_s can also be estimated by equation (1.1). As the flow velocity increases, resonance occurs at corresponding modes. Hereafter, the flow velocity refers to the gap flow velocity unless otherwise noted. Since, in this work, tube array vibration responses were studied in a wind tunnel, the tube bundle could be affected by the acoustic resonance excitation mechanism. Our predictions presented later on, however, show that, in this case, the acoustic resonance excitation mechanism does not apply.

The vortex shedding frequency increases with flow velocity for which the maximum value, in the experiments, was 15*m/s*. Therefore one may write:

$$f_s = \frac{SV}{D} \Rightarrow f_s = \frac{(0.5)(15)}{0.04} = 187.5Hz \tag{1.3}$$

The acoustic natural frequency for the first mode (*i=1*) is:

$$f_i = \frac{ic}{2W} \Rightarrow f_1 = \frac{(300)}{2(0.3)} = 500Hz \tag{1.4}$$

As the above theoretical estimation shows, the tube bundle natural frequency is out of the acoustic natural frequency range by an acceptable safety margin. This was confirmed by our tests in which we observed no acoustic noise. Although acoustic resonance is one of the most important mechanisms in gas-phase cross flow, it does not apply in the present work.

1.3 A review of fluidelastic instability for external cross flows

1.3.1 Development of stability criterion

Since the mid-1960s, several models and theories have been proposed to formulate fluidelastic instability in tube bundles subjected to cross flow. Based on the experimental mode shape and measured fluidelastic forces, in which the, fluidelastic force is defined as the motion-dependent fluid force component that is proportional to the displacement of a cylinder, Connors (1970) developed a simple stability criterion for a tube bundle subjected to air flow as:

$$\frac{U_{pc}}{fD} = K\left(\frac{2\pi\zeta m}{\rho D^2}\right)^n \tag{1.5}$$

In this theory, fluidelastic instability is expressed in terms of a dimensionless velocity, U/fD, and a dimensionless mass-damping term, $2\pi\zeta m/\rho D^2$, where U_c is the critical velocity for fluidelastic instability, f the tube natural frequency, D the tube diameter, ζ the damping ratio, ρ the density of the fluid, and m the tube mass per unit length, which includes the hydrodynamic mass and the mass of the fluid inside the tube. In the simplest model, the exponent n is 0.5, and the fluidelastic constant K is usually determined experimentally.

Roberts (1966) was probably the first to discuss fluidelastic instability in cross-flow. He studied the aeroelastic behavior of a row of cylinders with pitch-to-diameter ratio P/D of 1.5 in a wind tunnel. Roberts identified the forgoing dimensionless parameters to dominate the formulation of fluidelastic instability. Although Roberts'

expression is somewhat more complicated, an approximate simplified expression can be deduced from his experimental data.

$$\frac{U_{pc}}{fD} = 9.8\left(\frac{2\pi\zeta m}{\rho D^2}\right)^{0.5} \tag{1.6}$$

In this expression, U_p is the pitch velocity, which is defined as:

$$U_p = U_\infty \frac{P}{P-D} \tag{1.7}$$

where U_∞ is the free stream velocity or the velocity that would prevail if the tube where removed.

Connors (1970) was probably the first to study fluidelastic instability in heat exchanger tube bundles. He did his experimental work in a wind tunnel. Connors proposed a quasi-static model to describe fluidelastic instability. This work led to the formulation of equation (1.5), in which $n = 0.5$. Connors reported a fluidelastic instability constant $K = 9.9$ for a tube row of $P/D = 1.41$, which is in agreement with Roberts' finding. Unfortunately, because of the lack of other data at the time, the value of $K = 9.9$ was used for tube bundles by some designers Pettigrew et al., (1991).

In the early 1970s, a comprehensive program was undertaken at the Chalk River Laboratories to study flow-induced vibration of nuclear heat exchangers. This work was done in collaboration with Canadian industry and universities. Realistic tube bundles of both triangular and square configurations of P/D between 1.23 and 1.57 were tested in

liquid flow. This work led Pettigrew et al. (1978) to recommend the following relationship:

$$\frac{U_{pc}}{fD} = 3.3\left(\frac{2\pi\zeta m}{\rho D^2}\right)^{0.5} \tag{1.8}$$

This was recognized as a design guideline to avoid fluidelastic instability in heat exchangers. The criterion suggested by Pettigrew et al., (1978) is reasonable in practice as may be seen when compared to available data on in-service heat exchangers which show no problems of tube wear or fatigue due to fluidelastic instability. Since the mid 70s, a great number of heat exchangers for the Canadian, American, and other nuclear industries were designed using this criterion.

1.3.2 Development of the theory

Since 1975, a large number of studies especially in the experimental domain were undertaken by researchers in various fields with the aim of understanding the mechanics behind the fluidelastic instability phenomenon. Eventually, several alternatives for the Connors' relation (Eq. 1.5) were proposed in the literature as the criterion of design. For a detailed review of the models available, the readers are encouraged to refer to the excellent work of Price (1995). Many interesting developments were made during recent years some of which deserve to be mentioned. The most interesting, from a theoretical standpoint, are the two instability mechanisms discussed in Chen (1987), Price (1995), Païdoussis et al., (1988), and Yetisir and Weaver (1993).

Generally, in a tube bundle, the fluid forces on one tube are affected by its motion and the motion of neighboring tubes. This creates an interaction between fluid forces and tube motion. Fluidelastic instability take places when the interaction between

the motion of individual tubes is such that it results in fluid force components that are both proportional to tube displacement and in-phase with tube velocities.

It is well accepted that there are two mechanisms underling flow-induced instability. The first, the damping controlled mechanism, manifests itself when the forces acting on the tube are in phase with its velocity. This mechanism needs only one degree of freedom to exist. The second, called stiffness controlled mechanism appears, when the fluid force is proportional to both the displacement and velocity of cylinders and needs at least two degrees of freedom to materialize. Indeed in fluidelastic stiffness controlled instability, the coupling fluidelastic forces are the main cause of instability Chen (1983 and 1984).

From the results obtained for tubes which are flexible only in the flow direction, it can be concluded that for the fluidelastic instability to occur, more than one flexible tube (one degree of freedom) is needed. Since the damping controlled mechanism needs only one degree of freedom to cause instability, we can deduce that it is only the stiffness controlled mechanism that produces the instability of the tubes flexible purely in the flow direction. For the stiffness controlled mechanism, the relative tube displacement governs the interaction between the various degrees of freedom of the system. Another interesting finding, for a fully flexible tube array (flexible in all directions) is that when instability takes place, the motion seems to occur mainly in the lift direction (Weaver and Lever 1982). Thus the stability of tube bundles in the flow direction did not raise many concerns. Recently, Mureithi et al., (2005), however, have demonstrated in experiments in a wind tunnel that fluidelastic instability can develop inside a tube array which is flexible only in the flow direction.

1.3.3 Fluidelastic instabilities in two-phase flow

In spite of the considerable role of two-phase flows in industrial applications, it was only in 1980 that some experimental results were reported on tube bundle fluidelastic instabilities subjected to transverse flow composed of a liquid-gas mixture. The delay was of course due to the high cost and technical requirements of such experimental studies. Among available works, those by Axisa et al., (1984 & 1985), Nakamura et al., (1991 and 2002), Mureithi et al., (2002), and Hirota et al., (2002) are of interest to this study.

The least-expensive and simplest method to simulate steam-water two-phase flow state is the use of air-water mixtures. A significant number of investigations concerning the vibrations of tube bundles subjected to transverse two-phase flows were carried out using this type of mixture (Axisa et al., 1988, Heilker and Vincent 1981, Pettigrew et al., 1989, Remy 1982, Taylor et al., 1988). Nowadays the tendency is to simulate the boiling phenomenon at nearly atmospheric conditions using cooling agents like Freon in order to replicate steam-water mixtures (Pettigrew et al., 1995, Feenstra et al., 2003, Nakamura et al., 1999). The main advantage of two-phase mixtures of cooling agents lies in the similarity of their properties with those of steam-water mixtures (ratio of density, surface tension, and viscosity). Moreover, the presence of interactions between the liquid and gas phases in the Freon mixture, such as evaporation and condensation, contributes to a better simulation of a real vapor and water flow. Obviously these elements do not exist in air-water flow.

1.4 Motivation for the present work

At the beginning of this chapter, the more important areas susceptible to fluidelastic instability, the upper U-bend section of nuclear steam generators, were explained. In order to increase the rigidity of U-tubes in the cross flow direction, all

steam generators used in the nuclear industry are equipped with special supports to stiffen the tube arrays in this critical area. This aims to increase the critical flow velocity of instability out of the range of flow velocities in the steam generators. These metal bar supports, called anti vibration bars (AVBs), are installed in a radial orientation in the U-bend region.

As stated previously, this study focuses on the uppermost U-bend region, in which the flow crosses a large number of tubes causing significant hydraulic resistance. This hydraulic resistance forces the flow to change direction. As a result, flow leaves the tube bundle at different angles of attack ranging from 0° to 90° (Figure 1.3). Since the tube bundle is excited by both straight and oblique cross flows, the current study will examine the instability phenomenon in a rotated, triangle tube bundle subjected to oblique single-phase cross flow.

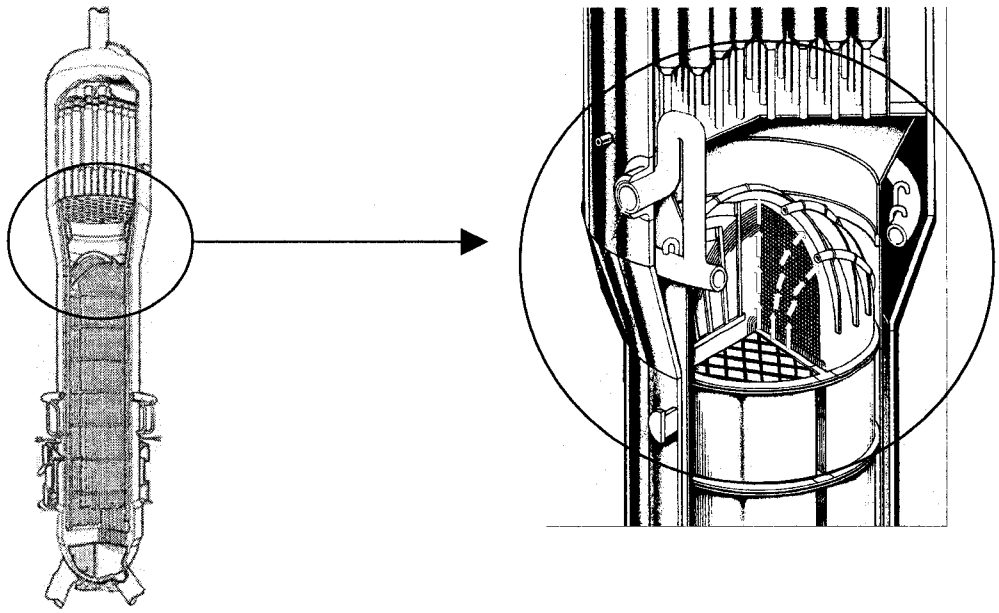

Figure 1.3 Flow stream alterations due to hydraulic resistance

1.5 Objectives

The research work on fluidelastic instability is divided in two categories. The first aims at obtaining a basic understanding of fluidelastic instability. This category is usually studied for well-defined and well-instrumented arrays of flexible cylinders in an otherwise rigid array of cylinders these are all installed inside wind tunnels or two-phase flow test sections.

The second category, on the other hand, aims at producing design information. Pettigrew and Taylor (1991) found that the only data from experiments where all tubes were free to vibrate are valid from a design point of view. This type of work is usually done on realistic heat exchanger tube bundles which are often studied in liquid flow. For two-phase flow, this method has been used only for a few cases, because of its high cost and other practical restrictions. However, this method often provides information much closer to real heat exchanger designs.

The current tests were performed in a wind tunnel with a tube array subjected to single-phase cross flow. Although single-phase flow tests do not represents two-phase flows, in many studies the air flow method is utilized due to its simplicity, less expensive equipment, and negligible flow damping.

1.6 Thesis layout

This thesis includes five chapters the first of which has been explained. The second chapter describes the equipment and the assembly of the experimental apparatus as well as the experimental methods. The experimental results are presented in the third chapter and subsequently analyzed in chapter four. Finally, chapter five concludes the project by discussing the implications of the research findings.

CHAPTER 2

TEST APPARATUS AND EXPERIMENTAL PROCEDURE

Within the framework of the second chapter, the means used to achieve the goals of this project will be examined. This chapter will thus be divided into two distinct parts. The first part will cover technical details on test section structure. The second part will be dedicated to the examination of the experimental methods.

2.1 Experimental assembly structure

2.1.1 Test section components

An approximate model was used to simulate the upper U-bend region in the nuclear steam generator.

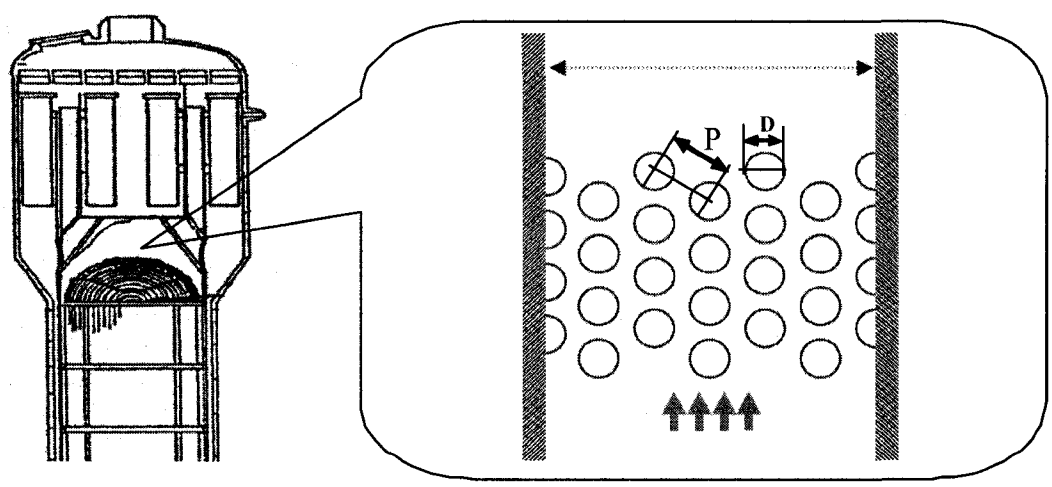

Figure 2.1 U-tube area of the steam generator and approximated experimental model

Figure 2.1 illustrates this experimental model. Testing was conducted in a wind tunnel with a 305mm ×305mm test section, in which the maximum flow velocity U_{max}

is 48.8m/s in the empty test section, and 8m/s with the array in place. The tube bundle shown in Figure 2.2 consists of an array of light-weight tubes with an outside diameter of 40.4mm, and a height of 288.9mm, placed in a rotated-triangular configuration with a pitch ratio of $P/D = 1.37$. The array consists of four rows by five columns, with alternately three and two-half tubes per row. The half tubes on the walls provided a uniform flow profile.

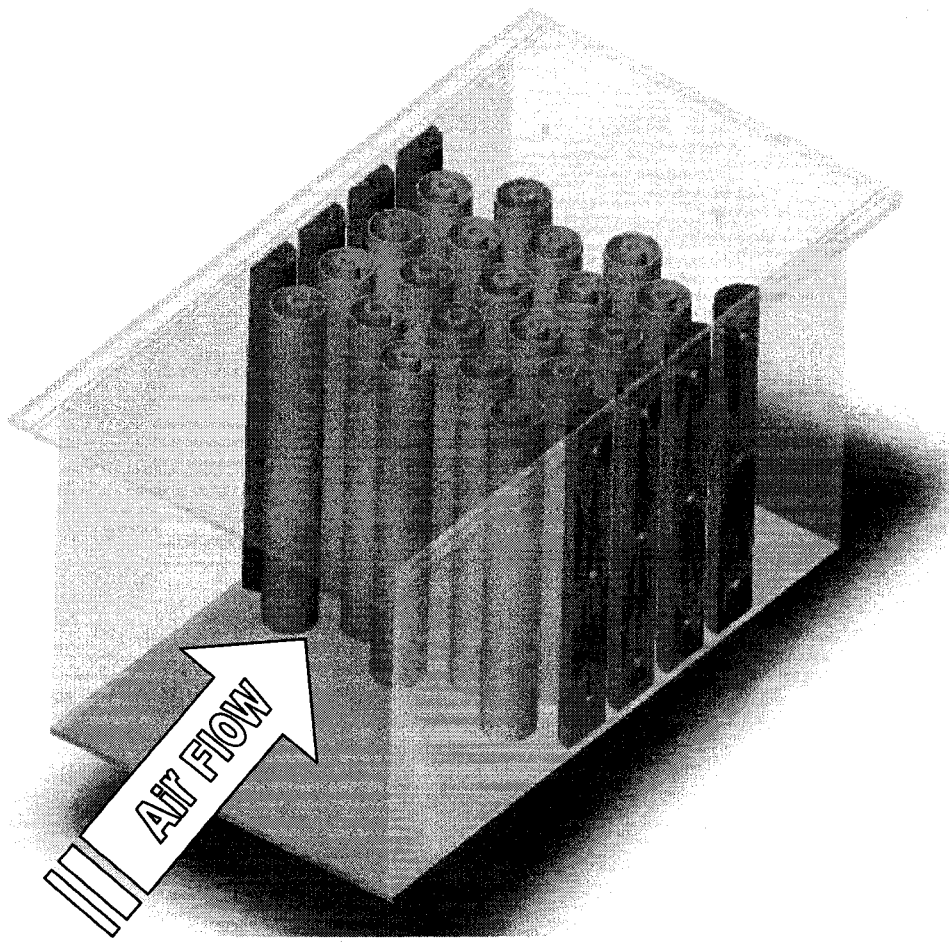

Figure 2.2 Test section and air flow direction

Each cylinder consists of a tube with a mild-steel thin plate fixed in the middle of the tube via a wooden plug as shown in figure 2.3. The mild-steel plate with a rectangular cross-section of 1.5mm ×15mm provides a unidirectional flexible tube bundle. The thin plate and tube assembly are rigidly fixed to the top of the test section

which provides a cantilever tube via the thin beam. The natural frequency of the assembly was 188Hz in the transverse direction, which in comparison to the natural frequency in the lateral direction, 19.44Hz, made the tube essentially rigid in this direction. Figure 2.3(a) and 2.3(b) illustrate an exploded view of the flexible tube assembly and assembled view of the flexible tube respectively.

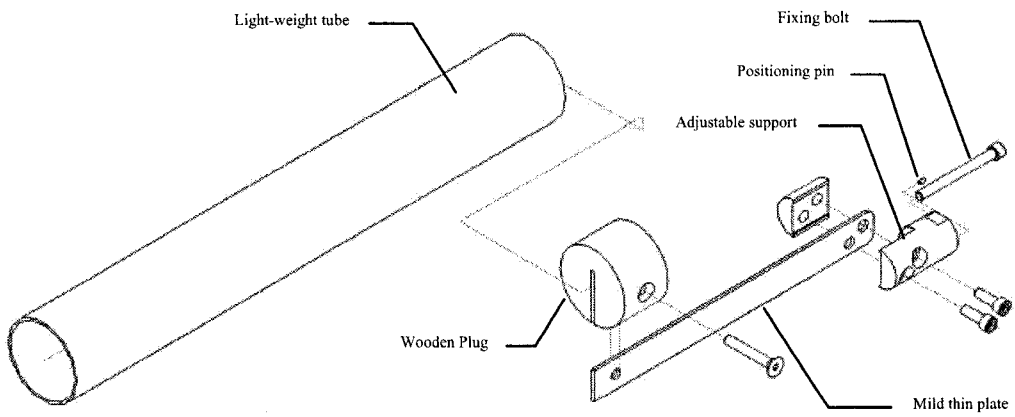

Figure 2.3(a) Exploded view of the flexible tube assembly

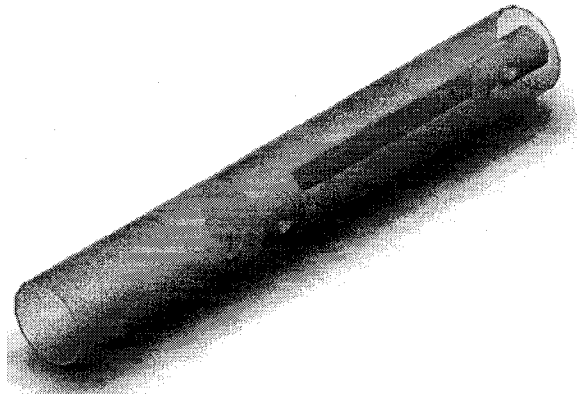

Figure 2.3(b) Assembled view of the flexible tube

A simple mechanism was designed to rotate the tubes axially to provide different flexibility orientations, resulting in various angles of attack ranging from 0° to 90° (Figure 2.4).

Also in order to cover a range of tube bundle configurations, each one of the tubes could be independently restrained from vibration, by means of an aluminum plug fitted at the free end. Appropriate technical drawings are given in appendix **A**.

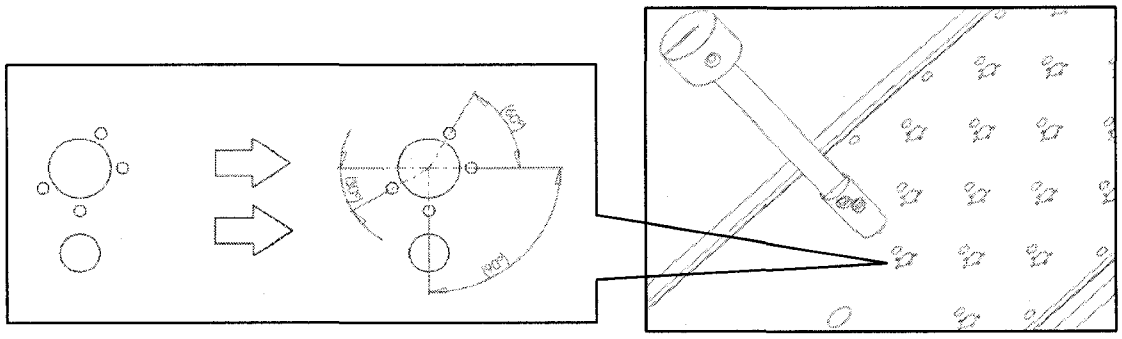

Figure 2.4 Positioning mechanism for the flexibility orientation

2.1.2 Wind tunnel specifications

Experiments were conducted in a wind tunnel Model 402 made by ELD, with a $305\text{mm} \times 305\text{mm}$ test section with a total power of 10hp, in which the maximum flow velocity was measured as 48 m/s in the empty test section, and 8m/s with the array in place. Figure 2.5 shows a photo of the open-loop ELD wind tunnel Model 402 utilized in the present work.

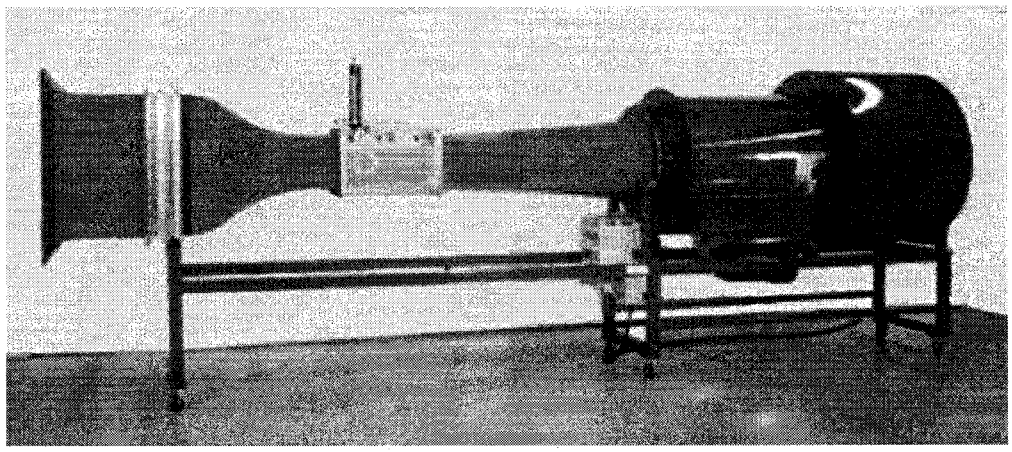

Figure 2.5 Open-loop ELD wind tunnel Model 402

2.2 Measurement equipment

2.2.1 Flow velocity measurement

The flow velocity is measured at the entry of the test section using a Pitot tube connected to an ultra low range Wet-Wet differential pressure Transducer "Validyne DP103". Pressure transducer is coupled to a digital converter.

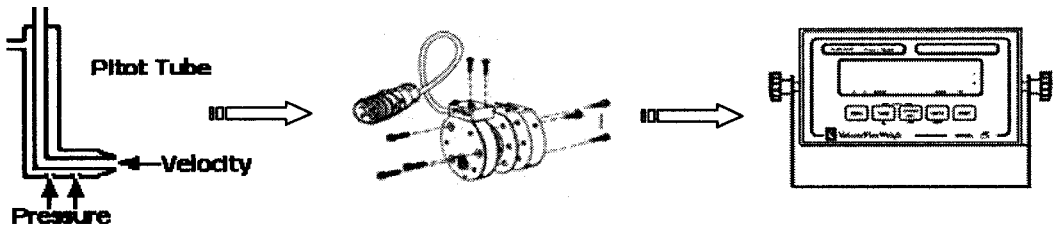

(a) (b) (c)

Figure 2.6 Flow velocity measurement chain

The Validyne DP103 transducer in figure 2.6 (b) is designed for very low differential pressure measurement applications where high accuracy is required under

rough physical conditions. With full scale ranges down to –0.008 psid (–0.56 cm H_2O), this instrument is used in the measurement of very low flow rates of gases where symmetrical pressure cavities are required for dynamic response.

The static pitot tube differential pressure is measured using a typical variable reluctance pressure transducer consisting of a diaphragm of magnetically permeable stainless steel clamped between two blocks of stainless steel (figure 2.7). Embedded in each block is an inductance coil on an E-shaped core. A pressure difference applied through the pressure ports deflects the diaphragm toward the cavity with the lower pressure, decreasing one gap and increasing the other. As the magnetic resistance varies with the gap, the diaphragm deflection increases the inductance of one coil and decreases the other.

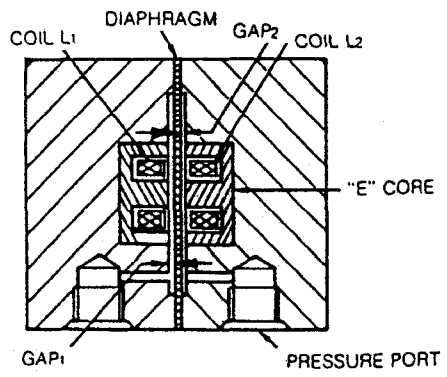

Figure 2.7 Typical transducer cross-section

The transducer connected in an AC bridge circuit is able to take advantage of the inductance variations in the transducer coil. Collected signals are transmitted to a digital transducer indicator adjusted for pressure engineering unit of$(In\ H_2O)$, consequently reading differential pressure digits will be in terms of$(In\ H_2O)$. Thus

$$\Delta P = \rho_{H_2O} \times g \times 0.0254 \times h \tag{2.1}$$

resulting from (2.1)

$$\frac{1}{2}V_1^2 \times \rho_{air} = \rho_{H_2O} \times g \times 0.0254 \times h \tag{2.2}$$

$$\boxed{V_1 = \sqrt{2 \times \frac{\rho_{H_2O}}{\rho_{air}} \times g \times 0.0254 \times h}} \tag{2.3}$$

where, h is the reading on the digital transducer indicator. The velocity V_1, corresponds to the upstream flow velocity which is identified as U_∞. The velocity inside the tube bundle between cylinders, which is called the Pitch velocity, U_P. For a rotated triangular tube bundle, it is calculated as follow:

$$U_P = \frac{P}{P-D} U_\infty \tag{2.4}$$

$$U_P = \frac{\frac{P}{D}}{\frac{P}{D}-1} U_\infty \tag{2.5}$$

$$\boxed{U_P = \frac{\frac{P}{D}}{\frac{P}{D}-1} \times \sqrt{2 \times \frac{\rho_{H_2O}}{\rho_{air}} \times g \times 0.0254 \times h}} \tag{2.6}$$

where, P is the pitch of the tube bundle and D is the tube diameter.

2.2.2 Instrumented tube calibration

Before the tube bundle was inserted into the wind tunnel test-section, the static strain displacement relation for every instrumented tube was determined via a careful

calibration. The latter was carried out using a micrometer to impose small displacements at the end of each instrumented tube. This gives the related calibration factor using a P3500 mobile strain indicator. Figure 2.9 illustrates the calibration factors in term of displacement for eight instrumented tubes.

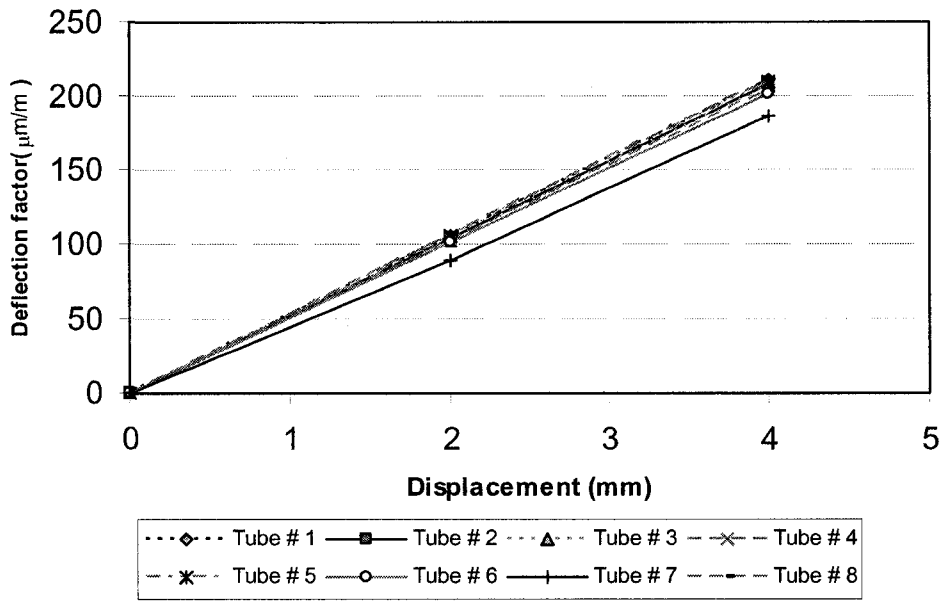

Figure 2.8 Tube displacement and relative deflection factor

	$\mu\varepsilon/mm$	Sensitivity(V/mm)	Sensitivity$(V/\%Dia)$
Tube # 1	**65.6**	**0.026**	**6.56E-03**
Tube # 2	**64.55**	**0.025**	**6.45E-03**
Tube # 3	**63.95**	**0.025**	**6.39E-03**
Tube # 4	**63.65**	**0.025**	**6.36E-03**
Tube # 5	**65.2**	**0.026**	**6.52E-03**
Tube # 6	**62.95**	**0.025**	**6.29E-03**
Tube # 7	**55.25**	**0.022**	**5.52E-03**
Tube # 8	**66.65**	**0.026**	**6.66E-03**

Table 2.1 Instrumented tubes calibration

To have a single voltage for a known deformation, a maximum factor of $2000\mu m/m$ for an output of $0.8V$ was used to convert the imposed deformation and to regulate the electrical signal. Therefore the sensitivity (V/mm) for each tube assembly is a product of $0.8/2000$ and the relative factor between displacement and tube deformation. Also for the purpose of having the amplitude as a function of tube diameter, the sensitivity is divided by the tube diameter (Table 2.1).

2.2.2 Tube structural damping and natural frequency measurement

The logarithmic decrement method is used to measure the structural damping in the time domain. With this method, the free vibration displacement amplitude response of a system to an impulse is measured and recorded. Logarithmic decrement is the natural logarithmic value of the ratio of the two adjacent peak values of displacement in free decay vibration and it is given by:

$$\boxed{\delta = \frac{2\pi\zeta}{\sqrt{1-\zeta^2}}} \tag{2.7}$$

The measured damping ratio for eight instrumented tubes is given in Table 2.2, corresponding figures may be found in appendix **B**.

Tube No.	1	2	3	4	5	6	7	8	Average
$f(Hz)$	19.5	19.45	19.5	19.3	19.8	19.5	19.3	19.3	19.45
$\zeta(\%)$	0.31	0.39	0.30	0.30	0.26	0.27	0.21	0.39	0.31

Table 2.2 Natural frequency and damping for eight instrumented tubes

To determine the natural frequency of the flexible tube, the Labview software uses a FFT algorithm. Figure 2.11 shows a typical measured natural frequency for tube # 1; corresponding figures for the eight instrumented tubes are given in Appendix **B**.

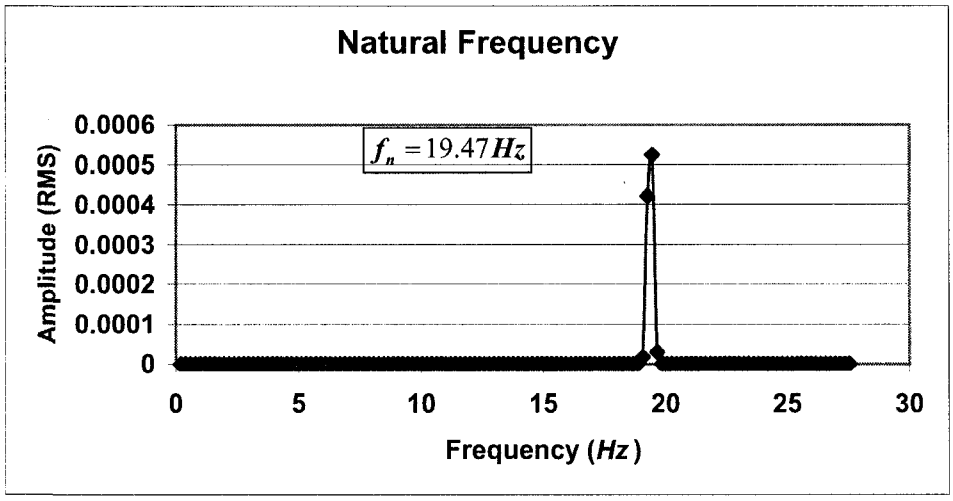

Figure 2.9 Natural frequency measurement

2.3 Experimental methods and procedure

2.3.1 More frequently used definitions

- **Critical velocity for fluidelastic instability**

In the available literature the critical velocity for fluidelastic instability, is defined by different criteria proposed by the different researchers. For example Heilker and Vincent (1981) used the velocity at which tube rattling occurred as a criterion, while Soper (1983) used the point at which a tangent to the post-critical response intersected the velocity axis.

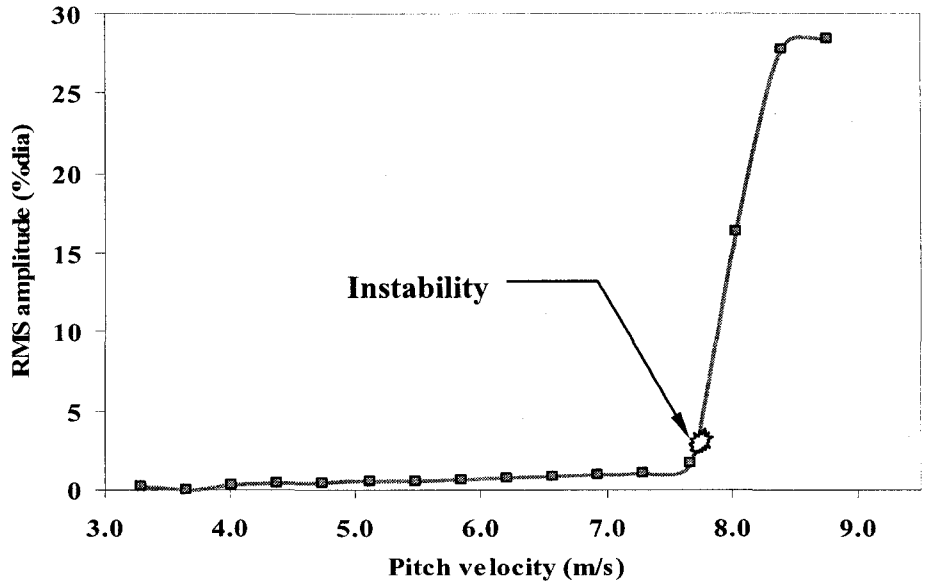

Figure 2.10 Well-defined fluidelastic instability

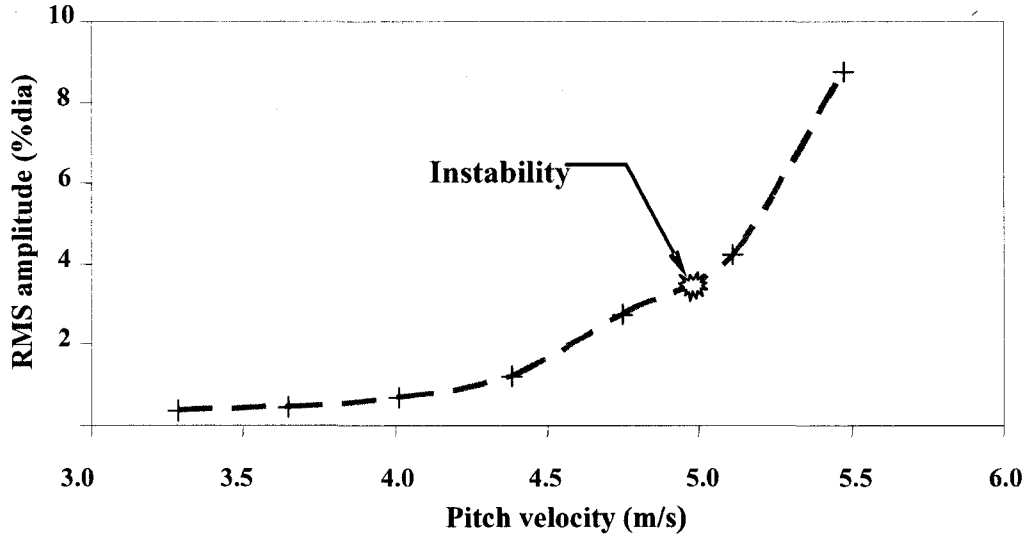

Figure 2.11 Less well-defined fluidelastic instability

Teh and Goyder (1988) took the velocity at which the damping appears to be nil. These differences are a great source of disparity in the data. Here we took a very practical approach as presented by Pettigrew and Taylor (1991). When the instability threshold is well defined, we simply took the flow velocity at which it occurs as the critical instability velocity, Figure 2.10. When it is not well defined, the velocity at which excessive vibration amplitude occurs has been taken, Figure 2.11.

This amplitude is dependent on the tube frequency and tube size (i.e. pitch ratio and rigidity). Here excessive amplitude means, vibration levels that normally not acceptable in heat exchangers and steam generators. Usually it is more than 2% of the tube diameter.

- **Tube natural frequency**

  The tube frequency in air, was used to analyze the data.

- **Damping**

  In gases, damping values in air are acceptable since fluid damping is not significant. Here the measured damping ratio in air is used in data analysis.

2.3.2 Tests procedure

Tests were performed on three different tube bundle configurations. All the tubes were originally designed as cantilever tubes. For the purpose of this study, each tube could be independently restrained from vibrating by means of a support inserted in the gap between the tube and the upper test-section window, hence simulating a rigidly fixed tube. Also each tube could be rotated axially, using a simple mechanism described in Section 2.1.1. This mechanism provides different flexibility orientations, which create various angles of attack ranging from 0° to 90° at four points for each tube bundle configuration. Each series of tests consisted of four principal flexibility orientations.

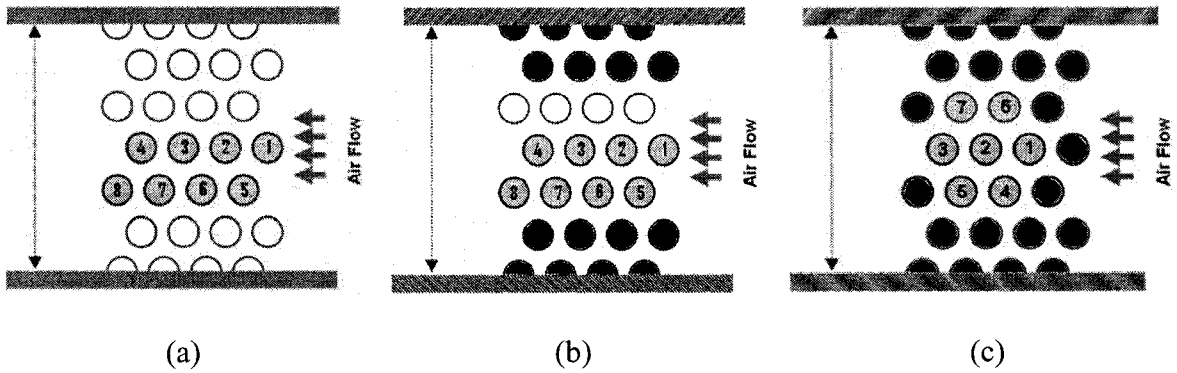

Figure 2.12 Three main tube bundle configurations
(a) Fully flexible tube bundle, (b) Three-column flexible tube bundle,
(c) Cluster tube bundle configuration

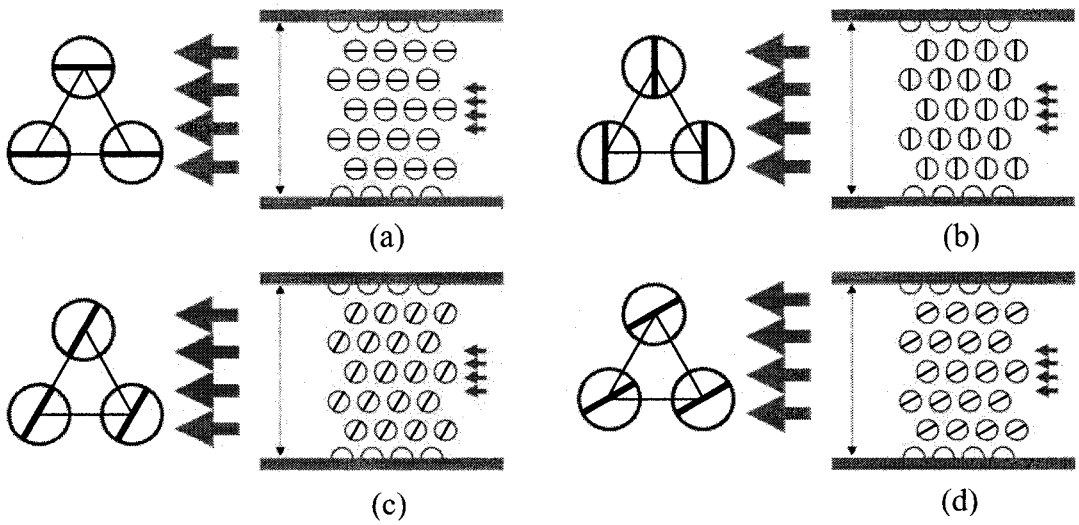

Figure 2.13 The main four tube flexibility orientations,
a) 90° to flow direction (cross flow), b) 0° to flow direction (in flow direction), c) 30° to flow direction, d) 60° to flow direction

For each test run, sufficient time was allowed for a steady state to be attained (usually several minutes). The flow velocity was recorded and r.m.s displacements

measured. The flow velocity was then increased gradually and the process repeated until the bundle was well into unstable regime.

For the single flexible tube configuration, Tube #2 is left flexible in the cluster configuration. Figure 2.12 and 2.13 show the main three tube bundle configurations and the main four tube flexibility orientations.

In the next chapter experimental results is discussed.

CHAPTER 3

EXPERIMENTAL RESULTS

In the second chapter, the test equipments and experimental methods utilized in the present work were described in details. In the present chapter, the experimental result will be examined. This chapter consists of two main sections, the first section presents the results of the fluidelastic instability tests, while the second section offers a stability comparison of for the various tube bundle configurations and flexibility orientations.

3.1 Fully flexible tube bundle

3.1.1 Stability behavior of the fully flexible bundle with tube motion in cross flow (Angle of attack 90°)

Eight instrumented tubes (labeled 1-8 Figure.2.12 (a)) were monitored within the fully flexible tube bundle. The vibration response for tube No.7 is given in Figure 3.1. The response spectra show that for low flow velocities, there is minimal excitation due to turbulence.

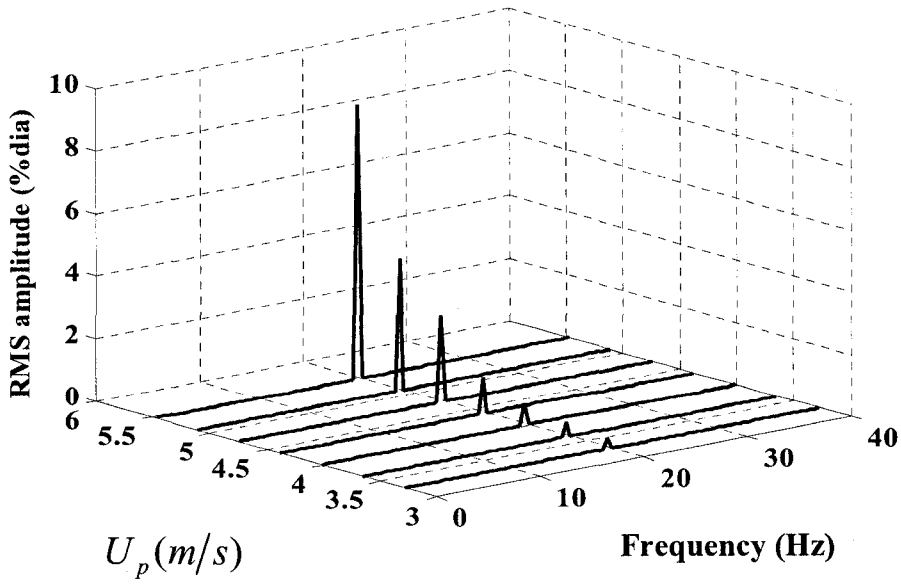

Figure 3.1 Response spectra variation with flow velocity for Tube No.7 in a fully flexible bundle, at a 90°angle of attack

At the pitch velocity $U_p = 4.75 m/s$, a strong instability developed. The r.m.s response amplitude variation with flow velocity is shown in Figure 3.2. Increasing the flow velocity to $U_p = 5.3 m/s$ resulted in increased peak amplitudes. Coincidentally with the large increase in vibration amplitude, a coalescence of the individual tube frequencies to a single modal frequency was observed as shown in Figure 3.3, confirming again the onset of fluidelastic instability.

Increasing the flow velocity to $U_p = 5.4 m/s$ resulted in peak amplitudes larger than the inter-cylinder gap which caused intermittent tube contact at the free ends. A sudden reduction in vibration amplitude was detected for tubes No.7 and No.4. A phase analysis showed that these two tubes are 180° out of phase and therefore a physical contact between the tubes occurred at this point.

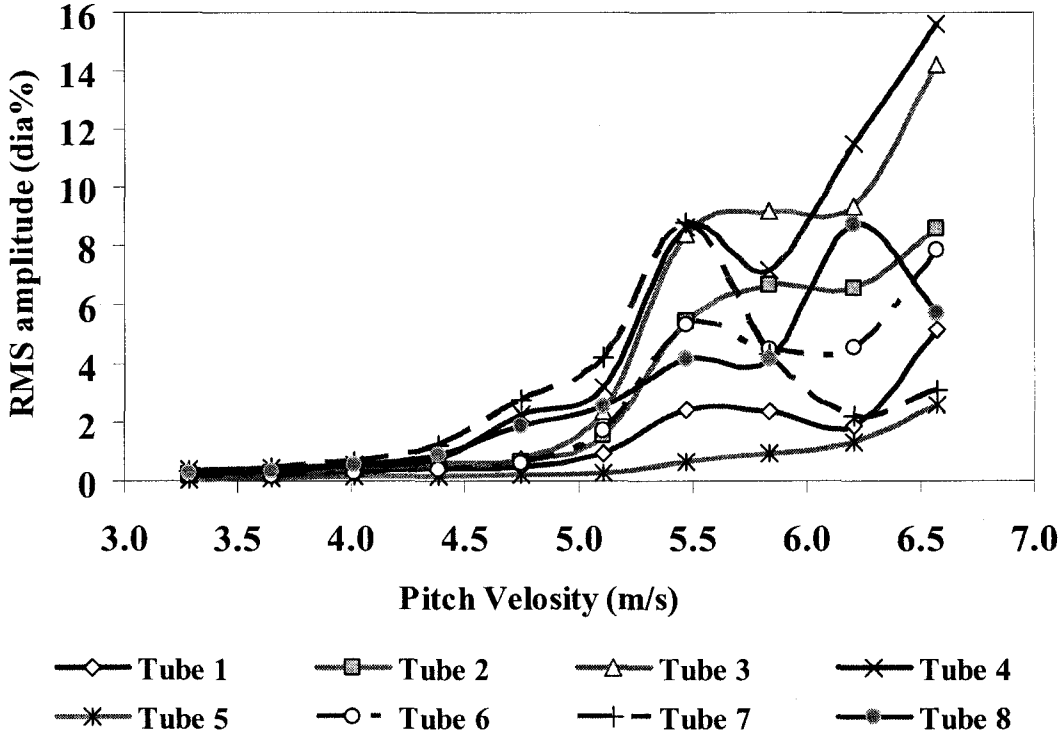

Figure 3.2 R.M.S vibration response for the fully-flexible tube bundle, at an angle of attack 90°

As shown in Figure 3.3, at a pitch velocity $U_p = 4.75\,m/s$ most of the tubes vibrated at two very close frequencies, confirming the onset of fluidelastic instability and, at pitch velocity $U_p = 5.0\,m/s$ all of the tubes vibrated at a single frequency. This latter experiment is used to validate the fluidelastic instability critical velocity obtained in the r.m.s vibration response results.

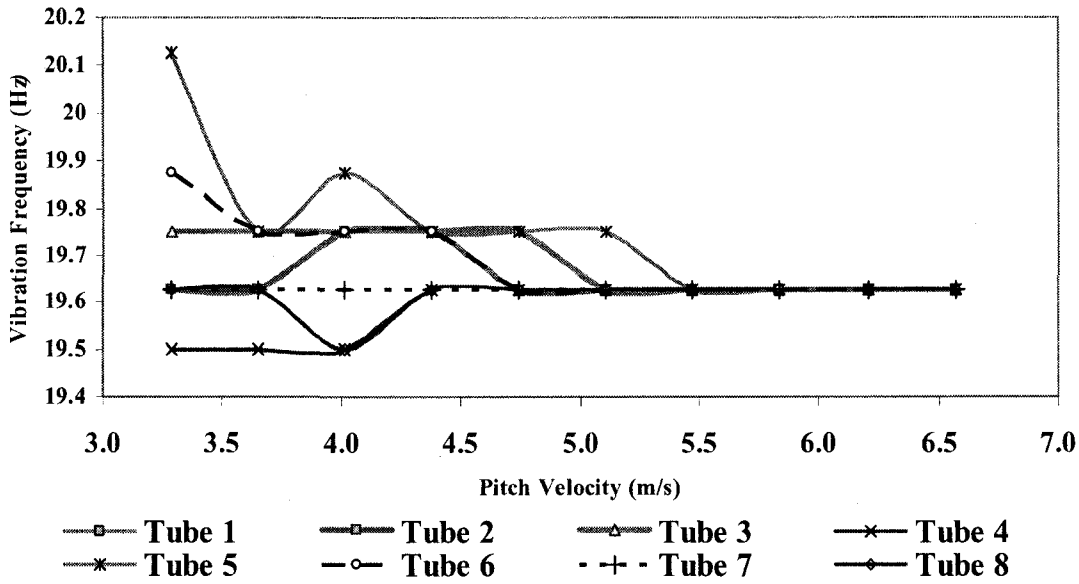

Figure 3.3 Response frequency versus flow pitch velocity for the flexible tube bundle, at a 90° angle of attack

3.1.2 Stability behavior of the fully flexible bundle with tube motion at 60° to the flow direction (Angle of attack 60°)

In the second series of tests, the tubes were rotated by 30 degrees resulting in a 60° angle of attack as shown in Figure 2.15(d). Of the eight instrumented tubes within the fully flexible bundle, the vibration spectra for tube No.7 given in Figure 3.4, shows that turbulence generates minimal excitation at low flow velocity.

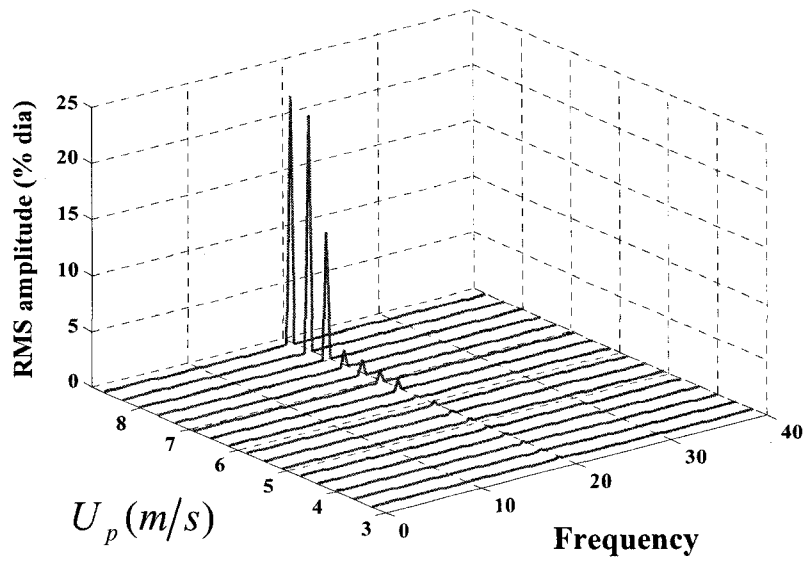

Figure 3.4 Response spectra variation with flow velocity for Tube No.7 in a fully flexible bundle, at a 60° angle of attack

The vibration response for the second and third tube columns (Figure 3.5) shows that the critical pitch velocity for the 60° angle of attack increases to $U_p = 7.7\,m/s$ and at a pitch velocity $U_p = 8.0\,m/s$ strong vibrations are observed. In this case a very typical fluidelastic instability phenomenon was observed in the r.m.s amplitude/flow pitch velocity diagram. In comparison to the 90° angle of attack, the r.m.s amplitude following fluidelastic instability increased by about a factor of two for the 60° angle of attack configuration.

Once more, coincidentally with the large increase in vibration amplitudes, a coalescence of the individual tube frequencies to a single modal frequency was observed at $U_p = 8.4\,m/s$.

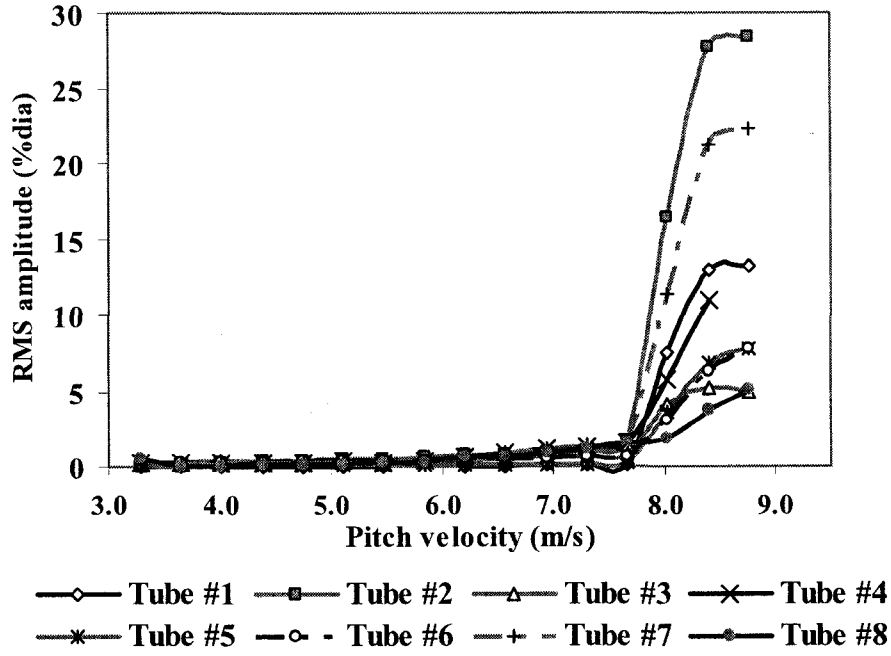

Figure 3.5 R.M.S vibration response for the fully flexible tube bundle, at a 60° angle of attack

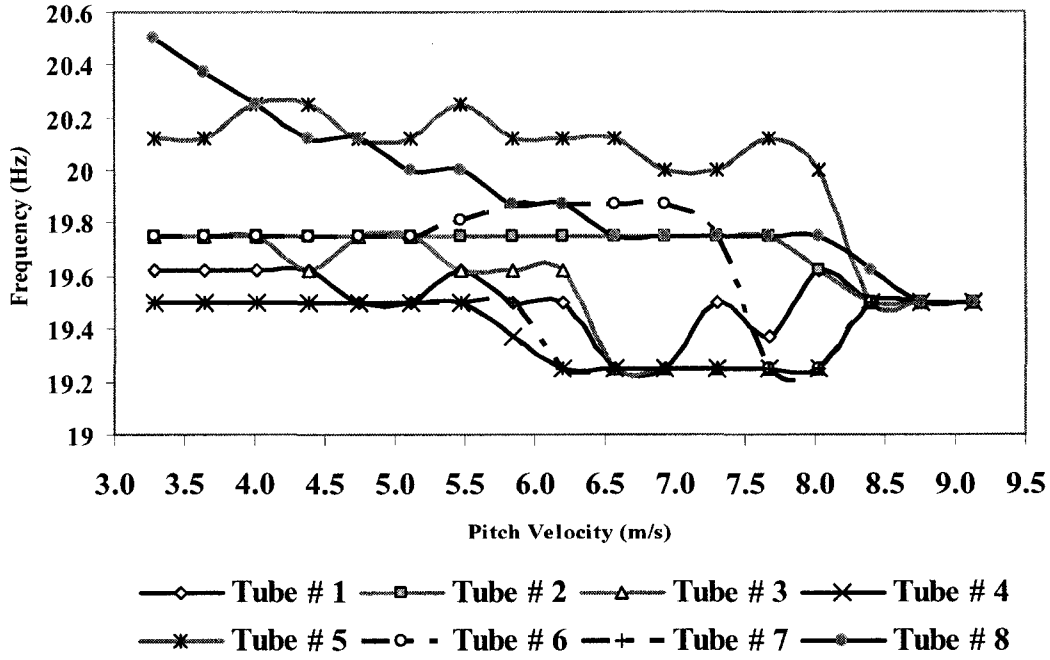

Figure 3.6 Response frequency versus flow pitch velocity for the flexible tube bundle, at a 60° angle of attack

3.1.3 Stability behavior of the fully flexible bundle with tube motion at 30° to the flow direction (Angle of attack 30°)

The tubes were rotated to a 30 degree angle of attack. The power spectra of the response are shown in Figure 3.7. The onset of fluidelastic instability is clearly defined when the flow velocity is increased gradually to $U_p = 8.3 m/s$. The amplitude plot of Figure 3.8 shows that the instability is occurs at a critical flow velocity $U_p = 8.3 m/s$ and at $U_p = 9.5 m/s$ the r.m.s vibration amplitude increases to 20% of the tube diameter.

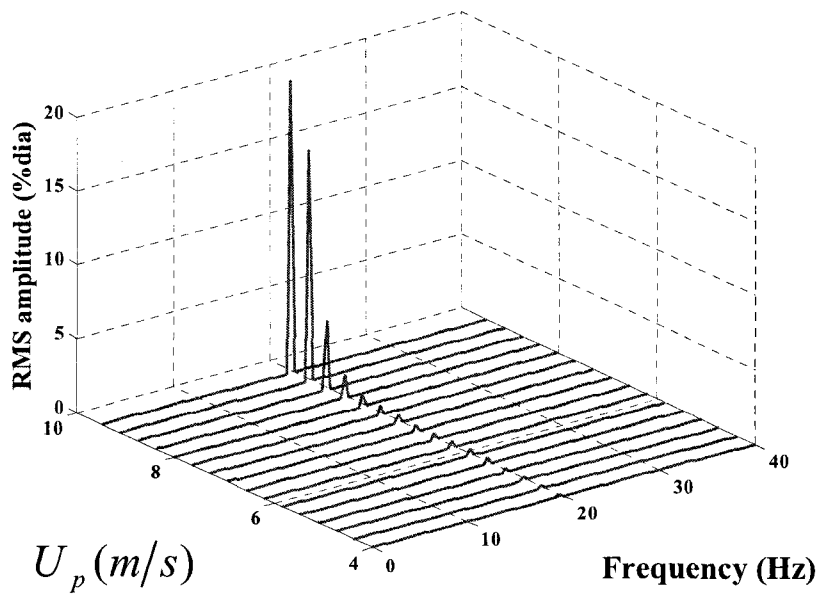

Figure 3.7 Response spectra variation with flow velocity for Tube No.4 in a fully flexible bundle, at an angle of attack 30°

As shown in Figure 3.8, instability occurs at a velocity higher than those for the 60° angle of attack configuration. Also larger r.m.s vibration amplitudes were recorded in comparison to the 90° angle of attack case.

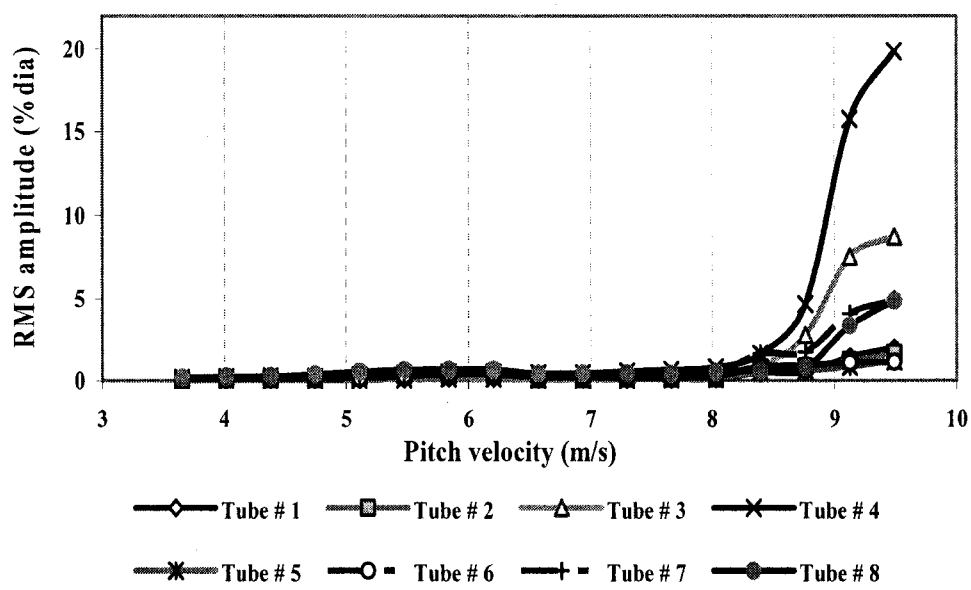

Figure 3.8 R.M.S vibration response for the fully flexible tube bundle, at a 30° angle of attack

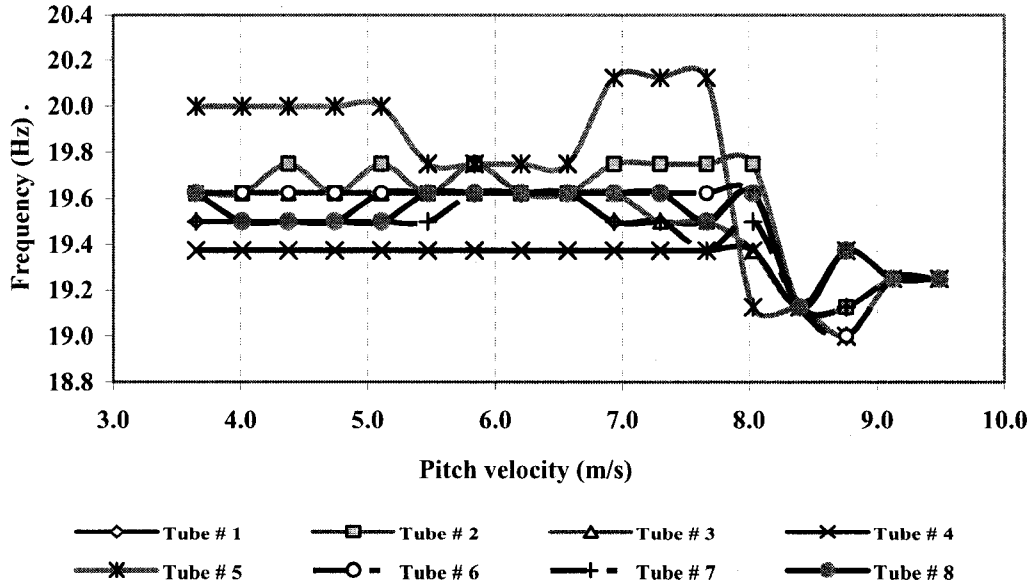

Figure 3.9 Response frequency versus flow pitch velocity for the flexible tube bundle, at a 30° angle of attack

Observation of fluidelastic instability at higher flow pitch velocity for the case of tube bundle flexibility at 30° angle of attack is supported by the coalescence of response frequencies with pitch flow velocity as shown in figure 3.9.

3.1.4 Stability behavior of the fully flexible bundle with tube motion in-line with the flow direction (Angle of attack 0°)

As the last step of the first series of tests, the tube motion was oriented in-line with the flow direction. For the fully flexible bundle, r.m.s vibration amplitudes in Figure 3.10 show that the critical pitch velocity increases to $U_p = 8.76 m/s$. At $U_p = 9.1 m/s$ the r.m.s vibration amplitude increases to 12% of the tube diameter.

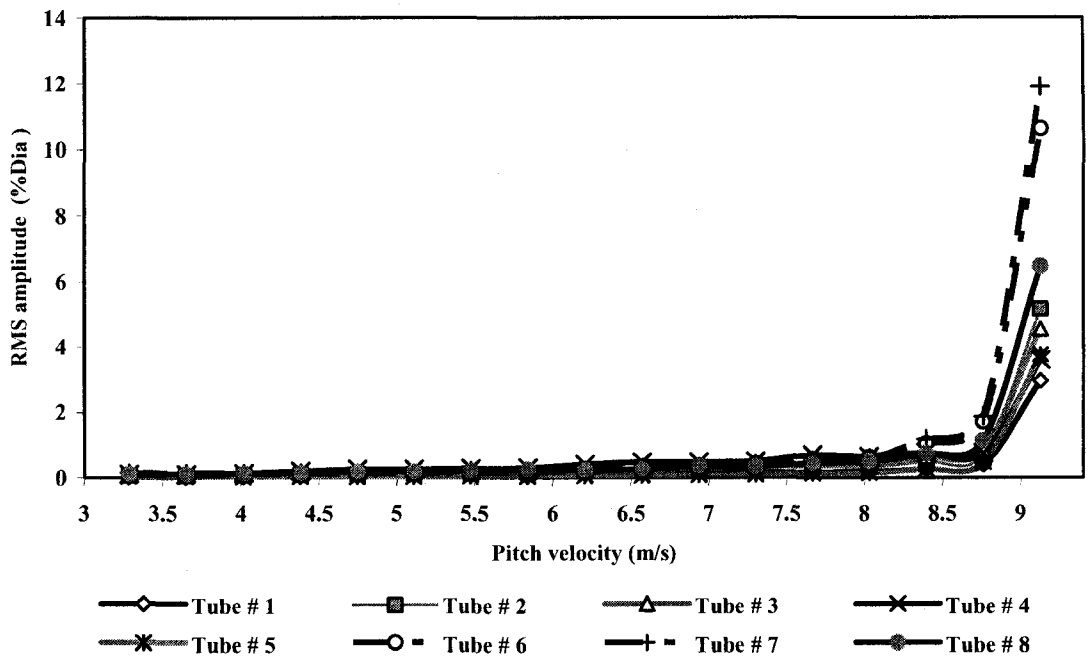

Figure 3.10 R.M.S vibration response for the fully flexible tube bundle, at a 0° angle of attack

The tube frequency information in Figure 3.11 shows that all the tubes vibrate at a single modal frequency at $U_p = 8.5 m/s$.

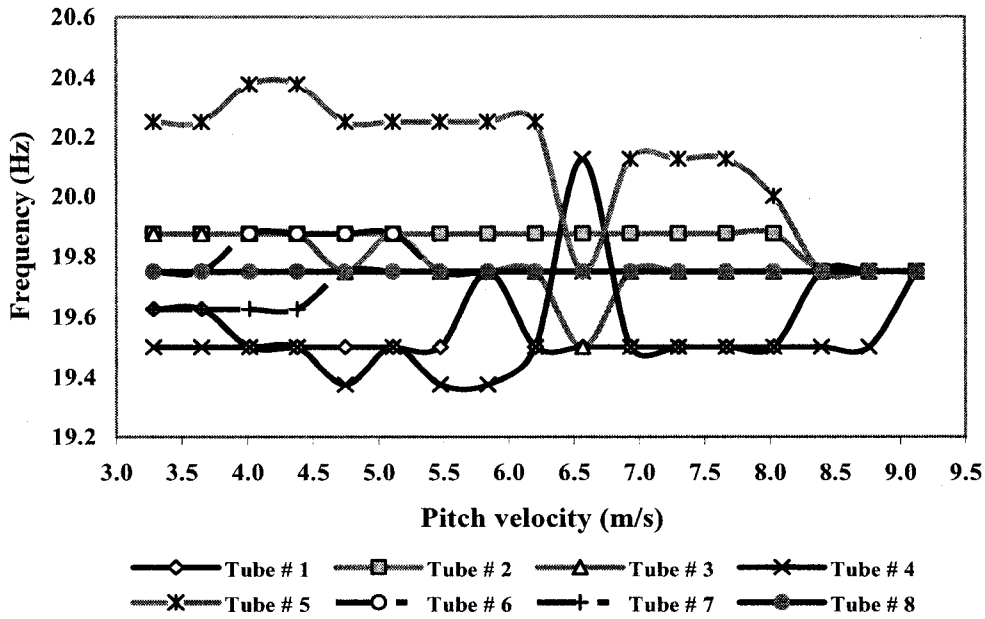

Figure 3.11 Response frequency versus flow pitch velocity for the flexible tube bundle, at a 0° angle of attack

3.2 Stability behavior of the three-column flexible tube bundle (two fixed adjacent columns)

In order to examine the effects of the number of flexible tubes in the bundle, a series of tests was conducted by fixing a number of flexible tubes within the tube array. As illustrated in figure 2.14(b) this configuration is called the "three-column" flexible tube bundle. As per section 3.1 the tests are carried out in four different steps by changing the tube flexibility direction.

In the second series of tests, the test section was modified by fixing two-side columns using an aluminum plug at the free end. Once again experimental tests were conducted within wind tunnel and for each test run, sufficient time was allowed for a steady state to be attained which would normally take several minutes. The flow velocity was recorded for post processing. The flow velocity was then incremented gradually and the process repeated until the bundle was well into the unstable regime.

3.2.1 Stability behavior of three-column flexible bundle with tube motion in cross flow direction (Angle of attack 90°)

As shown in Figure 3.12 for the flexibility orientation at 90° within the three-column flexible tube bundle, instability occurs at a velocity significantly higher than that for the fully flexible tube bundle.

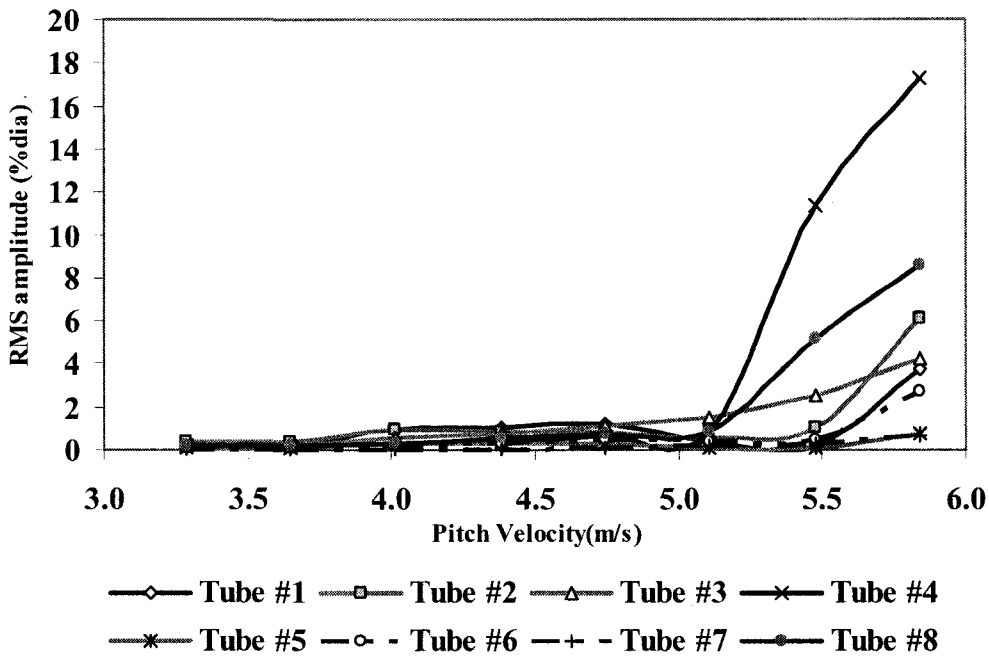

Figure 3.12 R.M.S vibration response for the three-column flexible tube bundle, at an angle of attack 90°

Tests were done for angles of attack ranging from 90° to 0°. The results are given in Table 3.1. The r.m.s response amplitude variation with flow velocity is shown in Figure 3.12. As depicted in this graph the fluidelastic instability critical flow velocity is $U_p = 5.3 m/s$ which is 11.5% higher than the value of $U_p = 4.75 m/s$ obtained for the fully flexible bundle. Also the frequency information given in Figure 3.13 shows that most of the tubes vibrate at a single modal frequency at $U_p = 5.8 m/s$.

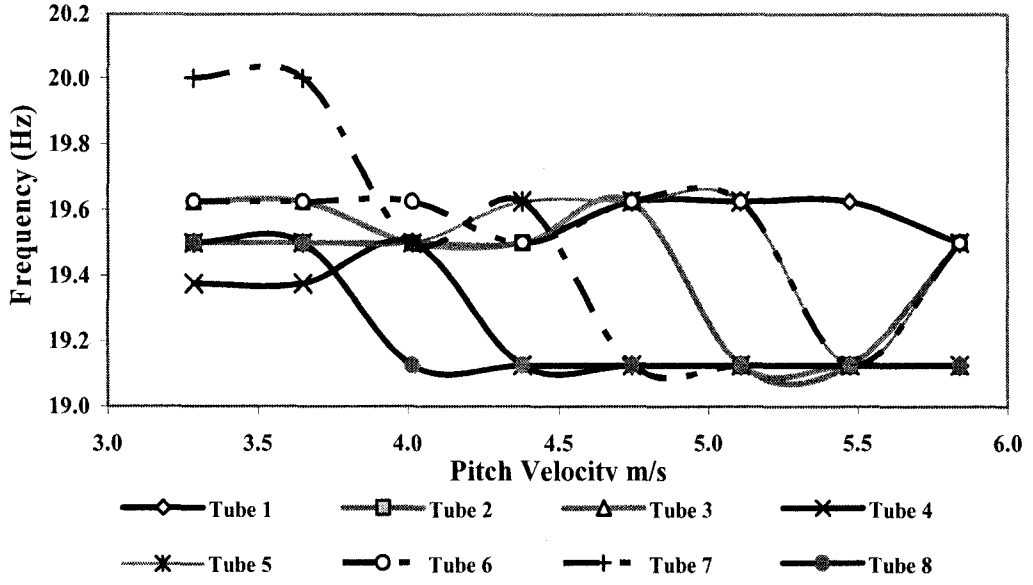

Figure 3.13 Response frequency versus flow pitch velocity for three-column flexible tube bundle, at a 90° angle of attack

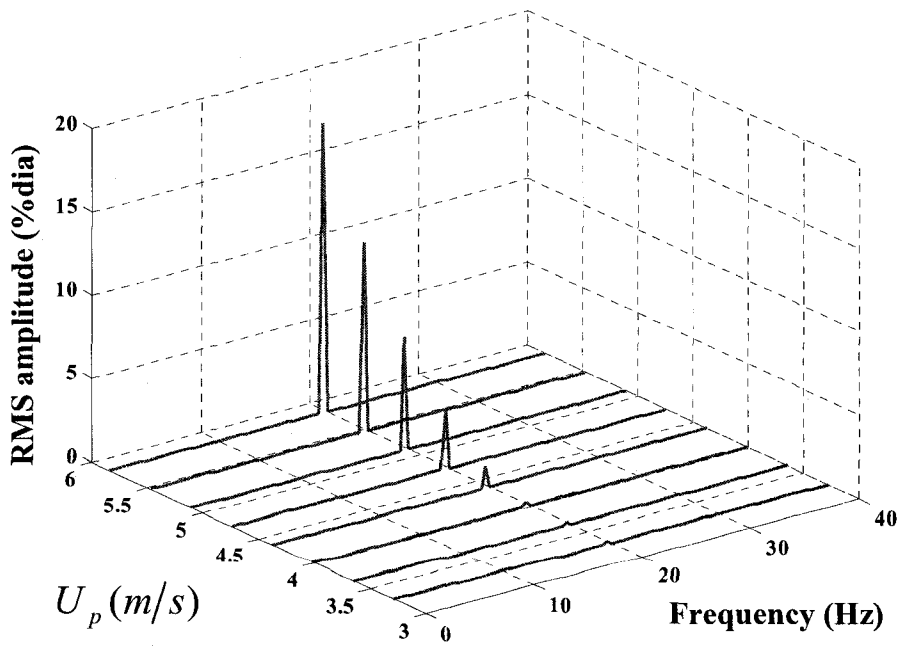

Figure 3.14 Response spectra variation with flow velocity for Tube No.4 in a three-column flexible bundle, at a 90° angle of attack

The increase in the fluidelastic instability critical velocity with a reduced number of flexible tubes is confirmed by the response spectra as illustrated in Figure 3.14.

3.2.2 Stability behavior of three-column flexible bundle with tube motion at 60° to the flow direction (Angle of attack 60°)

In the second step of the second series of tests, the flexible tubes were rotated by 60 degrees resulting in the angle of attack shown in Figure 2.15(d) considering two fixed side columns as illustrated in Figure 2.14(b). Of the eight instrumented tubes within the three-column flexible tube bundle, the vibration spectra for tube No.7 given in Figure 3.17, shows that, at low flow velocity, turbulence excitation is minimal effect the onset of fluidelastic instability occurs at a pitch velocity $U_p = 8.03 m/s$ as shown in Figure 3.15.

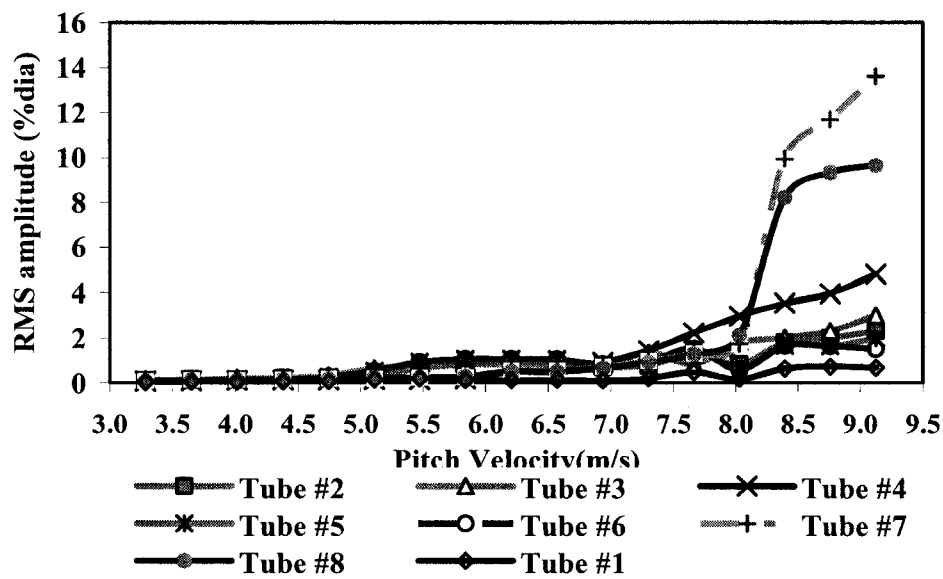

Figure 3.15 R.M.S vibration response for the three-column flexible tube bundle, at a 60° angle of attack

Coincidentally with the large increase in vibration amplitude, a coalescence of most of the individual tube frequencies to a single modal frequency was observed at the

same flow velocity, Figure 3.16. The increased critical flow velocity is also shown by the frequency response spectra given in Figure 3.17.

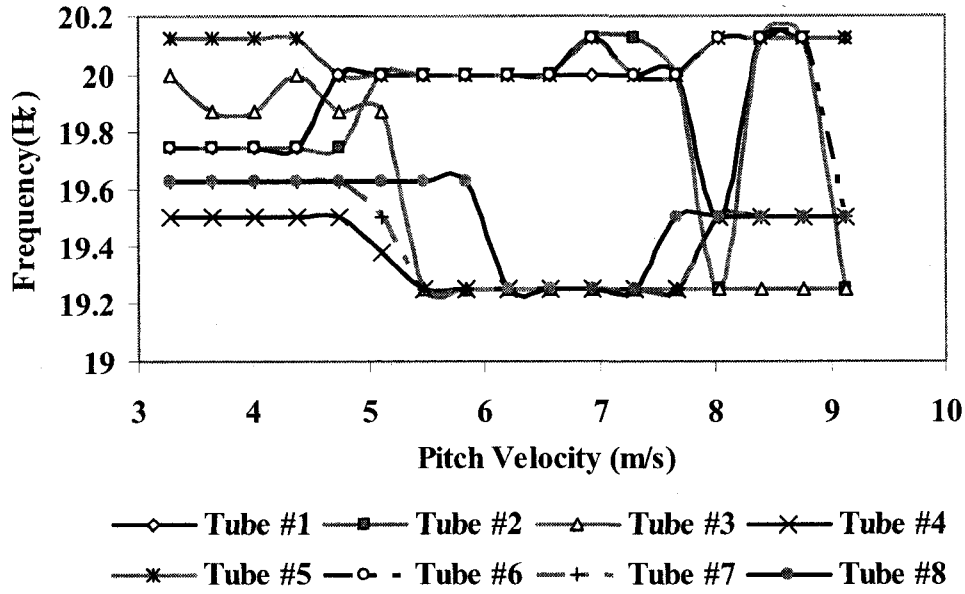

Figure 3.16 Response frequency versus flow pitch velocity for three-column flexible tube bundle, at a 60° angle of attack

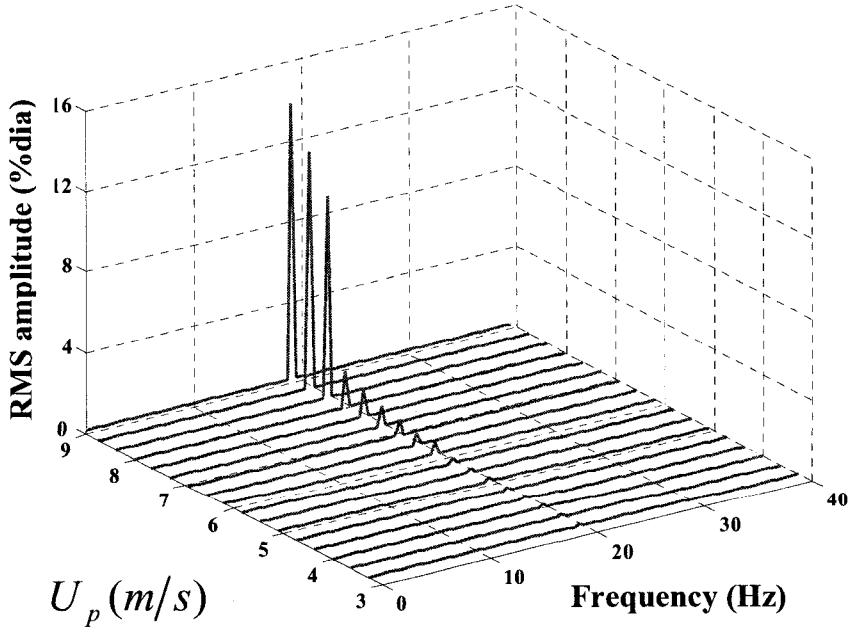

Figure 3.17 Response spectra variation with flow velocity for Tube No.4 in a three-column flexible bundle, at a 60° angle of attack

3.2.3 Stability behavior of three-column flexible bundle with tube motion at 30° to the flow direction (Angle of attack 30°)

The tubes were rotated to a 30 degree angle of attack within the three-column flexible tube bundle. The r.m.s vibration amplitude of the eight instrumented tubes is shown in Figure 3.18. The critical pitch velocity increased to $U_p = 8.4\,m/s$ and at $U_p = 8.75\,m/s$ the r.m.s vibration amplitude increased to 19% of the tube diameter.

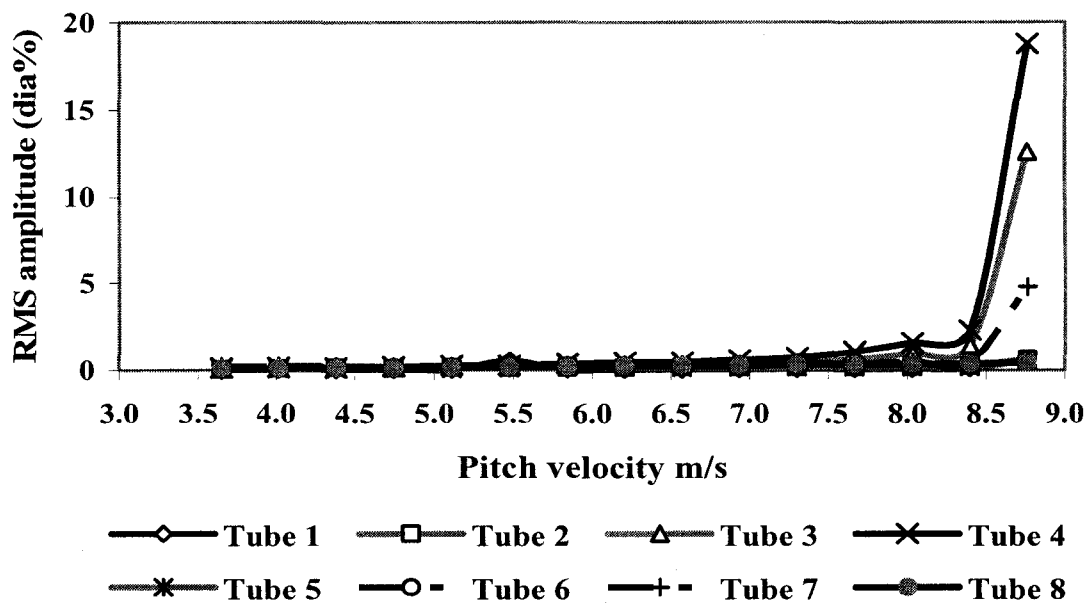

Figure 3.18 R.M.S vibration response for the three-column flexible tube bundle, at a 30° angle of attack

The higher critical pitch flow velocity for fluidelastic instability is also observed in Figure 3.19. The frequency information confirms that the critical velocity has increased by 4.5% in comparison to the 60 degree angle of attack configuration. This is also verified by the coalesce of tube vibration frequency to a single modal frequency. Increased critical flow velocity is also shown by the frequency response spectra illustrated in Figure 3.20.

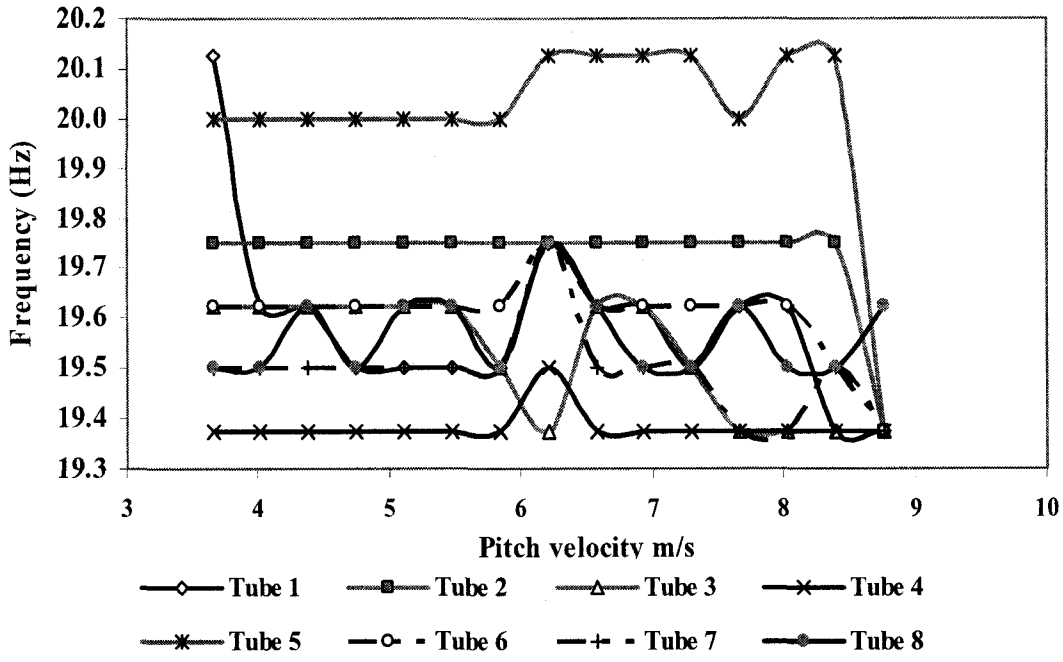

Figure 3.19 Response frequency versus flow pitch velocity for three-column flexible tube bundle, at a 30° angle of attack

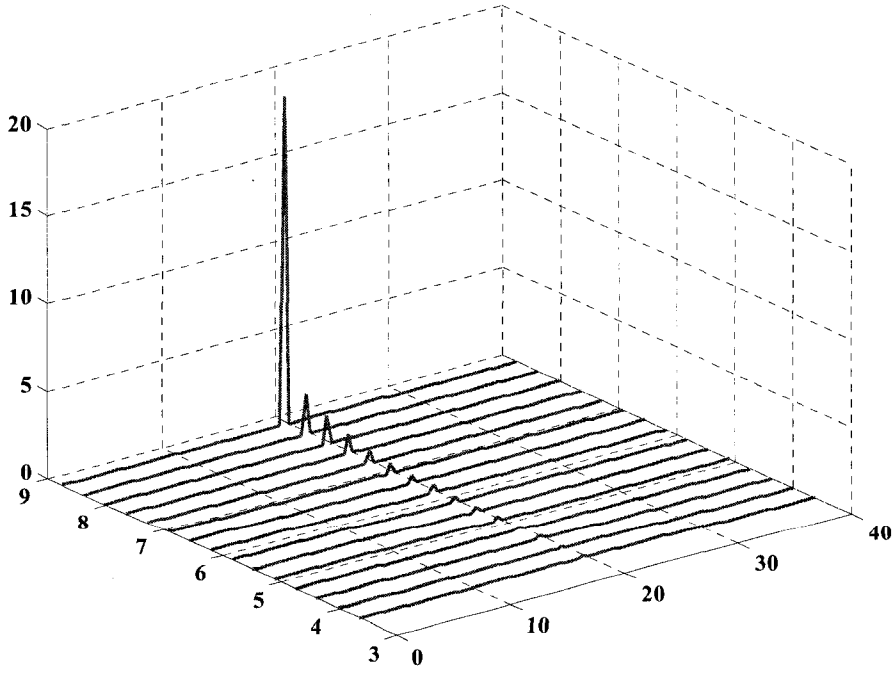

Figure 3.20 Response spectra variation with flow velocity for Tube No.4 in a three-column flexible bundle, at a 30° angle of attack

3.2.4 Stability behavior of the three-column flexible bundle with tube motion in-line with the flow direction (Angle of attack 0°)

As the last step of the second series of tests, the tube motion was oriented in-line with the flow direction. For the three-column flexible bundle, the r.m.s vibration amplitude in Figure 3.21 shows that the critical pitch velocity increases to $U_p = 9.12 m/s$. At $U_p = 9.85 m/s$ the maximum r.m.s vibration amplitude increases to 22% of the tube diameter.

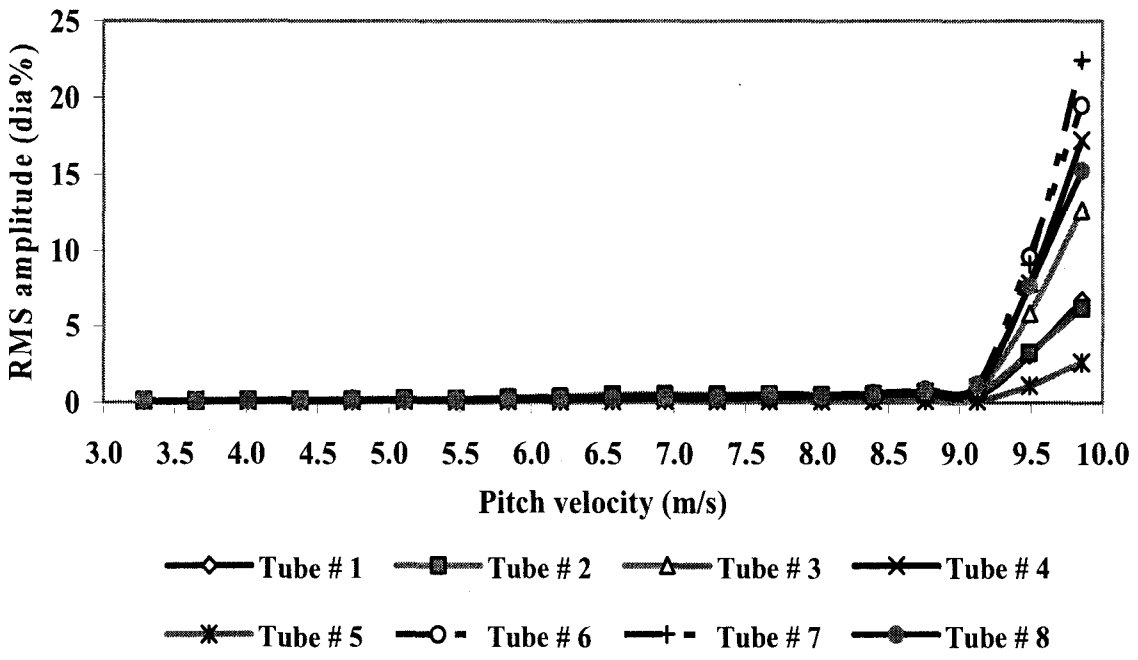

Figure 3.21 R.M.S vibration response for the three-column flexible tube bundle, at a 0° angle of attack

Once again monitoring the tube bundle response frequency versus flow pitch velocity for the three-column flexible tube bundle at 0° angle of attack (in line motion with flow direction) as shown in figure 3.22, proved that, the fluidelastic behavior is affected by changing in the angle of attack. This observable fact is also supported by the response spectra variation with flow velocity for tube No. 7 shown in Figure 3.23.

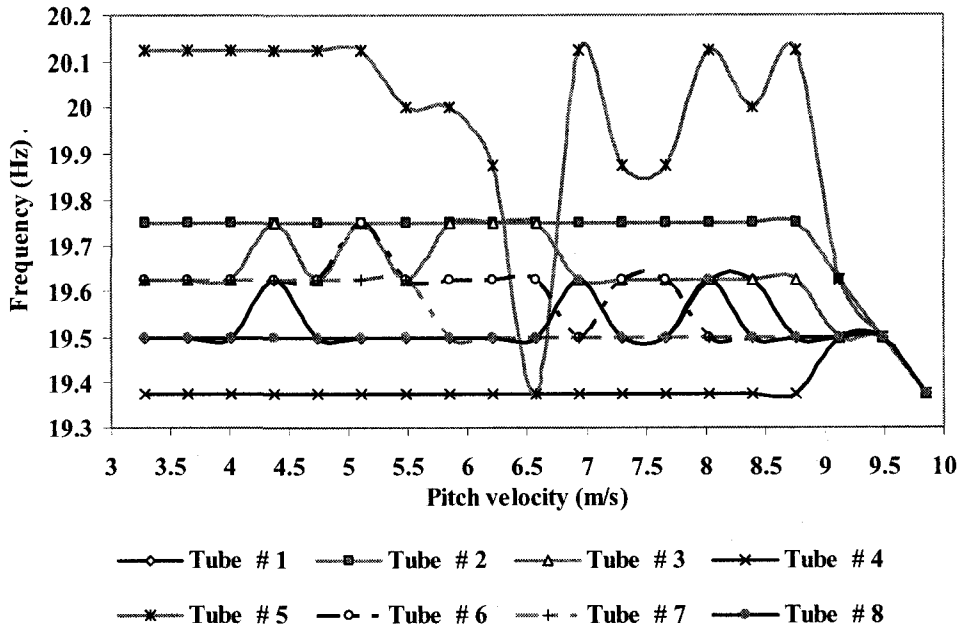

Figure 3.22 Response frequency versus flow pitch velocity for three-column flexible tube bundle, at a 0° angle of attack

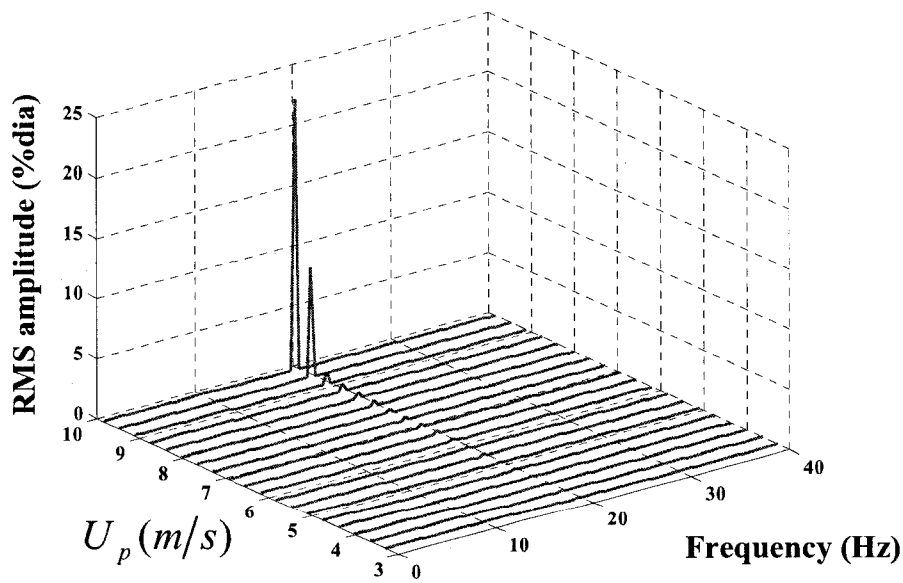

Figure 3.23 Response spectra variation with flow velocity for Tube No.7 in a three-column flexible bundle, at a 0° angle of attack

3.3 Stability behavior of the cluster tube bundle configuration

3.3.1 Stability behavior of cluster bundle configuration with tube motion in cross flow direction (Angle of attack 90°)

As shown in Figure 2.14(c), the seven tube cluster configuration is the classical unit that has been suggested as the minimal unit required for modeling a fully flexible tube bundle, Mureithi et al. (2005). In order to examine the fluidelastic instability behavior for the cluster configuration at different angles of attack a final series of tests was conducted in four steps. Figure 3.24 shows the vibration amplitude for the cluster configuration for a 90° angle of attack.

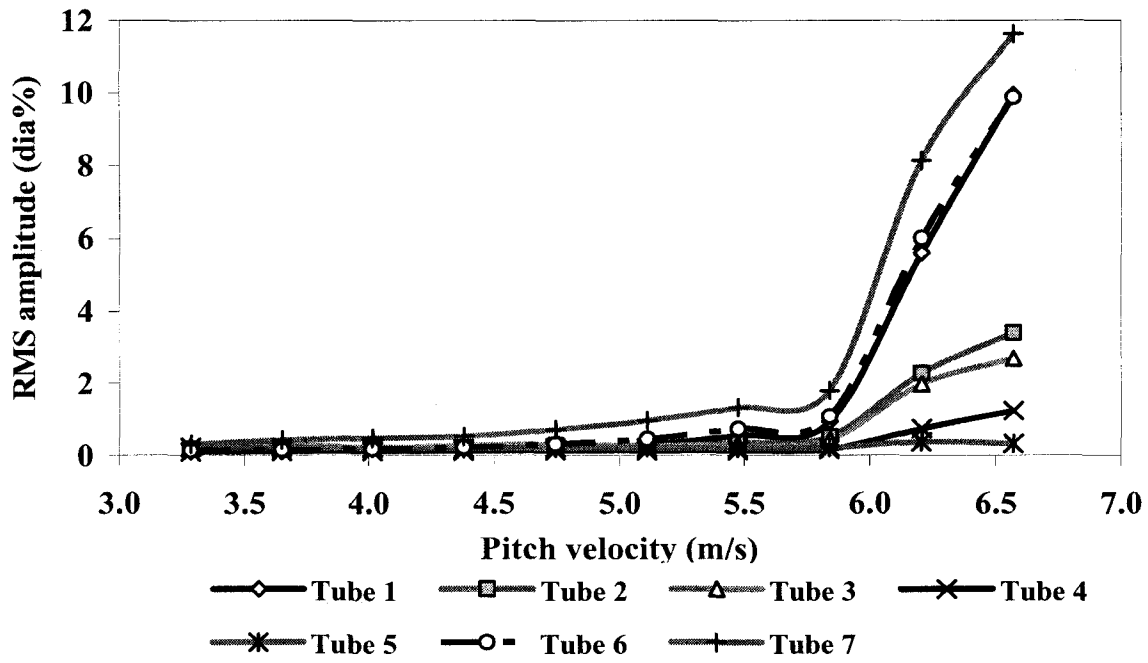

Figure 3.24 R.M.S vibration response for the cluster tube bundle configuration, at a 90° angle of attack

In this case the most remarkable result is the increased stability velocity to $U_p = 5.84\,m/s$ which is high relative to the three-column flexible and fully flexible tube bundle which have critical velocities of $U_p = 5.3\,m/s$ and $U_p = 4.75\,m/s$ respectively.

The latter result was confirmed by reviewing the frequency information curve and response spectra variation with flow velocity given in Figures 3.25 and 3.26.

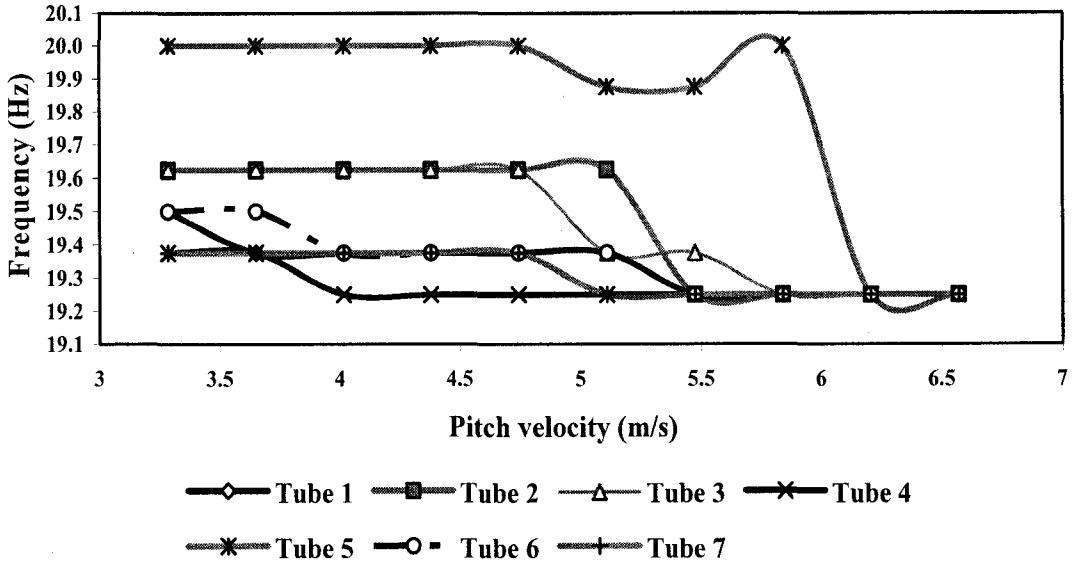

Figure 3.25 Response frequency versus flow pitch velocity for cluster tube bundle configuration, at a 90° angle of attack

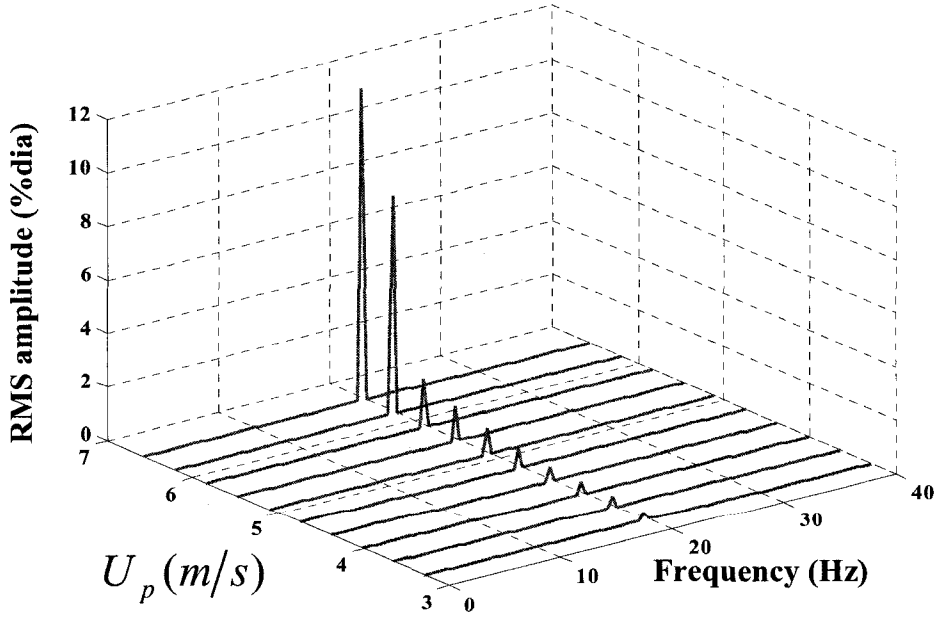

Figure 3.26 Response spectra variation with flow velocity for Tube No.7 in a cluster bundle configuration, at a 90° angle of attack

3.3.2 Stability behavior of cluster bundle configuration with tube motion at 60° to the flow direction (Angle of attack 60°)

Once more in this step seven flexible tubes were rotated to a 60 degree angle of attack in order to examine the effect of the flexibility orientation on fluidelastic instability in the cluster configuration. The r.m.s vibration amplitude for these seven instrumented tubes is shown in Figure 3.25. In comparison to the 90 degree angle of attack within the cluster tube bundle configuration the critical pitch velocity has increased to $U_p = 8.03 m/s$, and at $U_p = 8.4 m/s$ the r.m.s vibration amplitude increased to 7.8% of the tube diameter.

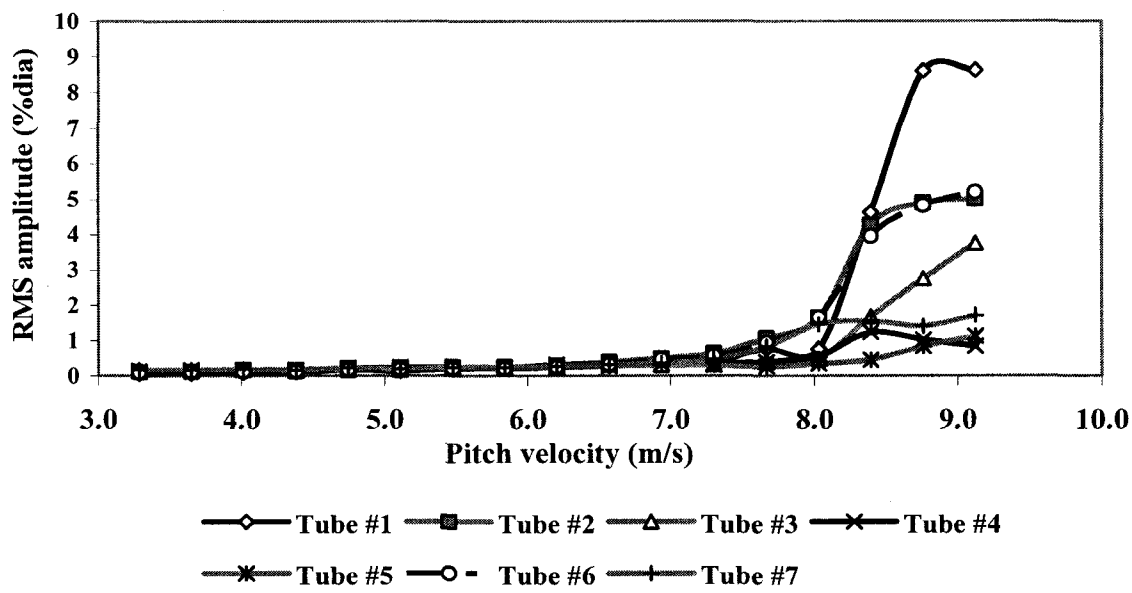

Figure 3.27 R.M.S vibration response for the cluster tube bundle configuration, at a 60° angle of attack

Similarly to the previous steps, increased critical flow velocity is confirmed from the response spectra and the frequency information diagrams. As previously showed at the fluidelastic instability threshold, most tubes vibrate at a single modal frequency. Using the response spectra diagram, it is easy to verify, by the sudden increase in

vibration amplitude at a certain flow velocity and frequency that the fluidelastic instability threshold is attained at a higher flow pitch velocity. Figures 3.28 and 3.29 show the frequency information and response spectra diagrams, respectively.

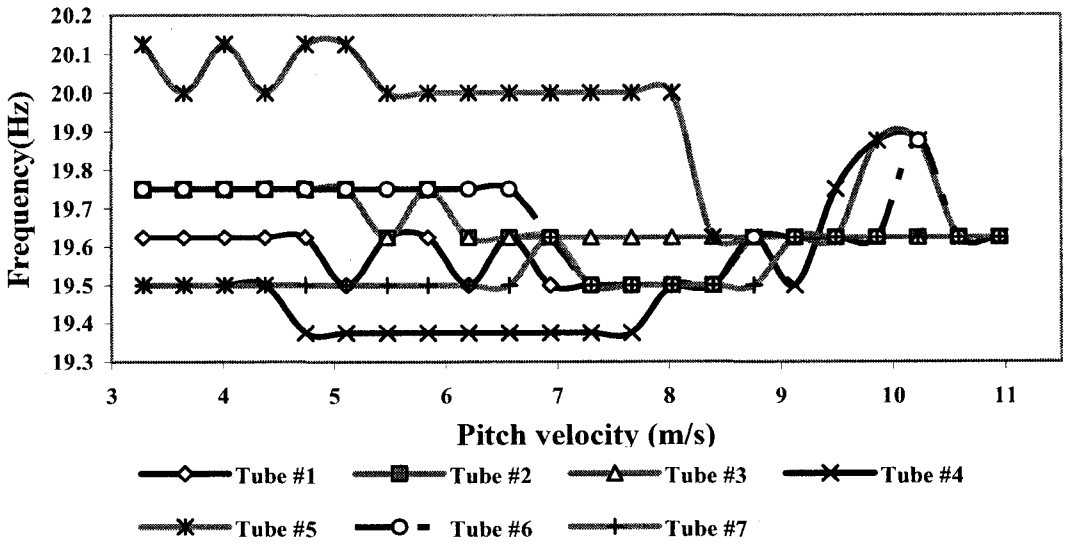

Figure 3.28 Response frequency versus flow pitch velocity for cluster tube bundle configuration, at a 60° angle of attack

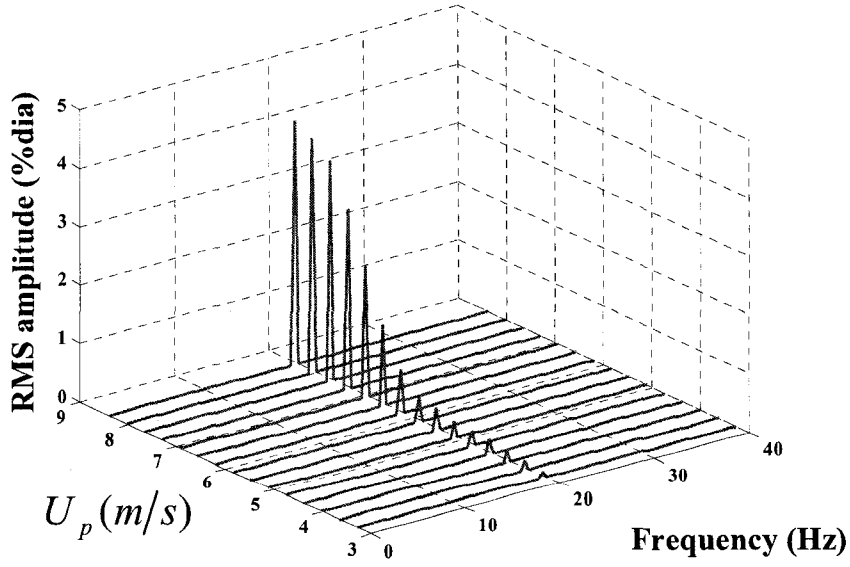

Figure 3.29 Response spectra variation with flow velocity for Tube No.2 in a cluster bundle configuration, at a 60° angle of attack

3.3.3 Stability behavior of cluster bundle configuration with tube motion at 30° to the flow direction (Angle of attack 30°)

The angle of attack was decreased further by a 30 degree rotation of the seven flexible tubes within the cluster tube bundle configuration. As shown in Figure 3.30 the instability occurs at a velocity significantly higher than that for 90° and 60° angles of attack. Also monitoring the tube bundle response amplitude with increasing flow velocity showed that the critical pitch flow velocity increased by 18% compared to the 60° angle of attack.

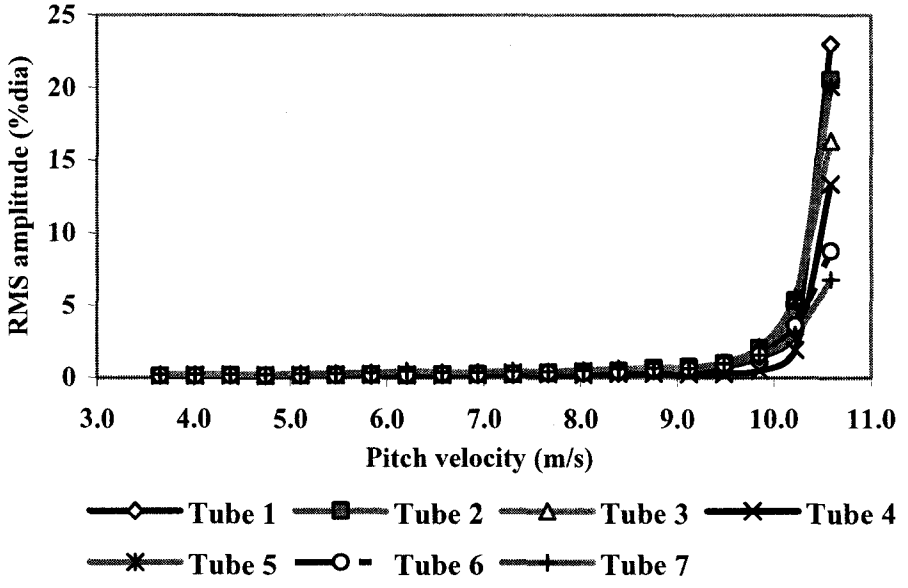

Figure 3.30 R.M.S vibration response for the cluster tube bundle configuration, at a 30° angle of attack

The increase in fluidelastic instability critical pitch velocity is also observed from frequency and the response spectra given in Figures 3.31 and 3.32 respectively.

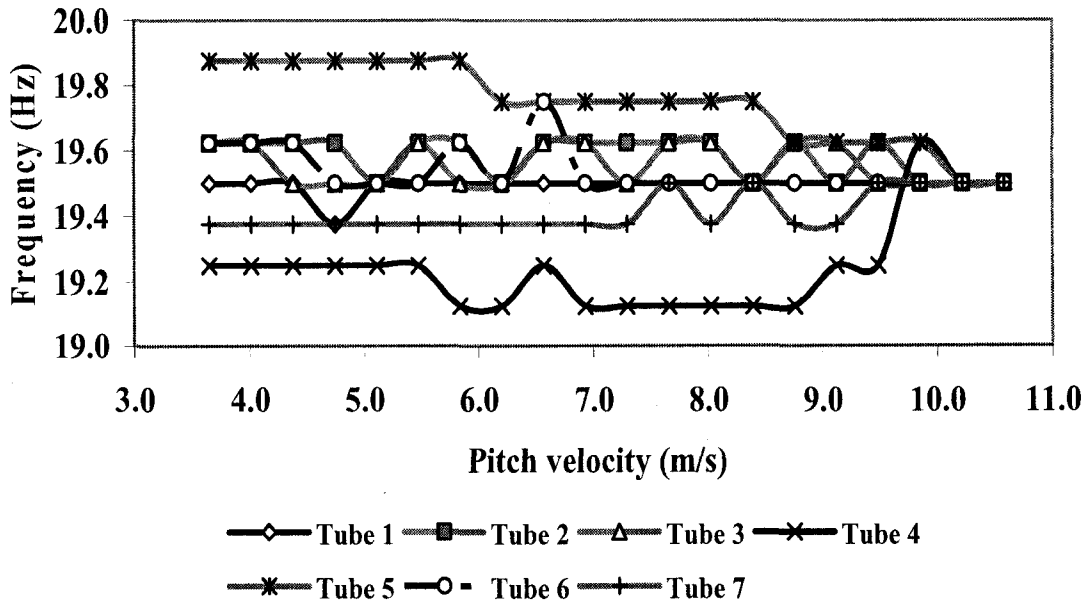

Figure 3.31 Response frequency versus flow pitch velocity for cluster tube bundle configuration, at a 30° angle of attack

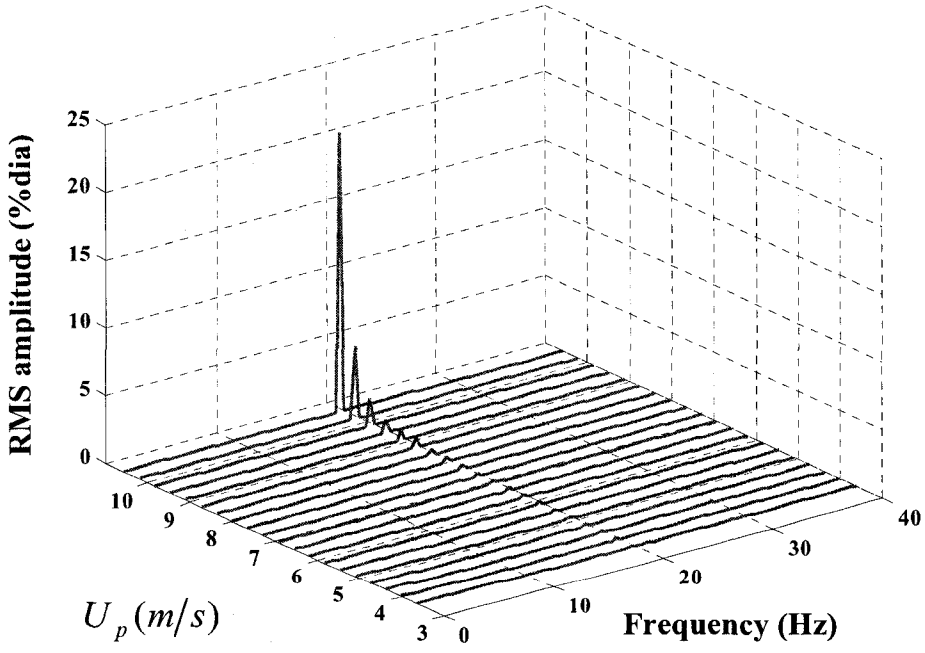

Figure 3.32 Response spectra variation with flow velocity for Tube No.2 in a cluster bundle configuration, at a 30° angle of attack

3.3.4 Stability behavior of cluster tube bundle configuration with tube motion in-line with the flow direction (Angle of attack 0°)

For the last series of tests, the tube motion was oriented in-line with the flow direction within the cluster tube bundle configuration, Figure 2.14(c) and 2.15(b).

For the cluster tube bundle configuration, the r.m.s vibration amplitude in Figure 3.33 shows that the critical pitch velocity increases to $U_p = 9.85 m/s$, and at $U_p = 10.5 m/s$ the r.m.s vibration amplitude increases to 10.7% of the tube diameter.

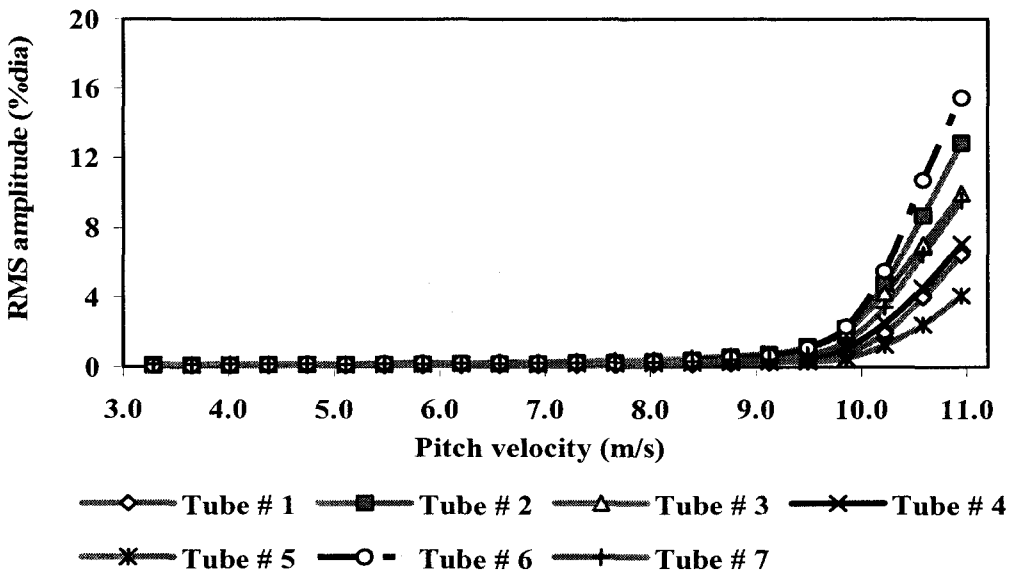

Figure 3.33 R.M.S vibration response for the cluster tube bundle configuration, at a 0° angle of attack

Once more to verify the increased critical pitch flow velocity for the reduced angle of attack within the cluster tube bundle configuration, frequency information and response spectra diagrams were examined. The frequency information and response spectra diagrams are given in Figures 3.34 and 3.35 respectively.

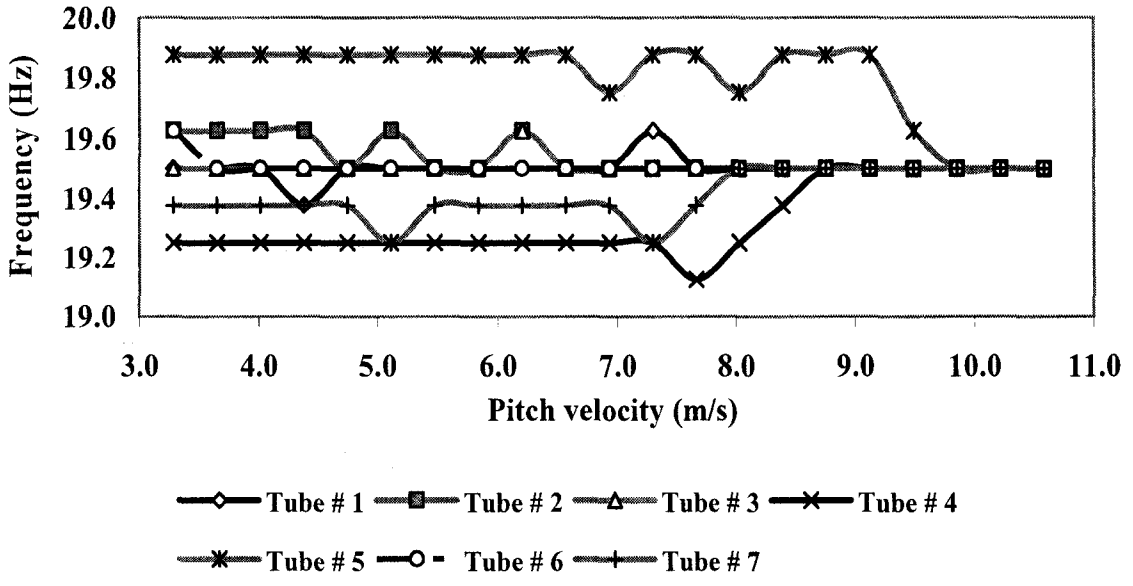

Figure 3.34 Response frequency versus flow pitch velocity for cluster tube bundle configuration, at a 0° angle of attack

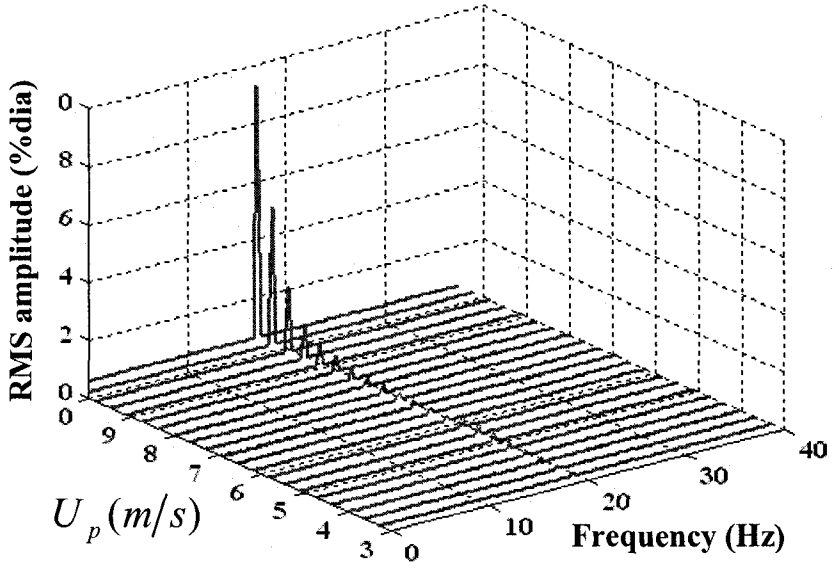

Figure 3.35 Response spectra variation with flow velocity for Tube No.2 in a cluster bundle configuration, at a 0° angle of attack

3.4 Stability behavior for two flexible cylinders

The case of drastically reduced number of flexible tubes is discussed next. Mureithi et al. (2005) demonstrated that the stability behavior changes significantly in the extreme case of two and then one cylinder flexible only in the flow direction. A series of tests was conducted to investigate these configurations for 90° and 60° angle of attack.

3.4.1 Stability behavior of two flexible cylinders at 90° angle of attack

Figure 3.36 shows response spectra for a test where Tubes No.2 and 3 in the middle column are flexible in cross flow.

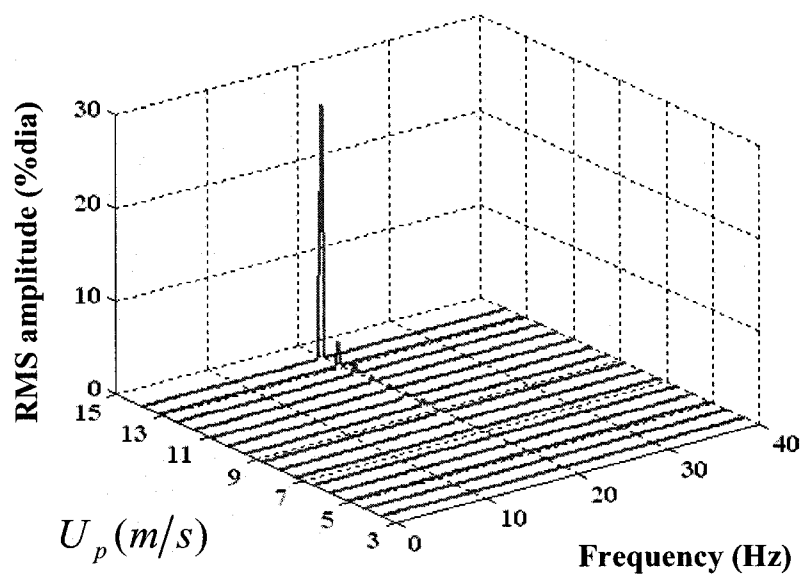

Figure 3.36 Response spectra variation with flow velocity for Tube No.2 in two flexible tube bundle configuration, at a 90° angle of attack

The spectra shown are those of tube No.2. The response amplitudes are slightly lower compared to the more flexible arrays, fluidelastic instability clearly occurs. This conclusion is supported by the amplitude and frequency trends in Figure 3.37 and 3.38, respectively.

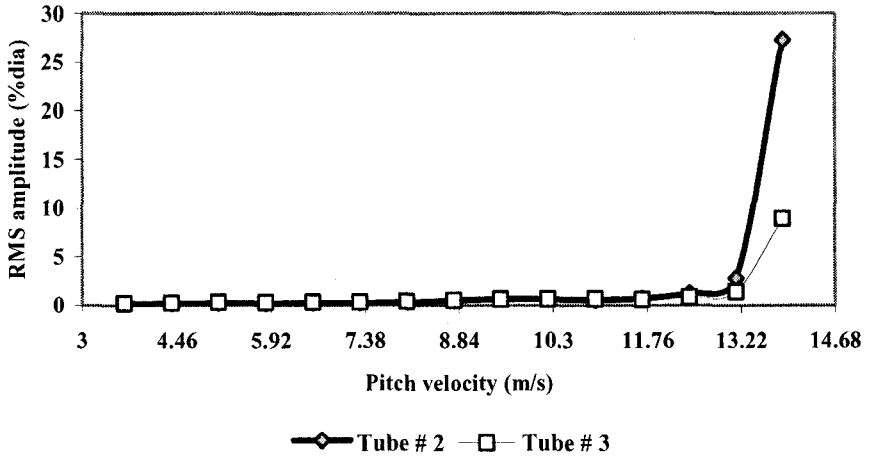

Figure 3.37 R.M.S vibration response for the two flexible tube bundle configuration, at a 90° angle of attack, Tube #2, 3(inline)

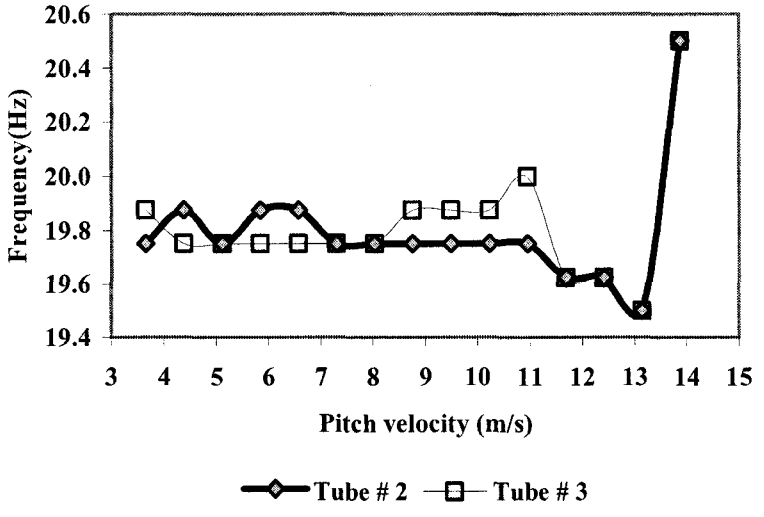

Figure 3.38 Response frequency versus flow pitch velocity for the two flexible tube bundle configuration, at a 90° angle of attack, tube #2,3(inline)

As shown in Figure 3.37, instability occurs at a velocity significantly higher than that for the more flexible configuration. The critical pitch velocity of 13.22 m/s is more than three times the critical velocity for the fully flexible array (i.e. 4.75 m/s).

Figure 3.39 shows the vibration response when the two flexible tubes are in neighboring columns, in this case Tubes No.3 and 7 were tested. The instability velocity of 16.4m/s is higher than that for the two flexible tubes in the same column Figure 3.37. The onset of fluidelastic instability is also less abrupt.

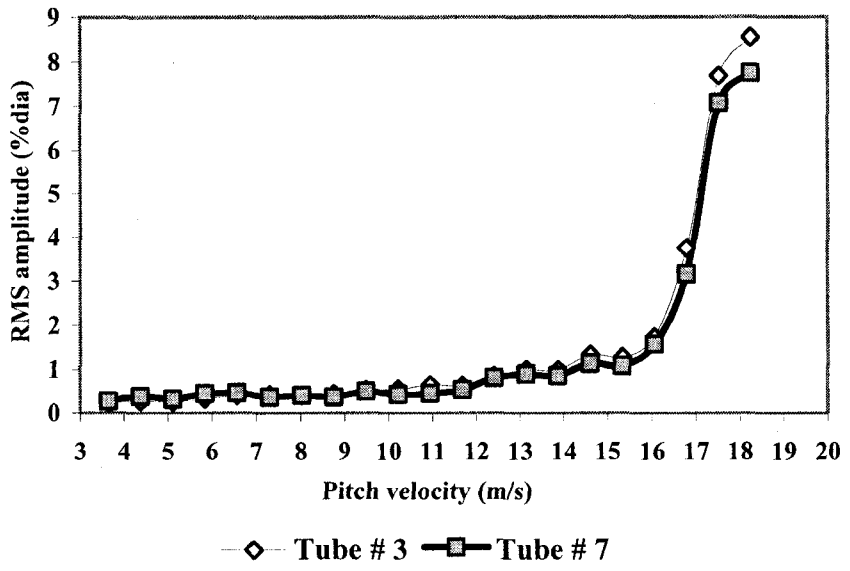

Figure 3.39 R.M.S vibration response for the two flexible tube bundle configuration, at a 90° angle of attack, Tube #3, 7 (neighboring columns)

3.4.2 Stability behavior of two flexible cylinders with tubes motion at 60° to the flow direction (Angle of attack 60°)

For the case of only two flexible tubes otherwise within a rigid tube array, the flexibility orientation was studied by changing the flexibility direction to 60° to provide a 60° angle of attack. Then the tests for the two flexible tubes configuration were repeated and the following results obtained.

Figure 3.40 shows the vibration response for two flexible tubes (#2&3) located in the same column with a flexibility angle of 60°.

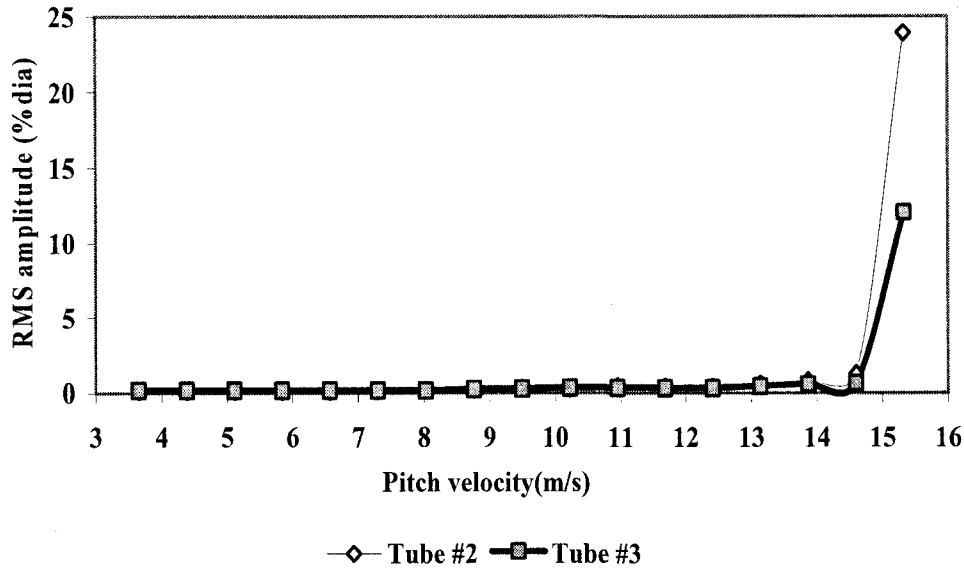

Figure 3.40 R.M.S vibration response for the two flexible tube bundle configuration, at a 60° angle of attack, Tube #2, 3 (inline)

The critical pitch velocity measured is 14.5 m/s, which is almost two times more than of the critical velocity for the fully flexible array (i.e. 7.75 m/s). The instability behavior is also apparent in the tubes frequency information given in Figure 3.41.

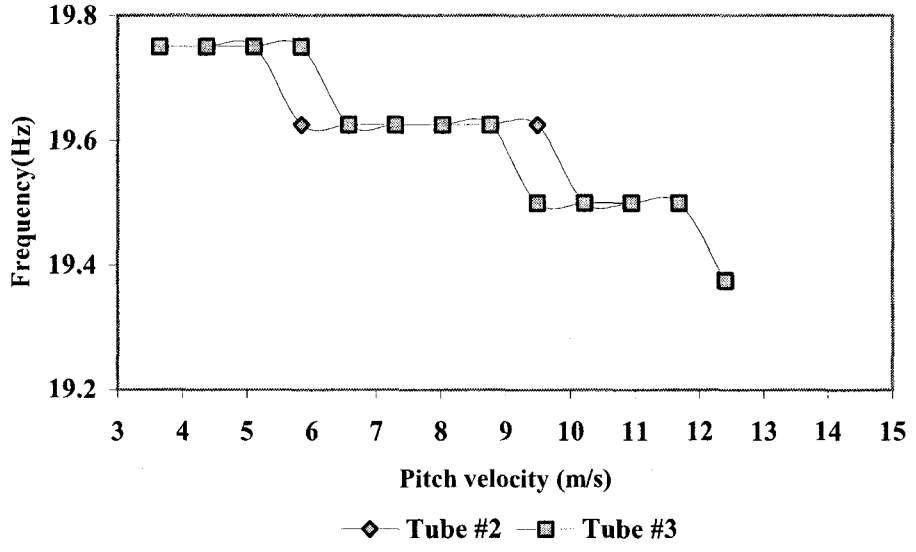

Figure 3.41 Response frequency versus flow pitch velocity for the two flexible tube bundle configuration, at a 60° angle of attack, Tubes #2, 3(inline)

Figure 3.42 shows the vibration response when the two flexible tubes are in neighboring columns. In this case Tube No.3 and 7 were tested. The instability velocity measured as 18.4m/s is higher than that for the two flexible tubes in the same column configuration.

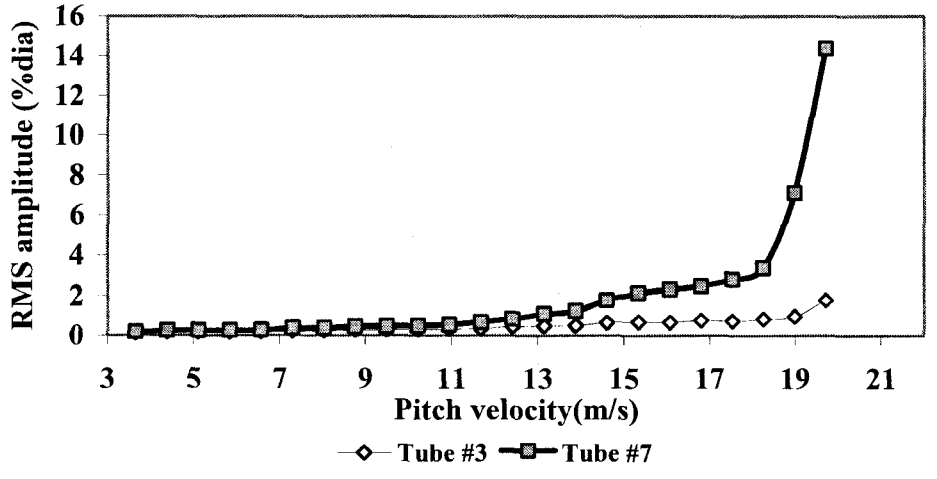

Figure 3.42 R.M.S vibration response for the two flexible tube bundle configuration, at a 60° angle of attack, Tubes #3, 7 (neighboring columns)

The increased fluidelastic instability pitch velocity is also observed in the frequency information given in Figure 3.43.

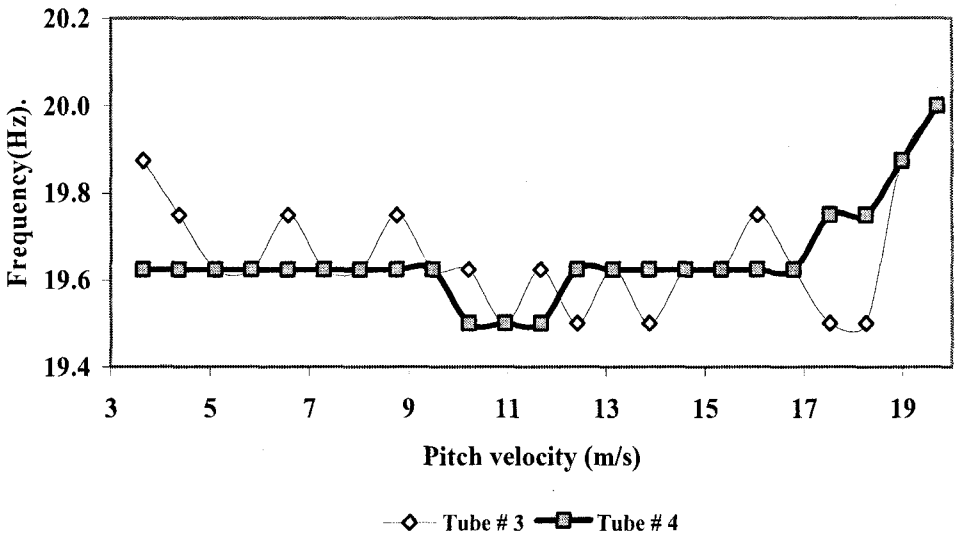

Figure 3.43 Response frequency versus flow pitch velocity for the two flexible tube bundle configuration, at a 60° angle of attack, Tubes #3, 7(neighboring columns)

CHAPTER 4

STABILITY ANALYSIS AND DISCUSSION

The series of tests presented in the forgoing chapters is rather classical and in some sense, the results are not surprising. Fluidelastic instability is now known to be strongly dependent on the angle between the flow direction and the tube bundle flexibility direction which we call the "*angle of attack*". The results obtained in the experimental tests, which are presented in the previous chapter, will be discussed in the individual sub-sections in the first section of this fourth chapter while a theory overview for fluidelastic instability mechanisms will be discussed in the second section.

4.1 Experimental data

4.1.1 Fully flexible tube bundle

The tests in the first series, tests are conducted within a fully flexible tube bundle. The tube flexibility direction was changed in four steps. The tests started with a 90° angle of attack which allowed for tube motion in the direction normal to the flow. Then in each next step the tubes were rotated by 30 degree to give a different angle of attack ending up with 0° (flexibility in the flow direction).

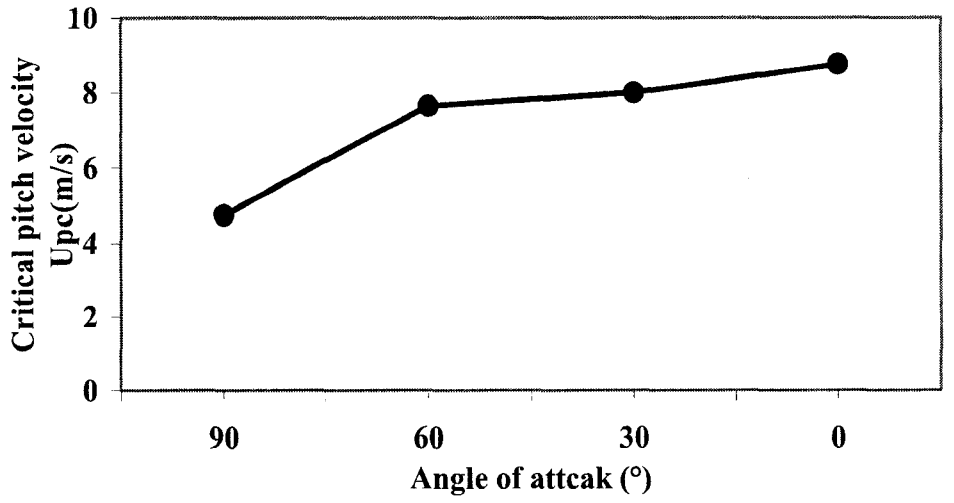

Figure 4.1 Critical pitch velocity versus flexibility orientation (angle of attack) for fully flexible tube bundle

The collected data shows how the fluidelastic instability critical velocity increases with decreasing angle of attack from 90 to 0°. The critical flow velocity for a 90° angle of attack is $U_{pc} = 4.75 m/s$ a 60° angle of attack increased by 61% to $U_{pc} = 7.65 m/s$. Reducing the angle of attack to 30° and finally to 0° increased critical flow velocity to $U_{pc} = 8.0 m/s$ and $U_{pc} = 8.75 m/s$ respectively. Figure 4.1 shows how the critical pitch flow velocity for the fluidelastic instability changes with decreasing in angle of attack.

4.1.2 Three-columns flexible tube bundle

In the second series of tests, which were performed with the three-column flexible tube bundle, the foregoing procedure was repeated and the critical pitch flow velocity for fluidelastic instability measured. The results presented in Chapter 3 shows that for a 90° angle of attack the critical pitch velocity was found to be $U_{pc} = 5.3 m/s$. It increased to $U_{pc} = 8.0 m/s$ for 60°.

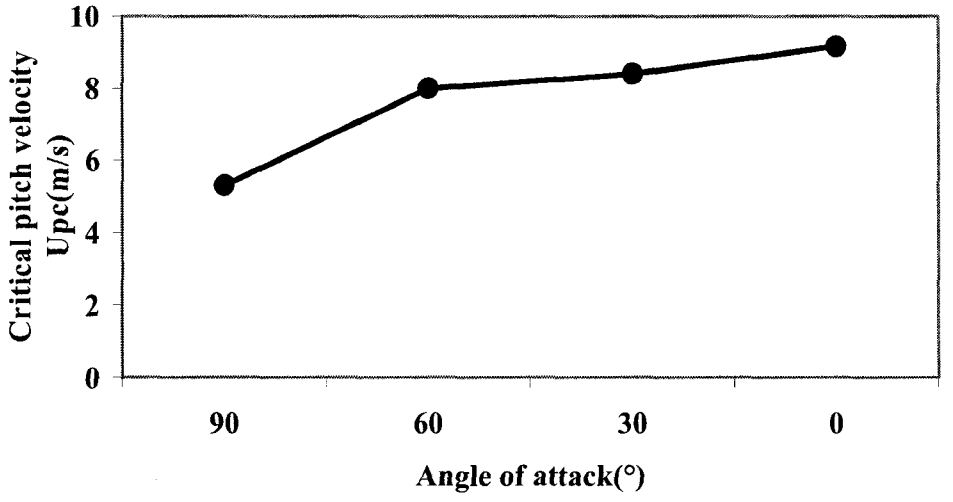

Figure 4.2 Critical pitch velocity versus flexibility orientation (angle of attack) for three-column flexible tube bundle

Reducing the angle of attack to 30° results in increased pitch flow velocity to $U_{pc} = 8.4\,m/s$. For a 0° angle of attack (inflow direction) the critical pitch velocity for fluidelastic instability obtained was $U_{pc} = 9.15\,m/s$. The critical velocity variation with angle of attack is illustrated in Figure 4.2.

4.1.3 Cluster tube bundle configuration

The critical pitch velocity variation with angle of attack for this configuration is given in Figure 4.3. The last series of tests were conducted with a cluster of seven flexible tubes. The collected data given in the third chapter shows how the critical flow pitch velocity changes with angle of attack. For a 90° angle of attack (motion normal to the flow), the critical flow pitch velocity is $U_{pc} = 5.85\,m/s$. It increases by 36% to $U_{pc} = 8.0\,m/s$ for a 60° angle of attack. For a 30° angle of attack the critical velocity is $U_{pc} = 9.5\,m/s$. Finally for the inflow direction (0° angle of attack) it is $U_{pc} = 9.85\,m/s$.

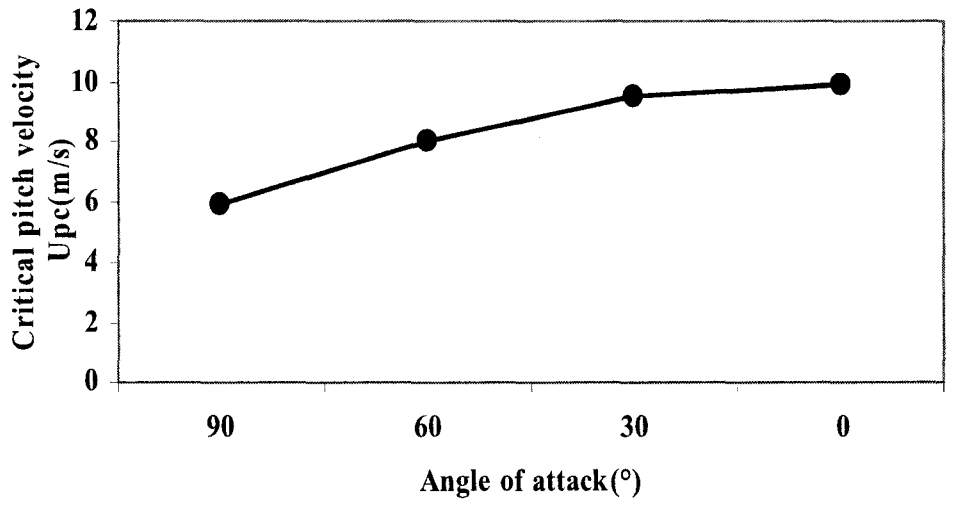

Figure 4.3 Critical pitch velocity versus flexibility orientation (angle of attack) for cluster tube bundle configuration

4.1.4 Stability behavior for two flexible cylinders

The case of a drastically reduced number of flexible tubes is discussed next. The Results given in the Section 3.4, show that the stability behavior changes significantly in the extreme case of only two flexible cylinders. Fluidelastic instability still occurs for two flexible cylinders. Two different configurations with tubes flexible only in the cross flow direction were tested. First the two flexible tubes were positioned in the same column (tube # 2,3 Figure 2.14a). Second, the two flexible tubes were located in the neighboring columns (tube #3, 7 Figure 2.14a).

The critical velocity at $U_{pc} = 13.2 m/s$ is more than double the critical velocity for the fully flexible array ($U_{pc} = 5.3 m/s$). The results show that in the case of two flexible cylinders, the relative position of the tubes is crucially important. Figure 3.37 shows the vibration response when the two flexible are in neighboring columns; in this case, Tubes No.3 and 7 were tested. The instability velocity of $U_{pc} = 16 m/s$ is higher than that for two tubes in the same column. For the case of flexibility in the flow direction, Mureithi et al. (2005), have experimentally shown that for two flexible

cylinders, the relative positions of the tubes is significantly important. They reported that the instability velocity for two tubes in neighboring columns is higher than for the case of two flexible tubes in the same column. This is in good agreement with what we have found in the present work.

This is not the case for two-phase flow. Violette et al. (2006), have experimentally shown that for fluidelastic instability to occur in a bundle of tubes flexible only in the drag direction, the flexible tubes must be located in two adjacent columns.

4.2 On instability mechanisms

In the previous chapter results from different tests were presented in detail. Here, in the second section of the fourth chapter a specific review of fluidelastic instability mechanisms is made. Fluidelastic instability is possible when the fluid dynamic forces on the tubes are proportional to tube motion. As mentioned in Chapter 1, it is well accepted that there are two mechanisms that can cause instability (Chen, 1987, Païdoussis and Price, 1988, Yetisir and Weaver, 1993). The first, the damping controlled mechanism, manifests itself when the energy absorbed from the fluid by the tubes exceeds the energy dissipated by damping. This mechanism needs only one degree of freedom to occur. The second, the stiffness controlled mechanism; is controlled by non-symmetric fluid dynamic stiffness effects and generally required relative motion between adjacent cylinders in the array, therefore it needs at least two degrees of freedom to materialize.

From the results obtained for the tubes flexible only in the flow direction, it can be concluded that there needs to be at least two flexible tubes for fluidelastic instability to occur. Since the damping controlled mechanism needs only one degree of freedom to cause instability, it can be deduced that it is only the stiffness controlled mechanism that

produced the instability for the tubes flexible only in the flow direction. This is in agreement with the finding of Mureithi et al in 2005.

Païdoussis and Price (1988) demonstrated with their theoretical model that the derivative of the lift coefficient (C_L) to displacement in the lift direction (y) must be negative and large ($\partial C_L/\partial y < 0$) for an instability by the damping controlled mechanism to occur for a tube that is free to vibrate only in the lift direction. By the same reasoning, the derivative of the drag coefficient (C_D) versus displacement in the drag direction (x) must be negative and large ($\partial C_D/\partial x < 0$) for an instability by the damping controlled mechanism to occur for a tube that is free to vibrate in the drag direction. Païdoussis et al. (1996) demonstrated experimentally in a wind tunnel within a rotated triangular tube bundle, that the derivative of the drag coefficient to the displacement in the drag direction is close to zero ($\partial C_D/\partial x \approx 0$). Therefore, no instability is possible for a single tube flexible only in flow direction inside a rigid array. The instabilities observed with tubes that are flexible only inflow direction is then caused only by the stiffness controlled mechanism. Violette et al. (2006) demonstrated experimentally in a set of two-phase flow tests that in order for the fluidelastic instability to occur in a bundle of tubes flexible only in the drag direction, the flexible tube must be located in two adjacent columns. But as Mureithi et al. (2005) experimentally showed and repeated in the present study, this is not the case for single phase flow, in which, instability can occur for a single column of tubes flexible only in the flow direction in a rotated triangular rigid array. This result is discussed in Section 4.1.4, by using collected data from the last series of tests presented in Chapter 3 Section 3.4. In the next section the fluid-dynamic theory presented by Païdoussis and Price (1987) will be used to understand the experimental results given in Chapter 3.

4.3 Fluidelastic instability result comparison

It is now confirmed that fluidelastic instability can occur in a rotated triangular tube bundle subjected to air cross flow with tube flexibility orientation in the flow direction (0°), at a 30 degree, 60 degree and 90° of angle of attack. The fluidelastic tests results in the previous chapter are now compared to existing data for the rotated triangle configuration on the instability map given in Figure 4.4, presented by Pettigrew et al. (1989). On this map, the horizontal axis is the mass-damping parameter and the vertical axis is the reduced velocity. The factor of K is the proportionality constant defined in the relation:

$$\frac{U_p}{fD} = K\left(\frac{2\pi m\zeta}{\rho D^2}\right)^{0.5} \tag{4.1}$$

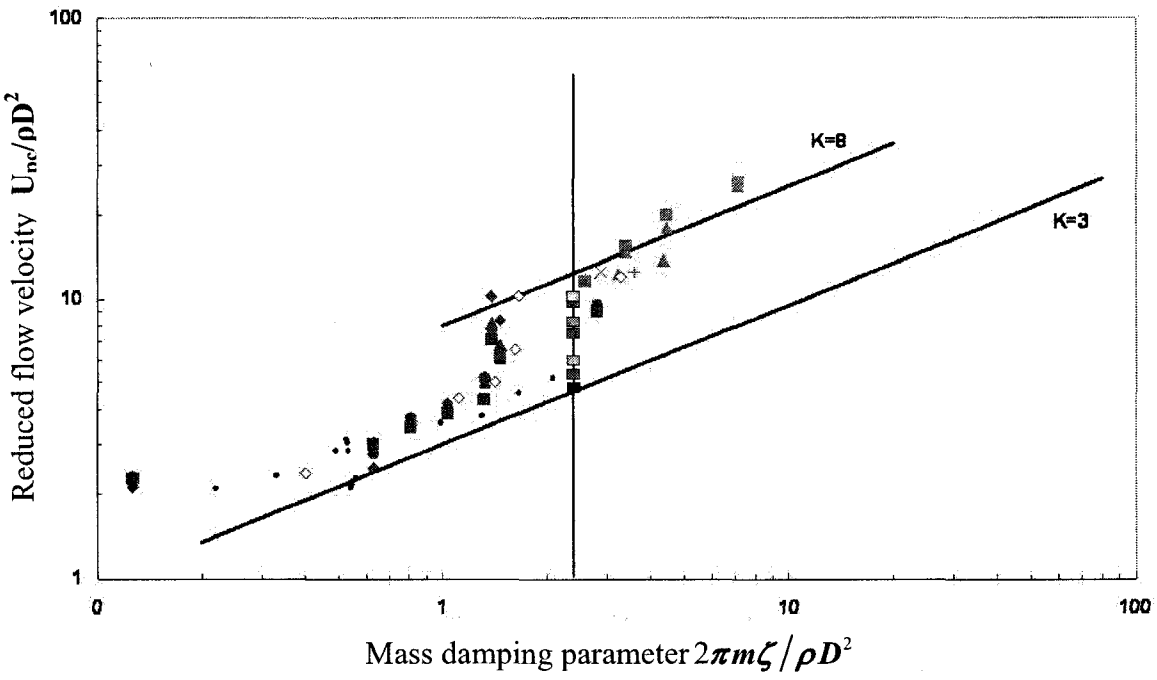

Figure 4.4 Stability map: full flexible tube bundle at a 90° angle of attack, three columns configuration at a 90° angle of attack, cluster configuration at a 90° angle of attack, full flexible tube bundle at a 60° angle of attack, three columns configuration at a 60° angle of attack, cluster configuration at a 30° angle of attack, cluster configuration at a 0° angle of attack seven tubes flexible only inflow direction in one column collated in the center of the test section(Violette et al. 2006), two flexible column only inflow direction(Violette et

al. 2006), + results for seven tubes flexible only in flow direction subjected to single phase flow (in a wind tunnel) (Mureithi et al. 2005), × wind tunnel results for one column tubes flexible only inflow direction, ▲ seven full-flexible tubes (axisymentical beam) subjected to two-phase flow (Violette et al. 2006), ■ two column full-flexible tubes (Violette et al. 2006), ● one full-flexible column (Violette et al. 2006), ◆ one single full flexible tube (Violette et al. 2006), ◇ one single flexible tube in lift direction (Violette et al. 2006), • full flexible tube array (Pettigrew et al.1989)

The experimental data for tubes that are flexible inflow direction and subjected to single-phase cross flow in a wind tunnel are found to be in good agreement with what Violette et al. reported in 2006 for the same tube bundle subjected to two-phase cross flow, $K \cong 8$. Also appearing in this figure is the results obtained by Mureithi et al. 2005, in a wind tunnel for a tube bundle similar to the one used in this study for two flexible bundle configurations: the central cluster and the single flexible column. Both configurations use tubes that are flexible in the flow direction. As is shown in Figure 4.4, the results are in good agreement with those obtained in the present study for the tubes flexible in the flow direction. On the other hand, Mureithi et al. (2005) reported an instability constant, $K = 5$ for a fully flexible tube bundle.

4.4 Modified quasi-steady theory

Consider an array of cylinders subjected to cross-flow as is partially shown in Figure 4.5.

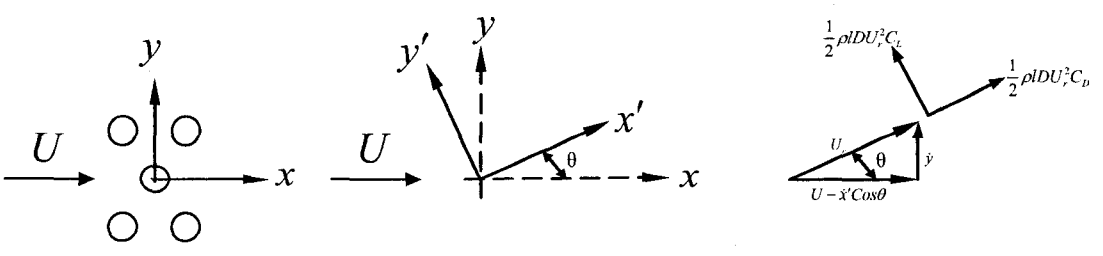

Figure 4.5a Cross-section of a small part of an array of cylinders in cross flow and velocity vector diagram

For simplicity, consider for the moment that all the cylinders are rigid, except one, which is flexibly mounted and motions of which are characterized by displacement only in the x' direction.

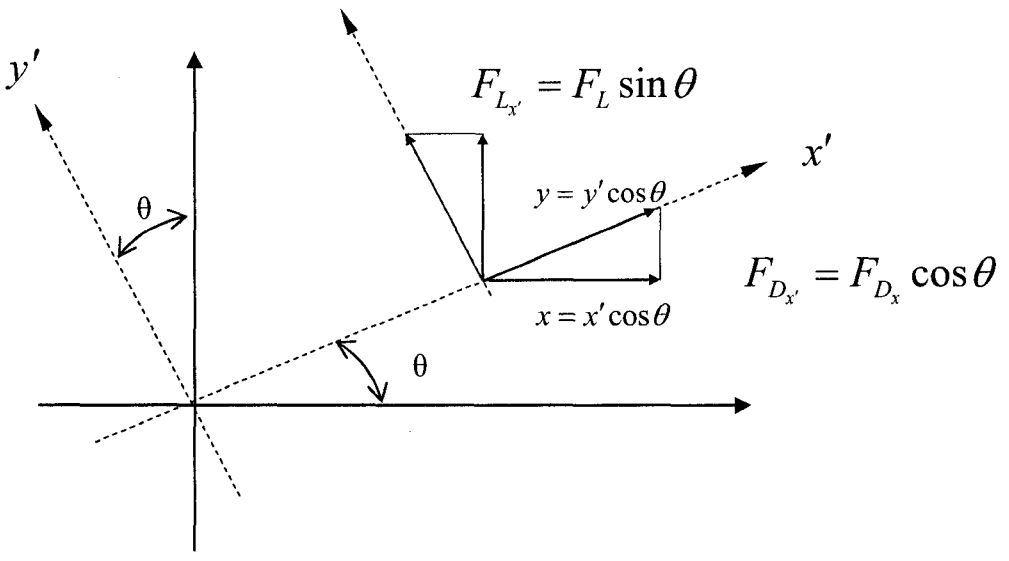

Figure 4.5b Displacement vectors for rotated flexibility angle by θ°

Then, assuming no mechanical coupling between motion in the x' and y' direction, the equation of motion of the cylinder in the x' direction may be written as:

$$ml\ddot{x}' + c\dot{x}' + kx' = F_{x'} \tag{4.2}$$

Where $F_{x'}$ is the fluid-dynamic force, m the mass per unit length of the tube, l the length of the cylinder, and c and k are the effective mechanical damping and stiffness of the cylinder, respectively.

According to the quasi-steady (or quasi static) theory, the forces acting on the oscillating cylinder are approximately the same as the static forces at each point of the

cycle of oscillation, provided that the approach velocity is properly adjusted to take into account the velocity of the cylinder, in the manner shown in the velocity vector in Figure 4.5 a and b.

Thus, $F_{x'}$ may be written as

$$F_{x'} = \frac{1}{2}\rho U_r^{\,2} lD\left(C_{L(x',y')} + C_{D(x',y')}\right), \tag{4.3}$$

where U_r, as shown in Figure 4.5 is the displacement velocity in the x' direction and defined as:

$$U_r^2 = \left(U - \dot{x}'\cos\theta\right)^2 + \left(\dot{x}'\sin\theta\right)^2 \tag{4.4}$$

$$U_r^2 = U^2 - 2U\dot{x}'\cos\theta + \dot{x}'^2 \tag{4.5}$$

In equation 4.3, $C_{(x,y)}$ is the effective component of the lift and drag coefficients in the x' direction, which for small displacement about the equilibrium position may be expressed in linearized form as:

$$C_{L_{x'}} = C_{L_0} + \frac{\partial C_L}{\partial y'}\Delta y' + \frac{\partial C_L}{\partial x'}\Delta x'$$

$$C_{L_{x'}} = C_{L_0} + \frac{\partial C_L}{\partial y}\frac{\partial y}{\partial y'}\Delta y' + \frac{\partial C_L}{\partial x}\frac{\partial x}{\partial y'}\Delta y' + \frac{\partial C_L}{\partial x}\frac{\partial x}{\partial x'}\Delta x' + \frac{\partial C_L}{\partial y}\frac{\partial y}{\partial x'}\Delta x'$$

For small displacement $x' = \Delta x'$ and $y' = \Delta y'$, also, according to Figure 4.5b: $y = y'\cos\theta$, $x = x'\cos\theta$, $y = x'\sin\theta$, and with respect to $C_{L_0} = 0$ and $\partial C_L / \partial x = 0$, $C_{L_{x'}}$ reduces to:

$$C_{L_{x'}} = \frac{\partial C_L}{\partial y} y' \cos\theta + \frac{\partial C_L}{\partial y} x' \sin\theta$$

And similarly for the drag coefficient in the x' direction $C_{D_{x'}}$ may be expressed in liearized form as:

$$C_{D_{x'}} = C_{D_0} + \frac{\partial C_D}{\partial x} y' \frac{\cos^2\theta}{\sin\theta} + \frac{\partial C_D}{\partial x} x' \cos\theta$$

Replacing $C_{L_{x'}}$ and $C_{D_{x'}}$ into the Equation 4.3 results:

$$F_{x'} = \frac{1}{2}\rho U^2{}_r lD\left(\frac{2\partial C_L}{\partial y} x' \sin^2\theta + C_{D_0}\cos\theta + \frac{2\partial C_D}{\partial x} x' \cos\theta\right) \qquad (4.6)$$

Using the flow velocity definition given in Equation 4.5 within Equation 4.6 gives:

$$F_{x'} = \rho U^2 lDx'\left(\frac{\partial C_L}{\partial y}\sin^2\theta + \frac{\partial C_D}{\partial x}\cos^2\theta\right) - \rho UlDC_{D_0}\dot{x}'\cos^2\theta \qquad (4.7)$$

The discussion so far has been in terms of traditional quasi-steady fluid-dynamics. It is known, however, that there is a time-lag between cylinder displacement and the fluid-dynamic forces generated thereby. This may be thought to be related to the delay in the two fluid streams on either side of the cylinder readjusting to the changing configuration as the cylinder oscillates (Lever & Weaver 1982); alternatively, it may be thought to be associated with retardation that the fluid experiences as it nears the cylinder, notably in the vicinity of a stagnation point, in conjunction with inter-cylinder positions having mean-while changed as a result of cylinder motions (Price & Païdoussis 1984, 1986). Perhaps this time-lag may most easily be conceived as a delay in the viscous wake adjusting continuously to the changing conditions imposed by the vibrating cylinder. Here we use an approximation for this time-delay as presented by Price & Païdoussis (1987), and the time delay τ, may be expressed as

$$\tau = \mu D/U \tag{4.8}$$

The effect of varying μ on stability was investigated by Price & Païdoussis (1984), they showed that for a rotated triangular array ($\boldsymbol{P/d} = 1.375$), $\mu = 1$ gives the best agreement between theory and experiment. Thus $\mu = 1$, will be used in all of the calculations in this paper. Assuming harmonic motion, such that $x = x_0 e^{(iP\tau)}$, the combination of equations of (4.2) and (4.7) gives:

$$ml\ddot{x}' + c\dot{x}' + kx' = \rho U^2 lDx' e^{ip\tau}\left(\frac{\partial C_L}{\partial y}\sin^2\theta + \frac{\partial C_D}{\partial x}\cos^2\theta\right) - \rho UlDC_{D_0}\dot{x}'\cos^2\theta \tag{4.9}$$

By replacing of $x' = x_0' e^{iPt}$, $\dot{x}' = x_0' ipe^{iPt}$ and $e^{iP\tau} = \cos P\tau + i\sin P\tau$ into Equation (4.9) it may rewritten by its real and imaginary components as:

$$-mlP^2 + iPc + K - \rho U^2 lD\frac{\partial C_L}{\partial y}\sin^2\theta\cos P\tau - \rho U^2 lD\frac{\partial C_D}{\partial x}\cos^2\theta\cos P\tau$$
$$-\rho U^2 lDi\frac{\partial C_L}{\partial y}\sin^2\theta\sin P\tau - \rho U^2 lDi\frac{\partial C_D}{\partial x}\cos^2\theta\sin P\tau + \rho UlDiPC_{D_0}\cos^2\theta = 0$$

(4.10)

Equating the real and imaginary parts of Equation (4.10) to zero yields the critical values for the natural stability: $U = U_c, p = p_c$.

$$-P^2 + \omega^2 - \rho U^2 D \frac{\partial C_L}{\partial y} \frac{\sin^2\theta}{m} \cos P\tau - \rho U^2 D \frac{\partial C_D}{\partial x} \frac{\cos^2\theta}{m} \cos P\tau = 0$$

$$2Pi\omega\zeta - \rho U^2 Di \frac{\partial C_L}{\partial y} \frac{\sin^2\theta}{m} \sin P\tau - \rho U^2 Di \frac{\partial C_D}{\partial x} \frac{\cos^2\theta}{m} \sin P\tau + \rho UDiPC_{D_0} \frac{\cos^2\theta}{m} = 0$$

(4.11)

For a single flexible tube within a rotated triangular tube bundle, and fluid-force coefficients measured by Price & Païdoussis in 1986, the critical upstream flow velocity for different angles of attack ranging from 0° to 90° is given in Table 4.2.

Using Equation 4.10, the fluidelastic instability behavior for the rotated triangular array can be easily explained. Since fluidelastic instability is possible when the energy absorbed from the fluid by the tubes exceeds the energy dissipated by damping, then damping variation with flexibility angle will be discussed.

It is well known that fluid damping in the flow direction is larger than fluid damping in cross flow, often almost twice (Price & Païdoussis 1986 & 1988). The imaginary part of the Equation 4.11 represents fluid damping. These terms are also function of the angle of attack θ. i.e. the maximum value of these terms occurs when $\theta = 0°$ (inflow direction) therefore increased fluid damping results in higher critical flow velocity. For the same reason, for a 90° angle of attack ($\theta = 90°$) the fluid damping term is minimum, which means that the tube bundle is very unstable leading to the lowest critical velocity.

For the cases of $\theta = 30°$ and $60°$ angle of attack it can easily seen that while $\cos^2 30 \succ \cos^2 60$ fluid damping decreases form 30° to 60° and as a result the fluidelastic instability critical velocity decreases from 30° to 60°.

For the cases of a drastically reduced number of flexible tubes in the array e.g. three-column flexible and cluster configuration, the reduction in the number of flexible tubes results in increased tube bundle effective structural stiffness and causes higher critical flow velocity for fluidelastic instability.

Flexibility Angle	Upstream Critical velocity	
	Numerical	Experimental
0	130	$\succ$ 8m/s
10	72.28	--
20	23.16	--
30	10.4	$\succ$ 8m/s
40	5.87	--
50	3.4	--
60	2.38	6.2
70	1.76	--
80	1.52	--
90	1.48	2.8

Table 4.1 summary of experimental and numerical results

4.5 Comparison with experimental data

Figure 4.6 shows that, for the available data, the experimental results are in qualitative agreement with those from the theoretical model. As mentioned in the Table 4.1, the critical velocities for fluidelastic instability within 0° and 30° angle of attack because the maximum flow velocity of the wind tunnel was about 8m/s with the array in place.

The results from available experimental data for fluidelastic instability from fully flexible, three-columns flexible and cluster configuration arrays can be compared with

results from the single flexible cylinder model. It is seen in Figure 4.6 and 4.7 that the theoretical curve gives a slightly lower bound for fluidelastic instability. However the agreement between the single flexible cylinder model and the experimental data for different tube bundle configurations with flexibility angle ranging from 90° to 0°, is generally acceptable.

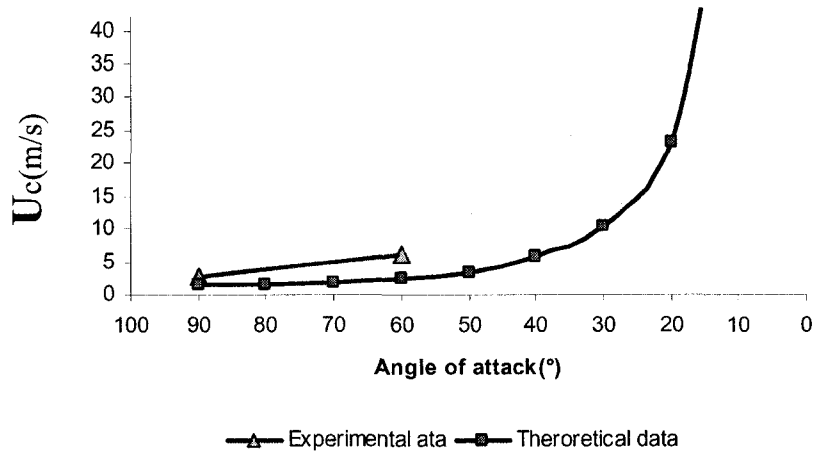

Figure 4.6 Upstream velocity variations with angle of attack comparison

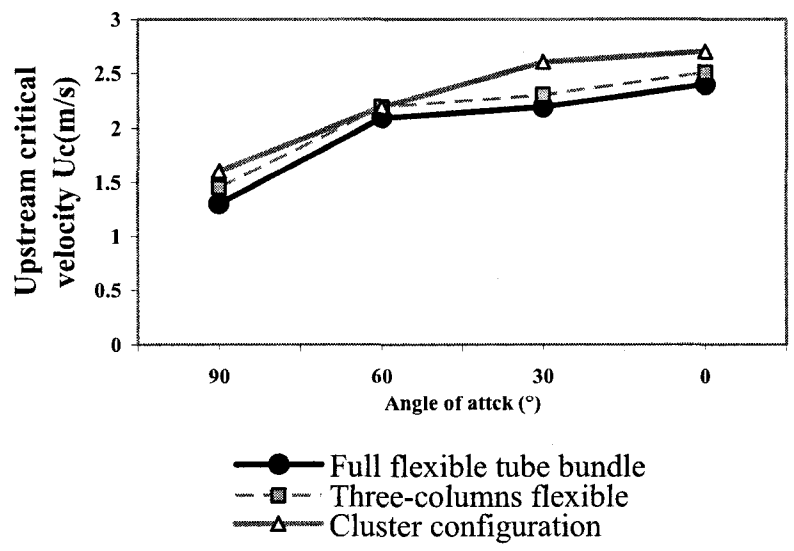

Figure 4.7 Upstream velocity variations with angle of attack for three configurations

Results summary

Angle of Attack	90°		60°		30°		0°	
	$\frac{2\pi m\zeta}{\rho D^2} = 2.47$							
Pitch velocity (m/s)	U_{pc}	K	U_{pc}	K	U_{pc}	K	U_{pc}	K
Fully Flex.	4.75	3.84	7.65	6.19	8.0	6.5	8.75	7.1
Three-Column	5.3	4.28	8.0	6.5	8.4	6.63	9.15	7.4
Cluster	5.85	4.72	8.0	6.5	9.5	7.7	9.85	7.97
Single tube	10.2	9.6	22.5	21.2	--	--	--	--

Table 4.2 Summary of experimental results and instability constant K

CHAPTER 5

CONCLUSIONS

An experimental program to conduct fluidelastic instability tests in single phase flow was completed. The principal objective of this work was to determine experimentally how the fluidelastic instability behavior of a rotated triangular tube bundle changes with tube flexibility angle. The main conclusions drawn from the current work are as follows:

- Fluidelastic instability can take places in a rotated triangular tube bundle that is flexible either in the flow direction or the direction normal to the flow.
- Fluidelastic instability is strongly dependent on the angle between the flow direction and the tube bundle flexibility direction which we call the "angle of attack".
- Increasing the angle of attack results in a decrease in the fluidelastic instability critical velocity.
- Increasing the number of flexible tubes in the array results in a reduced fluidelastic instability critical velocity for all angles of attack.
- A range of fluidelastic instability constant (K) between "3.8 and 8" were found for a range of angle of attack from 90 to 0 degree respectively.
- Fluidelastic instability can occur within single a flexible column (even with only two flexible tubes) in a rotated triangular tube bundle flexible in the flow direction
- The results obtained in single phase flow were found to be in good agreement with reported by Violette(2006) for two-phase flow, except for the single flexible column configuration in which the tubes were flexible only in the flow direction.

Future work

The tests in air-flow presented here are exploratory tests to investigate fluidelastic instability in oblique cross flow. To arrive at final conclusions regarding the stability behavior in actual steam generators, two-phase flow tests are required.

In the last step of the present study, a two-phase flow test section was modified by a simple mechanism to let the tubes to rotate axially. Thus tube bundle flexibility orientation can be changed from 0° to 90° degree in every 30 degree. This will enable tests at different angles of attack in two-phase flow. Appropriate technical drawings are given in appendix **C**.

REFERENCES

AXISA, F., VILLARD, B., GIBERT, R. J., HETSRONI, G., SUNDHEIMER, P. 1984, "Vibration of Tube Bundles Subjected to Air-Water and Steam-Water Cross Flow: Preliminary Results on Fluidelastic Instability", *Proceedings of ASME Symposium on Flow-Induced Vibrations*, Vol. 2, New Orleans, LA, pp. 269-284.

AXISA, F., BOHEAS, M. A., VILLARD, B., GIBERT, R. J. 1985, "Vibration of Tube Bundles Subjected to Steam-Water Cross Flow: a Comparative Study of Square and Triangular Pitch Arrays", *8th International Conference on Structural Mechanics in Reactor Technology*, Paper No. B1/2, Bruxelles, Belgium.

AXISA, F., WULLSCHLEGER, M., VILLARD, B., and TAYLOR, C., 1988 "Two-Phase Cross-flow Damping in Tube Arrays," *Damping* 1988, PVP-Vol. 133, Proceeding of the ASME PVP conference, Pittesburgh, PA, pp. 9-15.

BENDAT, J. S., PIERSOL, A. G., "Engineering Applications of Correlation and Spectral Analysis", *John Wiley & Sons*

BENNETT, A. W., HEWITT, G. F., KEARSEY, H. A., KEEYS, R. K. F., LACEY, P. M. C. 1965, "Flow Visualisation Studies of Boiling at High Pressures", *Gust. Mech. Eng. Proc. 1965-1966*, pt 3C, pp. 260-270.

BLEVIN, R. D. 1974, "Fluidelastic Whirlwing of a Tube Row", *Journal of Pressure Vessel Technology*, Vol. 96, pp. 263-267.

BLEVIN, R. D. 1979, "Formulas for natural frequency and mode shape", New York *Van Nostrand Reinhold*

CHEN, S. S. 1983, "Instability mechanisms and stability criteria of a group of cylinders subjected to cross-flow": Part 1 and 2. ASME Journal of Vibration, Stress and Reliability in Design 105, 51-58 and 253-260.

CHEN, S. S. 1984, "Guidelines for the Instability Flow Velocity of Tube Arrays in Crossflow", *Journal of Sound and Vibration*, Vol. 93, pp. 439-455.

CHEN, S. S. 1987, "Flow-Induced Vibration of Circular Cylindrical Structures", *Hemisphere Publishing Corporation*

CONNORS, H. J. 1970, "Fluidelastic Vibration of a Tube Array Excited by Cross Flow", *Flow Induced Vibration in Heat Exchangers*, New-York, pp. 42-56.

FEENSTRA, P. A., WEAVER, D. S., NAKAMURA, T. 2003, "Vortex Shedding and Fluidelastic Instability in a Normal Square Tube Array Excited by Two-Phase Cross-Flow", *Journal of Fluids and Structures*, Vol. 17, pp. 793-811.

GOVIER, G. W., AZIZ, K. 1972, "The Flow of Complex Mixture in Pipes", *Van Nostran-Reinhold*, New-York.

GRANT, I. D. R. 1975, "Flow and Pressure Drop with Single-Phaseand Two-Phase in the Shell-Side of Segmentally Baffled Shell-and-Tube Heat Exchangers", NEL Report No. 590, *Nationnal Engineering Laboratory*, Glasgow, Scotland, pp. 1-22.

HEILKER, W. J., VINCENT, R. Q. 1981, "Vibration in Nuclear Heat Exchangers Due to Liquid and Two-Phase Flow", *Journal of Engineering for Power*, Vol. 103, pp. 358-366.

HEWITT, G. F., ROBERTS, D. N. 1969, "Studies of Two-Phase Flow Patterns by Simultaneous X-Ray and Flash Photography, AERE-M 2159.

HIROTA, K., NAKAMURA, T., KASAHARA, J., MUREITHI, N. W., KUSAKABE, T., and TAKAMATSU, H. 2002, "Dynamics of an In-Line Tube Array Subjected to Steam-Water Cross-Flow. Part III: Fluidelastic Instability Test and Comparison With Theory", *Journal of Fluids and Structures*, Vol. 16, No. 2, pp. 153-173.

LEVER, J. H., WEAVER, D. S. 1982, "A Theoretical Model for the Fluid-Elastic Instability in Heat Exchanger Tube Bundles", *Journal of Pressure Vessel Technology*, Vol. 104, pp. 147-158.

MUREITHI, N. W., NAKAMURA, T., HIROTA, K., MURATA, M., UTSUMI, S., KUSAKABE, T. and TAKAMATSU, H. 2002, "Dynamics of an In-Line Tube Array Subjected to Steam-Water Cross-Flow. Part II: Unsteady Fluid Forces", *Journal of Fluids and Structures*, Vol. 16, No. 2, pp. 137-152.

MUREITHI, N.W., ZHANG, C., RUËL, M., PETTIGREW, M. J. 2005, "Fluidelastic Instability Test on an Array of Tubes Preferentially Flexible in the Flow Direction" *Journal of Fluids and Structures*, paraîtra en 2005.

NAKAMURA, T., FUJITA, K., KAWANISHI, K., YAMAGUCHI, N., TSUGE, A. 1991, "Study on the Vibrational Characteristics of a Tube Array Caused by Two-Phase Flow Part 2 – Fluidelastic Vibration", *Flow-Induced Vibration and Wear*, PVP-Vol. 206, pp. 25-30.

NAKAMURA, T., KAZUO, H., KEN-ICHI, T., JIROU, K., HIROSHI, T. 1999, "On Positional Effect of Flexible Tubes in a Square Array Subjected to Freon Two-Phase Flow", *Flow-Induced Vibration*, PVP-Vol. 389, pp. 73-80.

NAKAMURA, T., HIROTA, K., WATANABE, Y., MUREITHI, N. W., KUSAKABE, T., and TAKAMATSU, H. 2002, "Dynamics of an In-Line Tube Array Subjected to Steam-Water Cross-Flow. Part I: Two-Phase Damping and Added Mass", *Journal of Fluids and Structures*, Vol. 16, No. 2, pp. 123-136.

OSHINOWO, T., CHARLES, M. E. 1974, "Vertical Two-Phase Flow. Part 1 – Flow Pattern Correlation", *Canadian Journal of Chemical Engineering*, Vol. 52, pp.25-35.

PAIDOUSSIS, M. P. 1983, "A Review of Flow-Induced Vibrations in Reactors and Reactor Components", *Nuclear Engineering and Design*, Vol. 74, pp. 31-60.

PAIDOUSSIS, M. P., PRICE, S. J. 1988, "The mechanisms underlying flow-induced instabilities of cylinder arrays in cross-flow", *Journal of Fluid Mechanic*, Vol. 187, pp. 45-59.

PAÏDOUSSIS, M. P., PRICE, S. J., MUREITHI, N. W. 1996, "On the Virtual Nonexistence of Multiple Instability Regions for Some Heat-Exchanger Arrays in Crossflow", *Journal of Fluids Engineering*, Vol. 118, pp.103-109.

PETTIGREW, M. J., SYLVESTRE, Y., CAMPAGNA, A. O. 1978, "Vibration Analysis of Heat Exchanger and Steam Generator Designs", *Nuclear Engineering and Design*, Vol. 48, pp. 97-115.

PETTIGREW, M. J., TAYLOR, C. E., KIM, B. S. 1989, "Vibration of Tube Bundles in Two-Phase Cross-Flow: Part 1 – Hydrodynamic Mass and Damping", *Journal of Pressure Vessel Technology*, Vol. 111, pp. 466-477.

PETTIGREW, M. J., TROMP, J. H., TAYLOR, C. E., KIM, B. S. 1989, "Vibration of Tube Bundles in Two-Phase Cross-Flow: Part 2 – Fluid-Elastic Instability", *Journal of Pressure Vessel Technology*, Vol. 111, pp. 478-487.

PETTIGREW, M. J., TAYLOR, C. E. 1991, "Fluidelastic Instability of Heat Exchanger Tube Bundles: Review and Design Recommendations", *Journal of Pressure Vessel Technology*, Vol. 113, pp.252-256.

PETTIGREW, M. J. 1994, "Two-Phase Flow-Induced Vibration: an Overview", *Journal of Pressure and Vessel Technology*, Vol. 116, pp. 233-253.

PETTIGREW, M. J., TAYLOR, C. E., JONG, J. H., CURRIE, I. G. 1995, "Vibration of a Tube Bundle in Two-Phase Freon Cross-Flow", *Journal of Pressure and Vessel Technology*, Vol. 117, pp. 321-329.

PETTIGREW, M. J., TAYLOR, C. E. 2003, "Vibration Analysis of Shell-and-Tube Heat Exchangers: An Overview – Part 1: Flow, Damping, Fluidelastic Instability", *Journal of Fluids and Structures*, Vol. 18, pp. 469-484.

PETTIGREW, M. J., TAYLOR, C. E. 2003, "Vibration Analysis of Shell-and-Tube Heat Exchangers: An Overview – Part 2: vibration response, fretting-wear, guidelines", *Journal of Fluids and Structures*, Vol. 18, pp. 485-500.

PETTIGREW, M. J., TAYLOR, C. E. 2004, "Damping of Heat Exchanger Tubes in Two-Phase Flow: Review and Design Guidelines", *Journal of Pressure Vessel Technology*, Vol. 126, pp.523-533.

PETTIGREW, M. J., ZHANG, C., MUREITHI, N. W., PAMFIL, D. 2004, "Detailed Flow Measurements in a Rotated Triangular Tube Bundle Subjected to Two-Phase

Cross Flow", *Proceedings of the 8th International Conference on Flow Induced Vibration*, Vol. 1, Paris, France, pp. 507-512.

PRICE, S. J., PAIDOUSSIS, M. P. 1984, "An Improved Mathematical Model for the Stability of Cylinder Rows Subject to Cross-Flow", *Journal of Sound and Vibration*, Vol. 97, pp. 615-640

PRICE, S. J., PAIDOUSSIS, M. P. 1986, "A Constrained-Mode Analysis of the Fluidelastic Instability of a Double Row of Flexible Circular Cylinders Subject to Cross-Flow: A Theoretical Investigation of System Parameters", *Journal of Sound and Vibration*, Vol. 105, pp. 121-142.

PRICE, S. J. 1995, "A Review of Theoretical Models for Fluidelastic Instability of Cylinder Arrays in Cross-Flow", *Journal of Fluids and Structures*, Vol. 9, pp. 463-518.

RAO, S. S. 1995, "Mechanical Vibrations, 3rd Ed", *Addison-Wesley*

REMY, R. M. 1982, "Flow-Induced Vibration of Tube Bundles in Two-Phase Cross-Flow", *Proceedings of the Third Conference on Vibration in Nuclear Plant*, Vol. 1, Kewsick, U.K., pp. 135-160.

ROBERTS, B. W. 1962, "Low Frequency Self-Excited Vibration in a Row of Circular Cylinders Mounted in an Air Stream", Ph.D. thesis,University of Cambridge.

SOPER, B. M. H., 1983, "The Effect of Tube Layout on the Fluid-Elastic Inistability of Tube bundles in Cross-Flow," ASME Journal of Heat Transfer, Vol. 105, Nov., pp. 755-750

TAYLOR, C.E., PETTIGREW, M. J., AXISA, F., VILLARD, B. 1988, "Experimental Determination of Single and Two-Phase Cross Flow-Induced Forces on Tube Rows", *Journal of Pressure Vessel Technology*, Vol. 110, pp. 22-28.

TAYLOR, C. E., CURRIE, I. G., PETTIGREW, M. J., KIM, B. S. 1989, "Vibration of Tube Bundles in Two-Phase Cross-Flow: Part 3 – Turbulence-Induced Excitation", *Journal of Pressure and Vessel Technology*, Vol. 111, pp. 488-500.

THE, C.E., and GOYDER, H. G. D., 1988, "Data for the Fluidelastic Instability of Heat Exchanger Tube Bundles," Flow Induced Vibration and Noise in Cylinder Arrays, Vol. 3, ASME-WAM, Chicago, pp. 77-94

ULBRICH, R., MEWES, D. 1994, "Vertical upward gas-liquid two-phase flow across a tube bundle", International Journal of Multiphase Flow, Vol. 20 No. 2, pp. 249-272.

VIOLETTE, R., PETTIGREW, M. J., MUREITHI, N. W. 2006, "Fluidelastic Instability of an Array of Tubes Preferentially Flexible in the Flow Direction Subjected to Two-Phase Cross Flow", *Journal of Pressure Vessels Technology,* Vol.128, pp. 1-12

WEAVER, D. S., SCHNEIDER, W. 1983, "The Effect of Flat Bar Supports on the Crossflow Induced Response of Heat Exchanger U-Tubes", *Journal of Engineering for Power*, Vol. 105, pp. 775-781.

WEAVER, D. S., FITZPATRICK, J.A., 1988.Arevirew of cross-flow induced vibrations in heat exchanger tube arrays. Journal of Fluids and Structures 16, 73-93.

YETISIR, M., WEAVER, D. S. 1993, "An Unsteady Theory for Fluidelastic Instability in an Array of Flexible Tubes in Cross-Flow. Part II: Results and Comparison with Experiments", *Journal of Fluids and Structures*, Vol. 7, pp. 767-782.

ZIADA, S., OENGÖREN, A. 2000, "Flow Periodicity and Acoustic Resonance in Parallel Triangular Tube Bundles", *Journal of Fluids and Structures*, Vol. 14, pp. 197-219.

Appendix A

Flexible Tube Assembly for Single-phase Flow Test Section

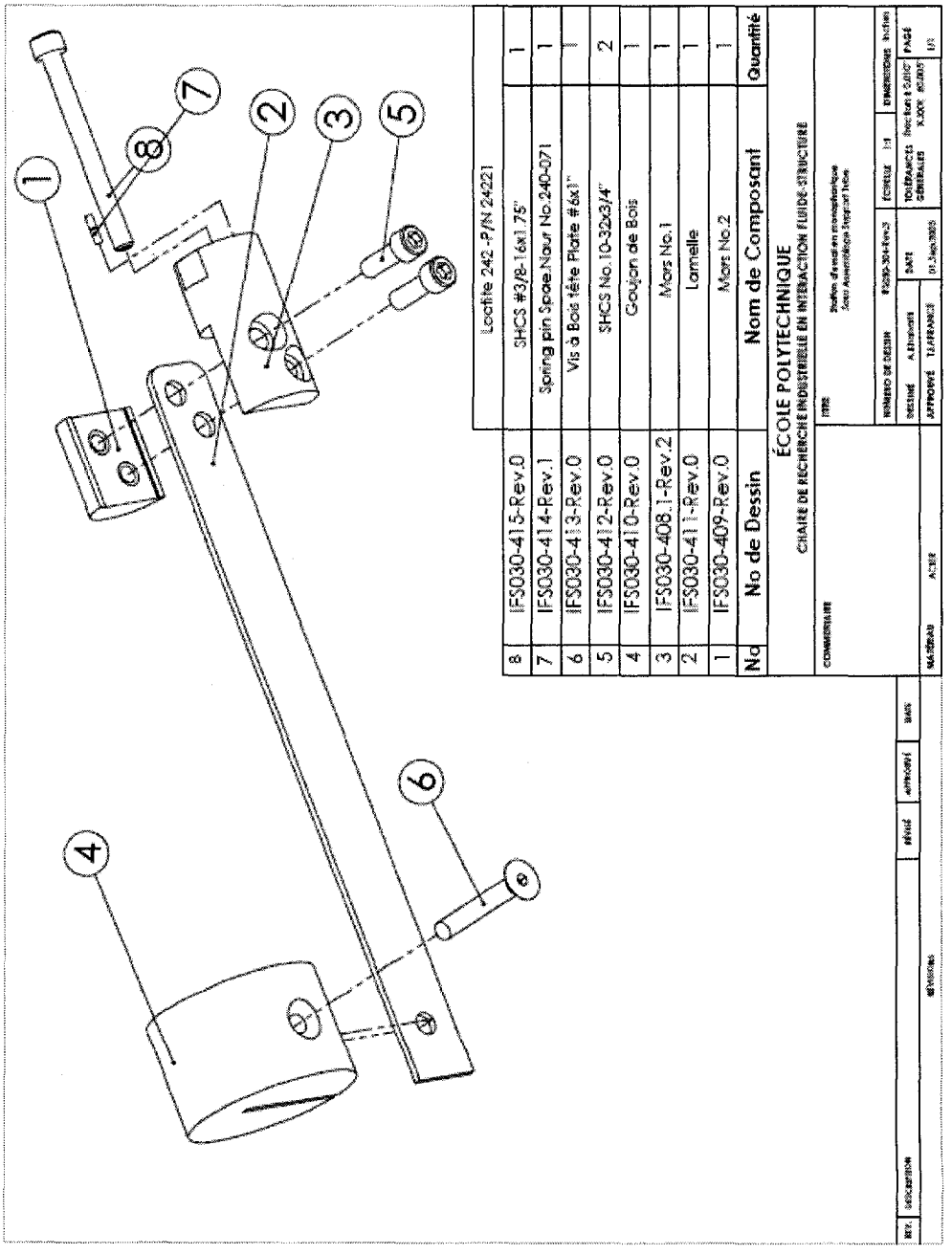

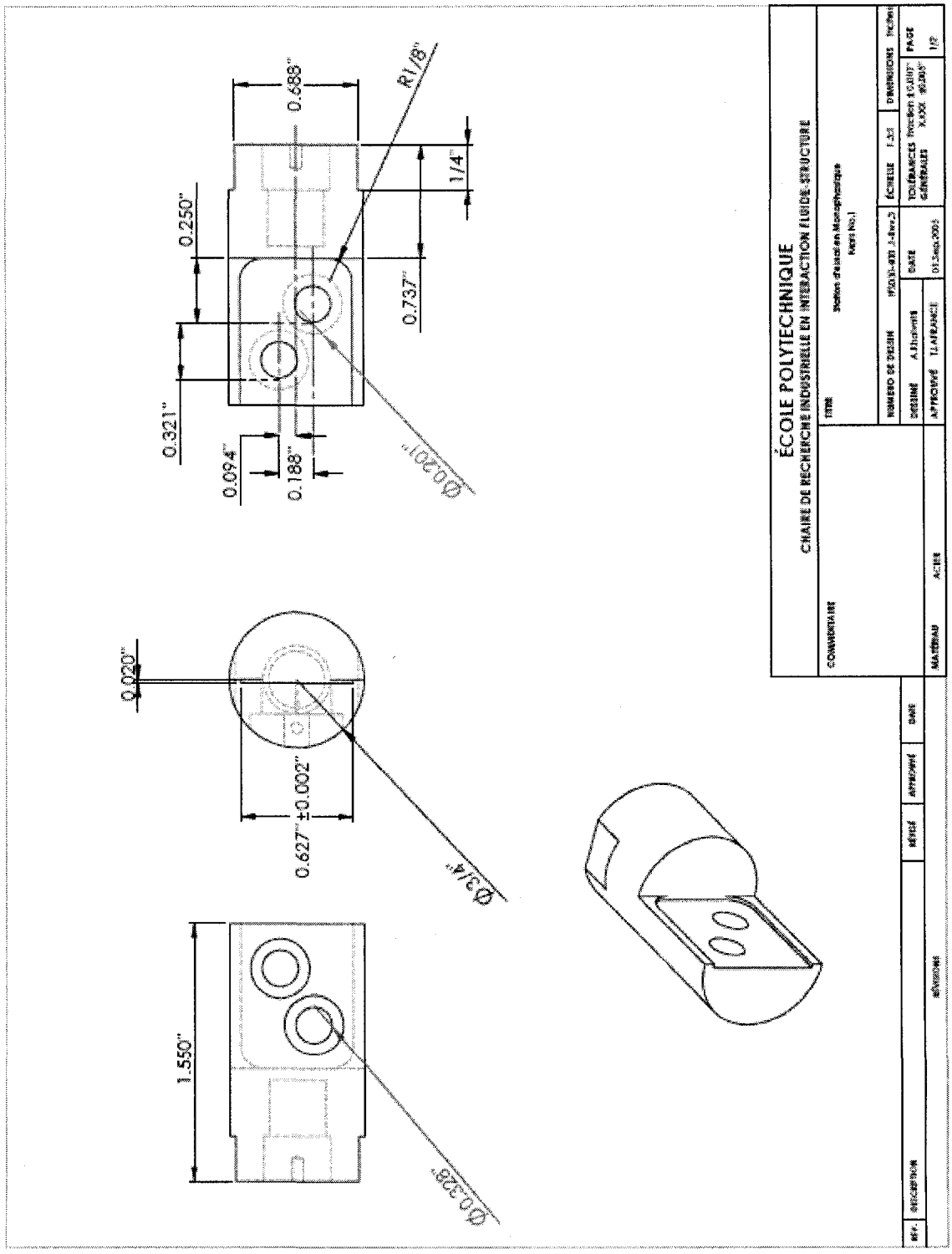
ÉCOLE POLYTECHNIQUE
CHAIRE DE RECHERCHE INDUSTRIELLE EN INTERACTION FLUIDE-STRUCTURE
0.688"
R1/8"
0.250"
1/4"
0.737"
0.321"
0.094"
0.188"
Ø0.201"
0.020"
0.627" ±0.002"
Ø3/4"
1.550"
Ø0.328"

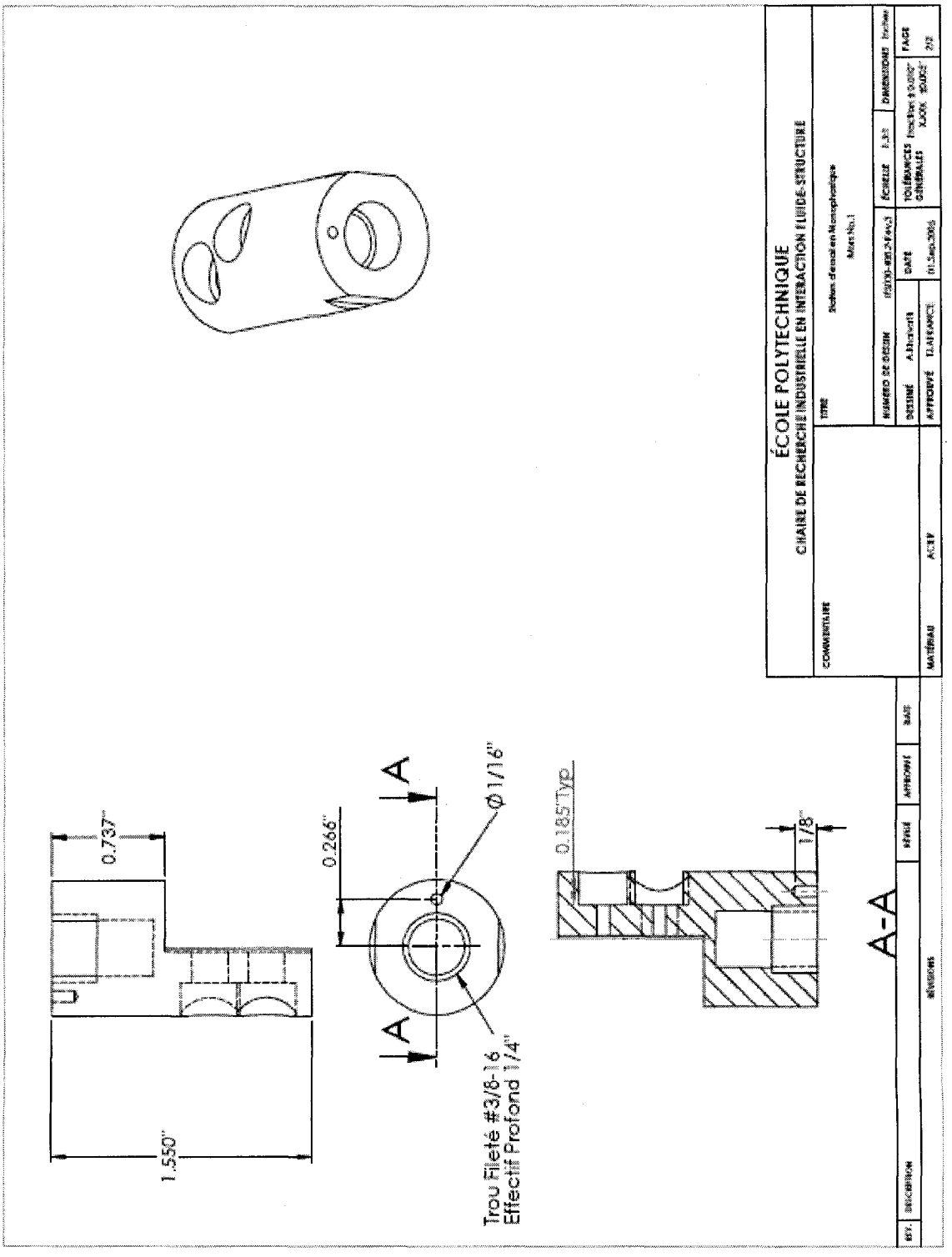
ÉCOLE POLYTECHNIQUE
CHAIRE DE RECHERCHE INDUSTRIELLE EN INTERACTION FLUIDE-STRUCTURE
0.737"
1.550"
0.266"
A
A
Ø1/16"
Trou Fileté #3/8-16
Effectif Profond 1/4"
0.185"Typ
1/8"
A-A

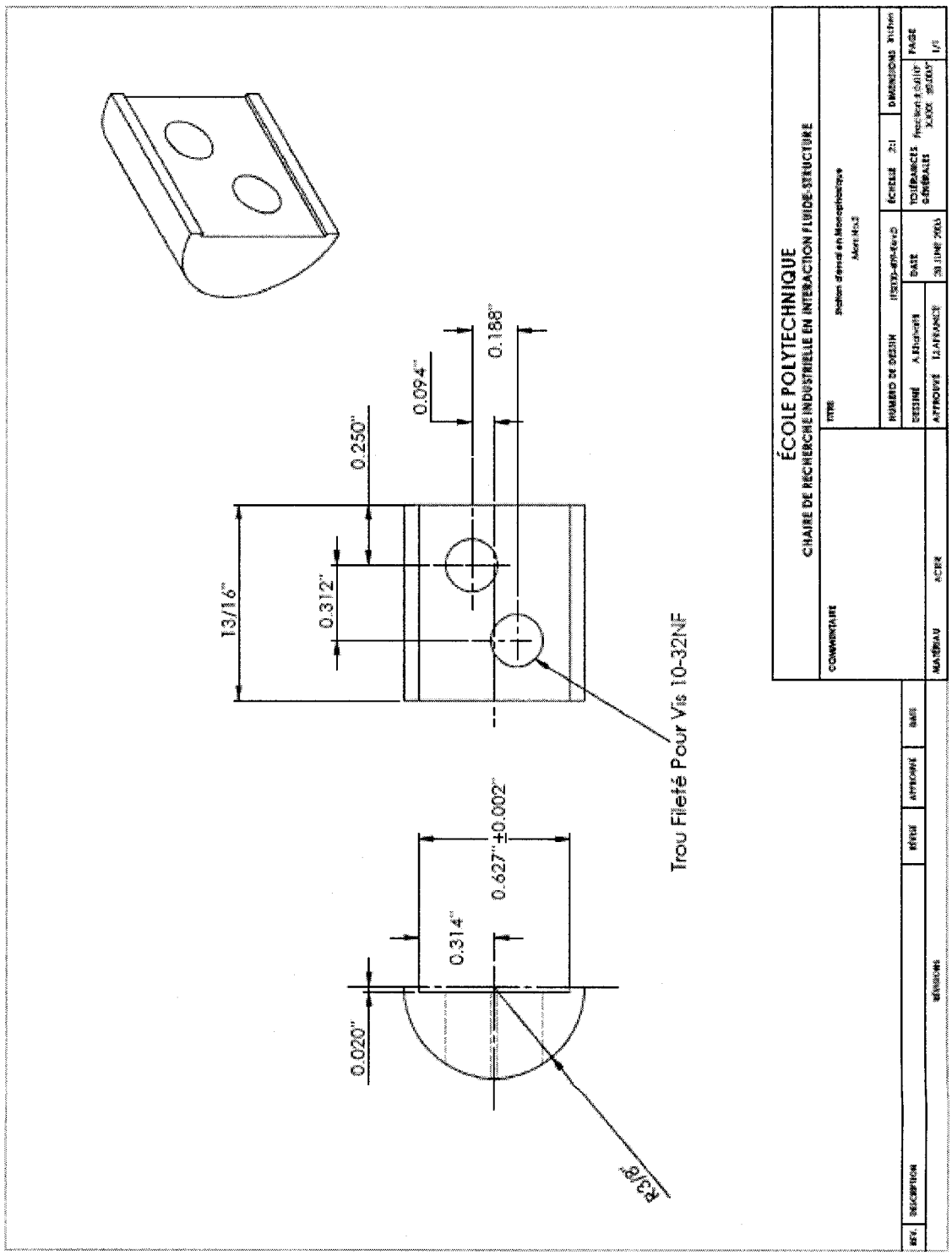
ÉCOLE POLYTECHNIQUE
CHAIRE DE RECHERCHE INDUSTRIELLE EN INTERACTION FLUIDE-STRUCTURE
13/16"
0.312"
0.250"
0.094"
0.188"
0.020"
0.314"
0.627" ±0.002"
R3/8"
Trou Fileté Pour Vis 10-32NF

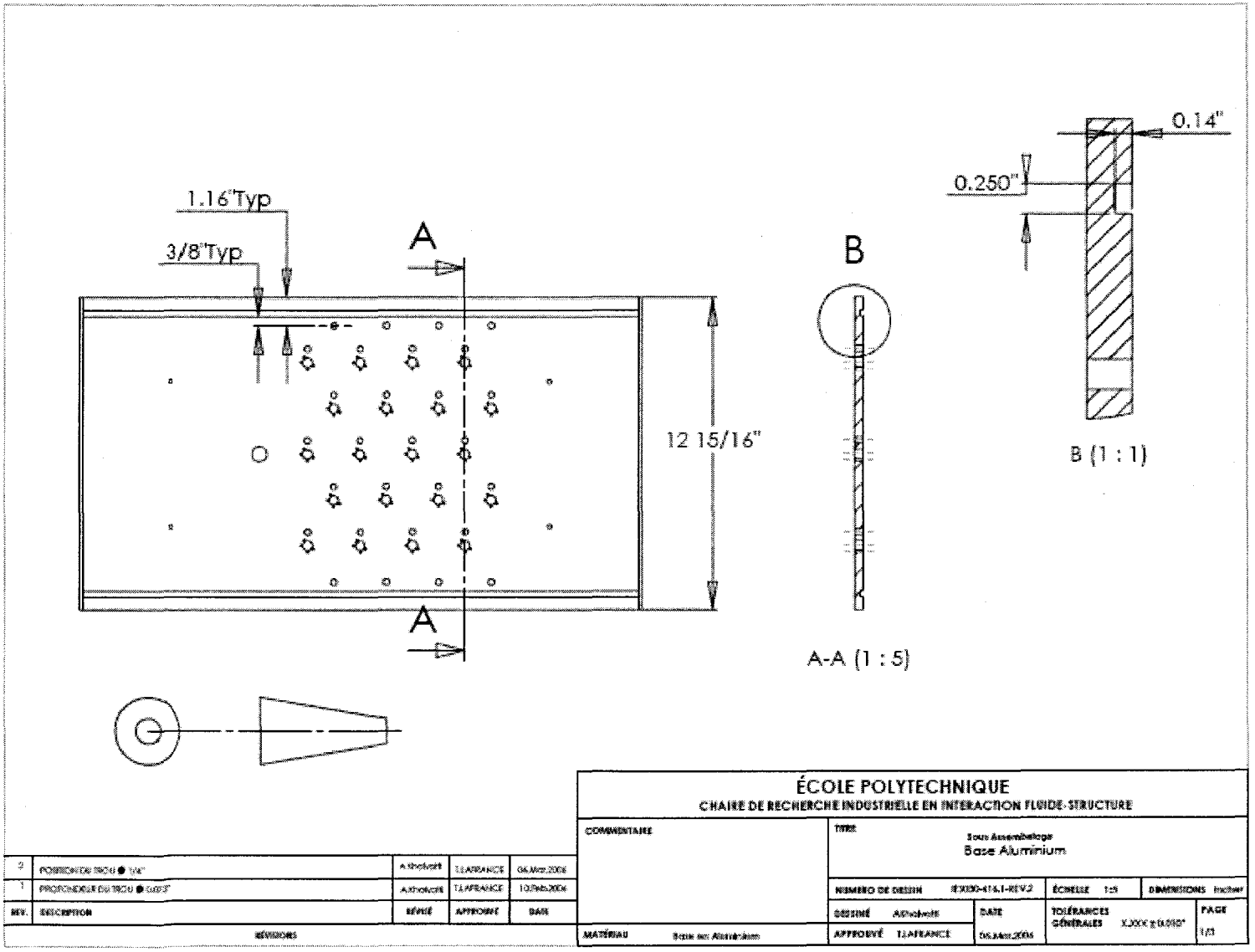
1.16"Typ
3/8"Typ
A
A
12 15/16"
B
A-A (1 : 5)
0.14"
0.250"
B (1 : 1)
ÉCOLE POLYTECHNIQUE
CHAIRE DE RECHERCHE INDUSTRIELLE EN INTERACTION FLUIDE-STRUCTURE
COMMENTAIRE
TITRE
Base Aluminium
NUMÉRO DE DESSIN
ÉCHELLE 1:5
DIMENSIONS Inches
DESSINÉ
DATE
APPROUVÉ T.LAFRANCE
TOLÉRANCES GÉNÉRALES
PAGE
MATÉRIAU
REV.
DESCRIPTION
RÉVISÉ
APPROUVÉ
DATE
RÉVISIONS

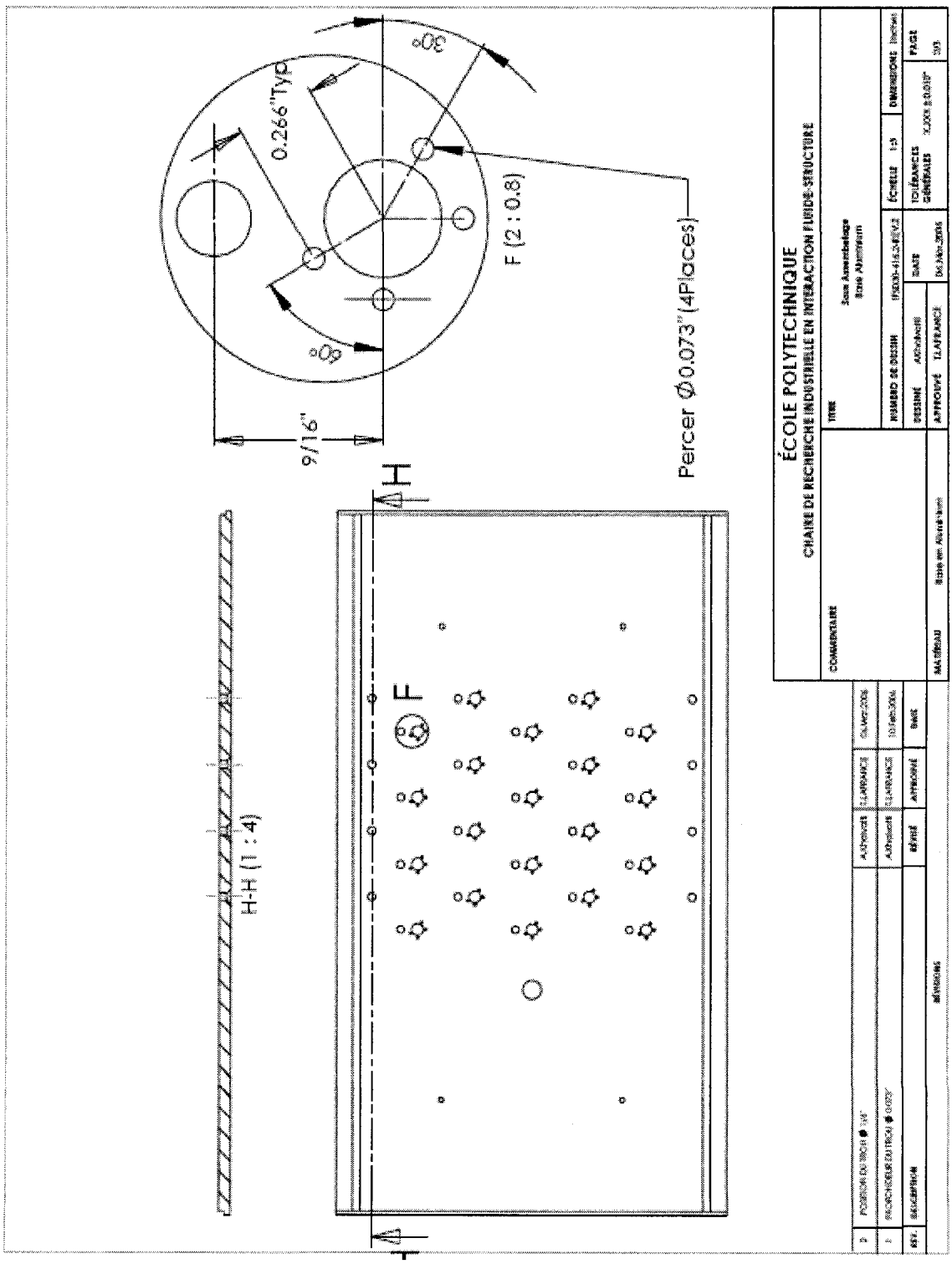
ÉCOLE POLYTECHNIQUE
CHAIRE DE RECHERCHE INDUSTRIELLE EN INTERACTION FLUIDE-STRUCTURE
0.266"Typ
30°
60°
F (2 : 0.8)
Percer Ø0.073" (4Places)
9/16"
H
H-H (1 : 4)
F

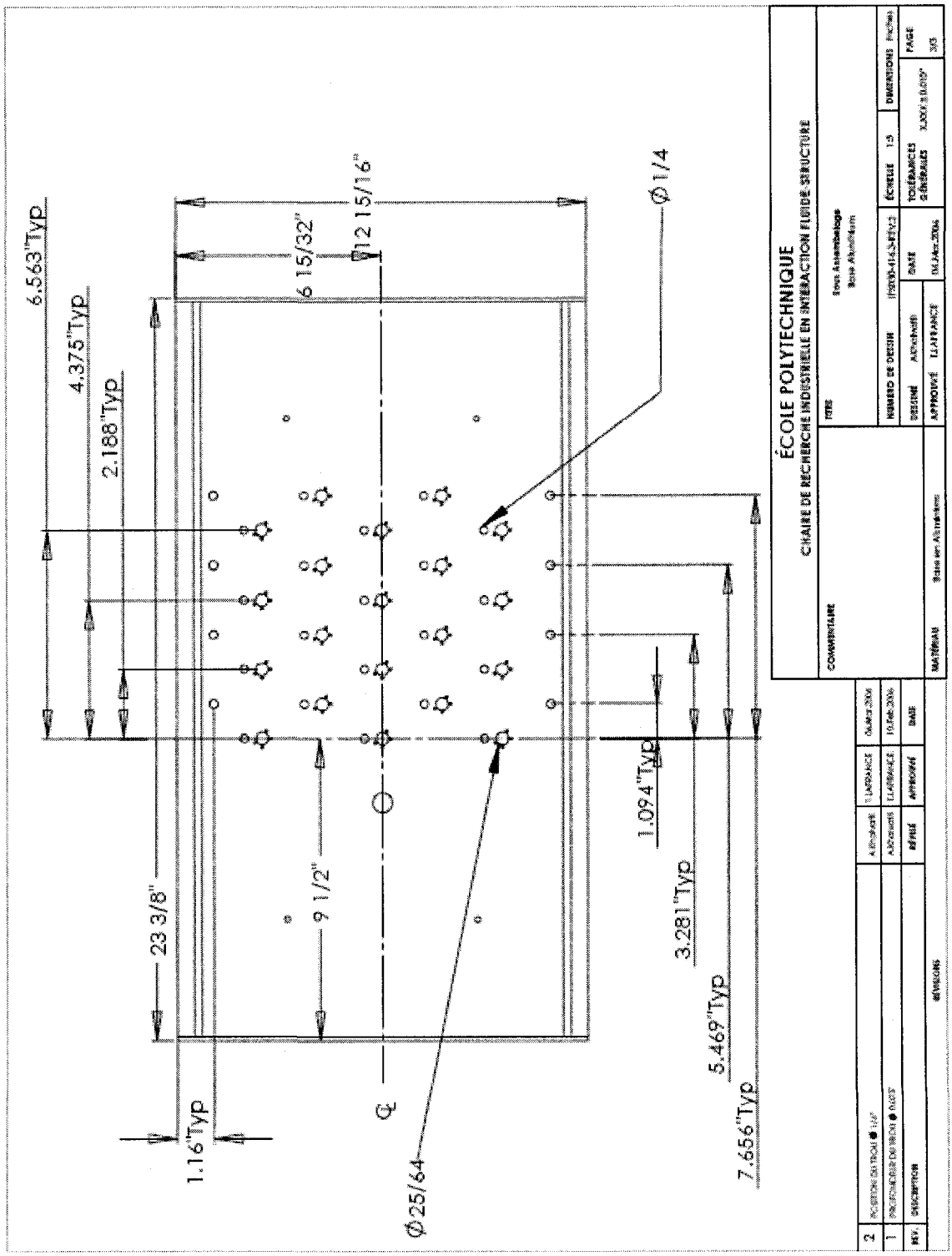
6.563"Typ
4.375"Typ
2.188"Typ
6 15/32"
12 15/16"
Ø1/4
23 3/8"
9 1/2"
1.094"Typ
3.281"Typ
5.469"Typ
7.656"Typ
1.16"Typ
Ø25/64
ÉCOLE POLYTECHNIQUE
CHAIRE DE RECHERCHE INDUSTRIELLE EN INTERACTION FLUIDE-STRUCTURE
COMMENTAIRE
TITRE
NUMÉRO DE DESSIN
ÉCHELLE
DIMENSIONS
DESSINÉ
DATE
TOLÉRANCES GÉNÉRALES
APPROUVÉ
MATÉRIAU
REVISIONS
REV.
DESCRIPTION
DATE

APPENDIX B

The measured damping ratio and natural frequency for eight instrumented tubes

Damping Factor for Tube #1

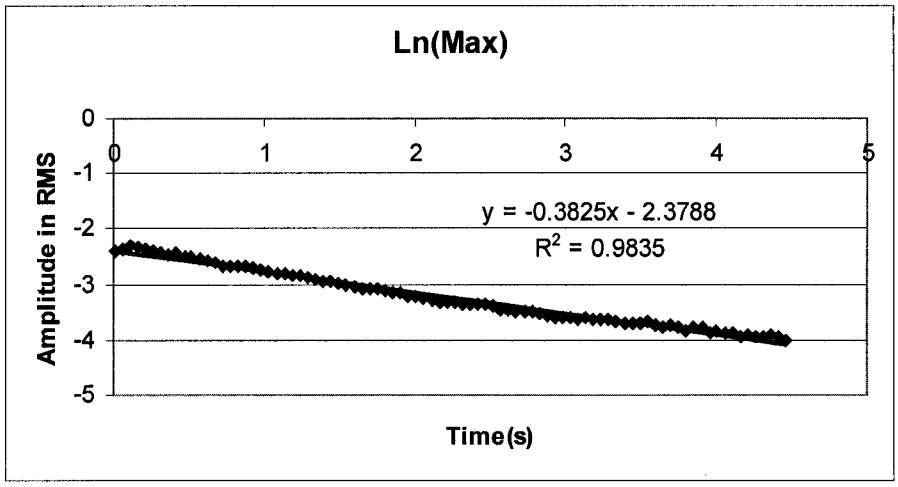

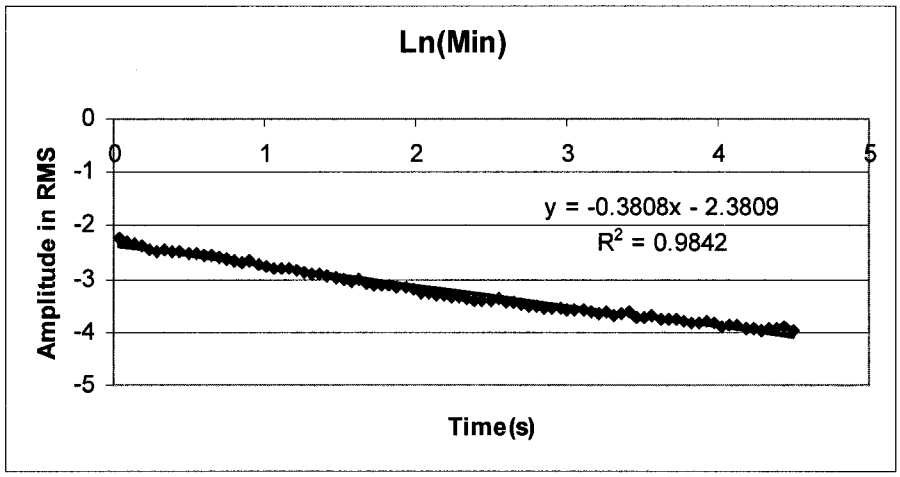

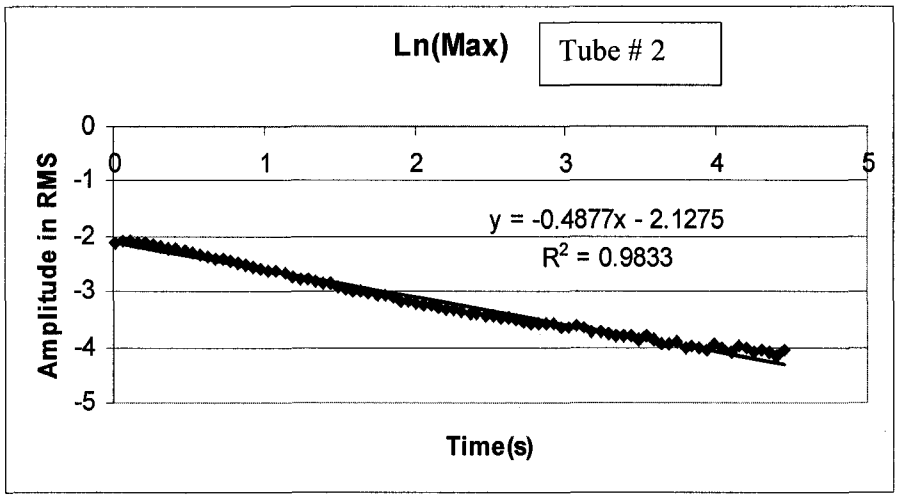
Ln(Max)
Tube # 2
Amplitude in RMS
0
-1
-2
-3
-4
-5
0
1
2
3
4
5
y = -0.4877x - 2.1275
R2 = 0.9833
Time(s)

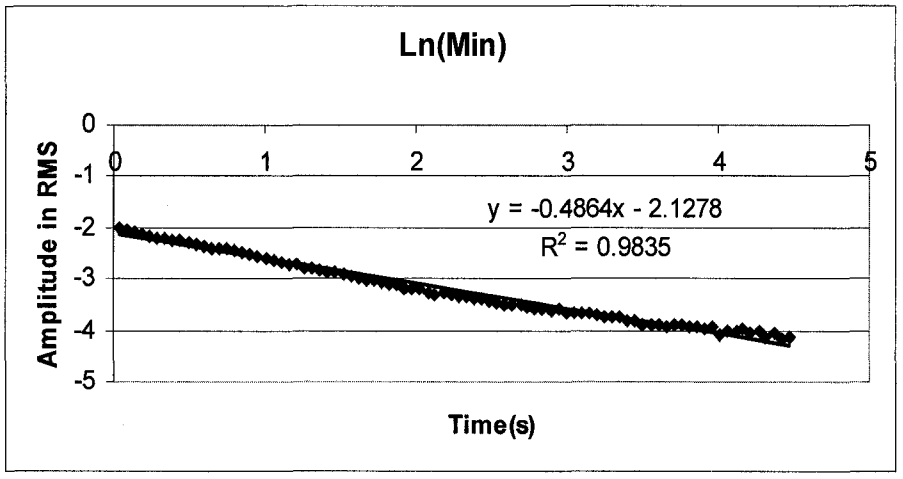
Ln(Min)
Amplitude in RMS
0
-1
-2
-3
-4
-5
0
1
2
3
4
5
y = -0.4864x - 2.1278
R2 = 0.9835
Time(s)

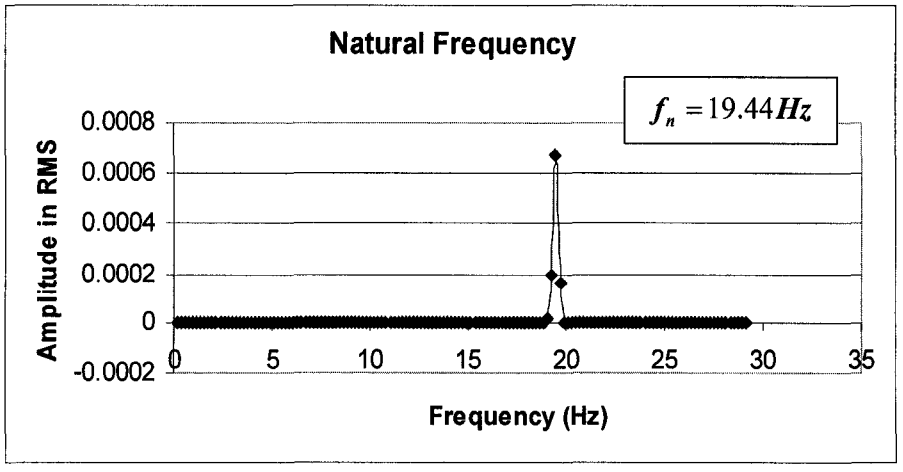
Natural Frequency
$f_n = 19.44 Hz$
Amplitude in RMS
0.0008
0.0006
0.0004
0.0002
0
-0.0002
0
5
10
15
20
25
30
35
Frequency (Hz)

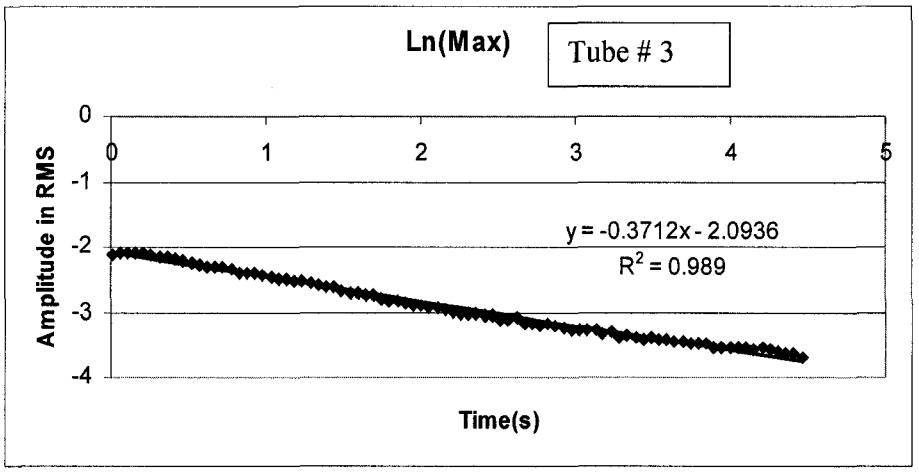
Ln(Max)
Tube # 3
Amplitude in RMS
0
-1
-2
-3
-4
0
1
2
3
4
5
y = -0.3712x - 2.0936
R2 = 0.989
Time(s)

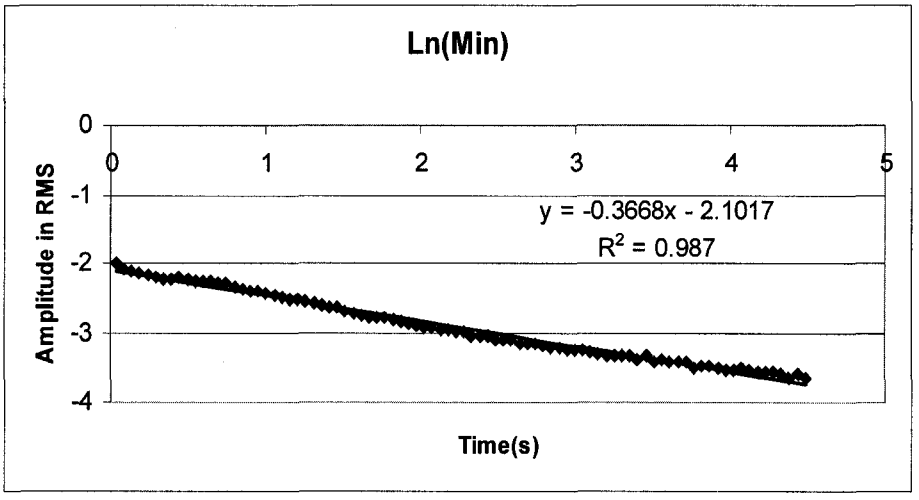
Ln(Min)
Amplitude in RMS
0
-1
-2
-3
-4
0
1
2
3
4
5
y = -0.3668x - 2.1017
R2 = 0.987
Time(s)

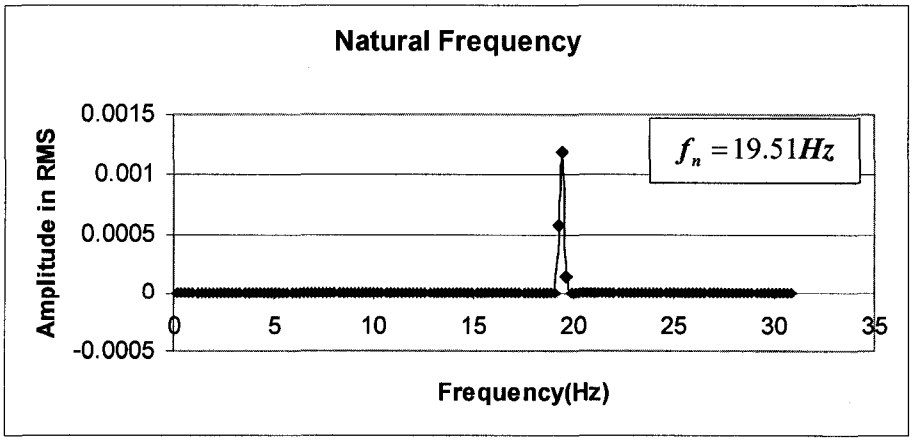
Natural Frequency
Amplitude in RMS
0.0015
0.001
0.0005
0
-0.0005
0
5
10
15
20
25
30
35
$f_n = 19.51Hz$
Frequency(Hz)

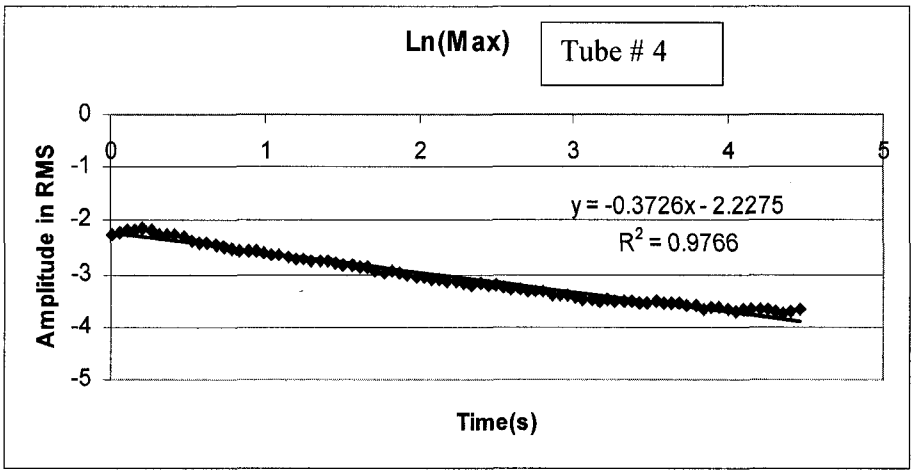
Ln(Max)
Tube # 4
Amplitude in RMS
0
-1
-2
-3
-4
-5
0
1
2
3
4
5
y = -0.3726x - 2.2275
R2 = 0.9766
Time(s)

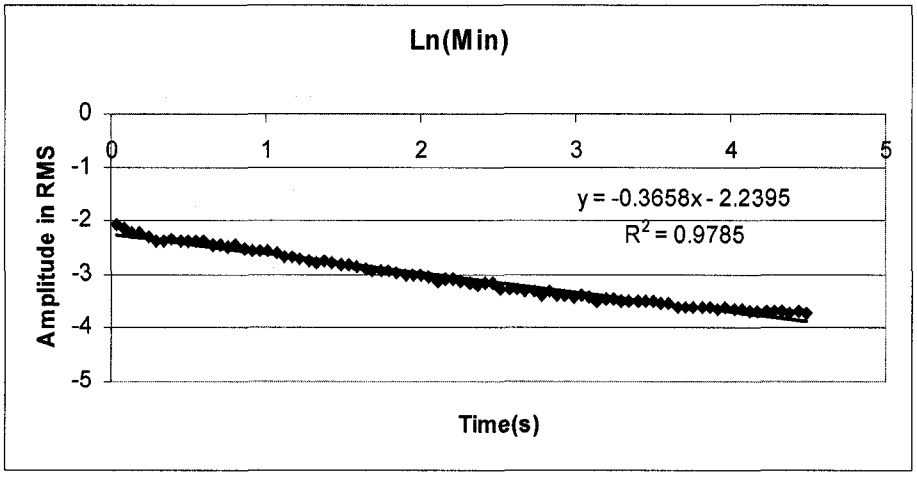
Ln(Min)
Amplitude in RMS
0
-1
-2
-3
-4
-5
0
1
2
3
4
5
y = -0.3658x - 2.2395
R2 = 0.9785
Time(s)

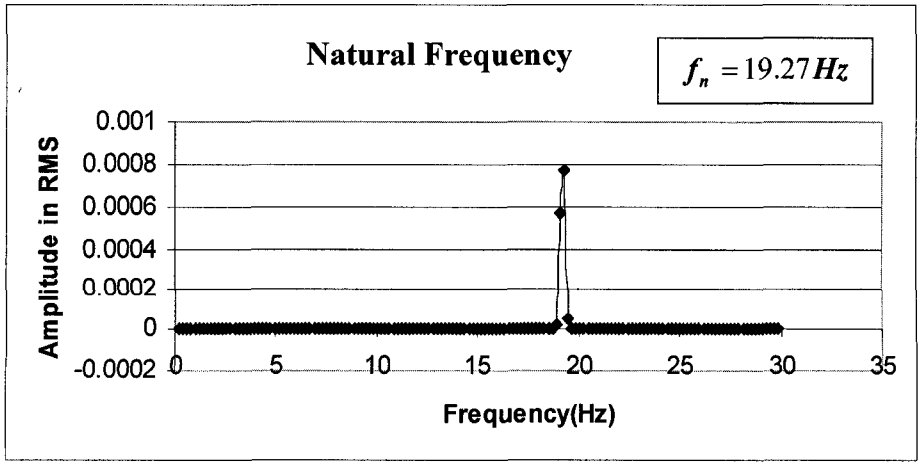
Natural Frequency
$f_n = 19.27 Hz$
Amplitude in RMS
0.001
0.0008
0.0006
0.0004
0.0002
0
-0.0002
0
5
10
15
20
25
30
35
Frequency(Hz)

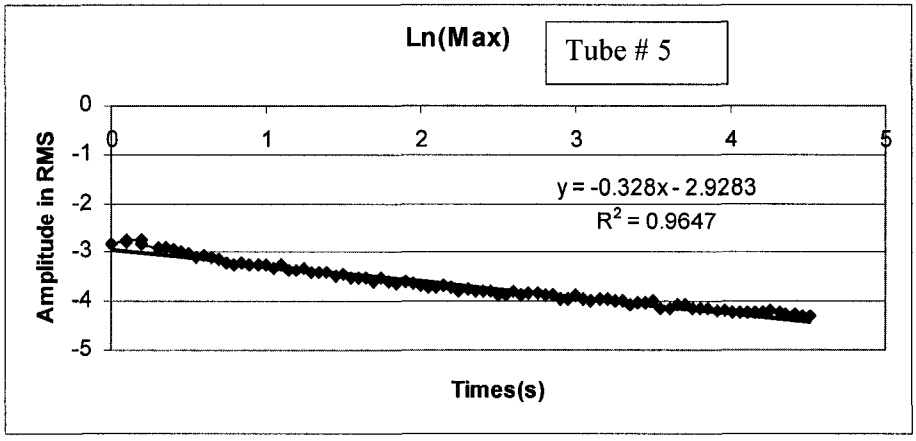
Ln(Max)
Tube # 5
Amplitude in RMS
0
-1
-2
-3
-4
-5
0
1
2
3
4
5
y = -0.328x - 2.9283
R2 = 0.9647
Times(s)

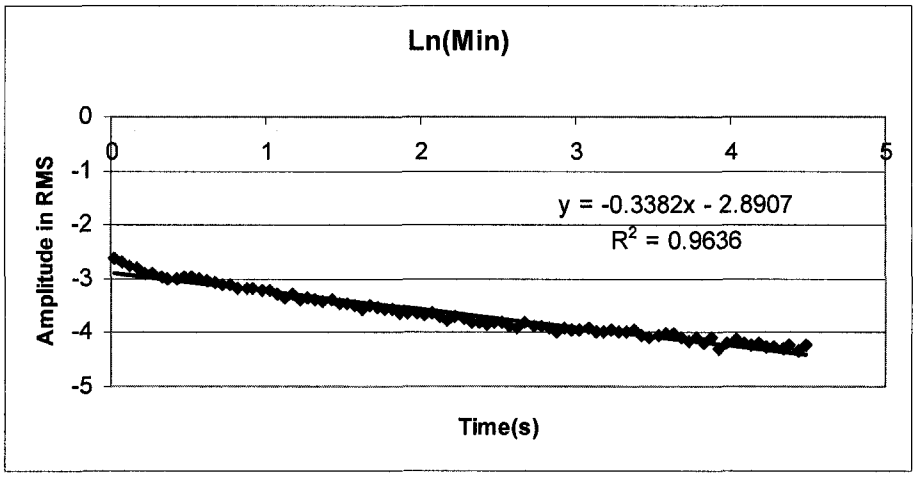
Ln(Min)
Amplitude in RMS
0
-1
-2
-3
-4
-5
0
1
2
3
4
5
y = -0.3382x - 2.8907
R2 = 0.9636
Time(s)

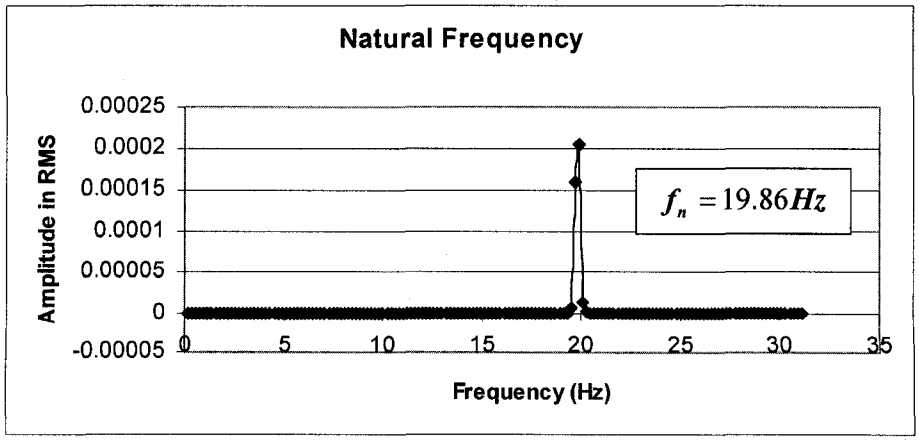
Natural Frequency
Amplitude in RMS
0.00025
0.0002
0.00015
0.0001
0.00005
0
-0.00005
0
5
10
15
20
25
30
35
$f_n = 19.86Hz$
Frequency (Hz)

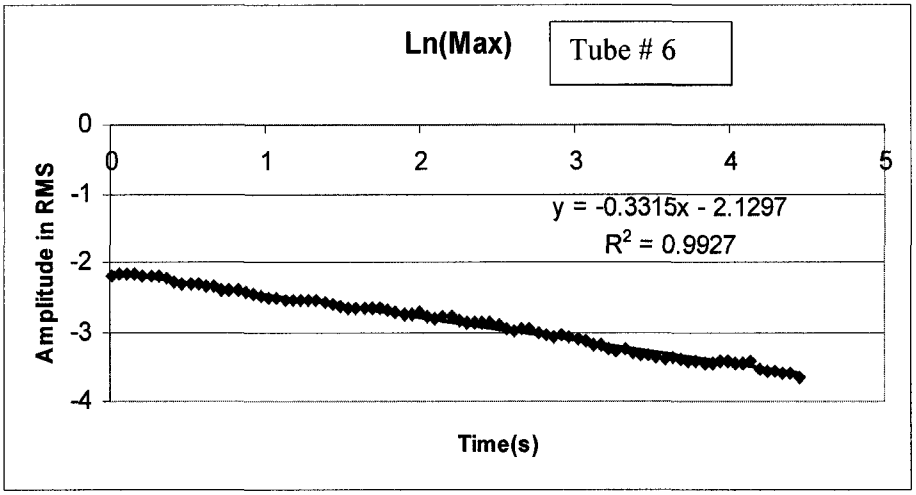
Ln(Max)
Tube # 6
y = -0.3315x - 2.1297
R2 = 0.9927
Amplitude in RMS
Time(s)

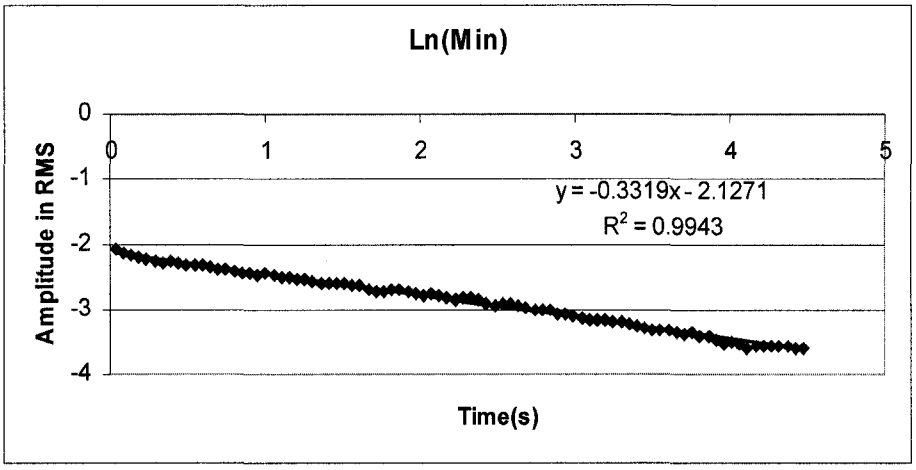
Ln(Min)
y = -0.3319x - 2.1271
R2 = 0.9943
Amplitude in RMS
Time(s)

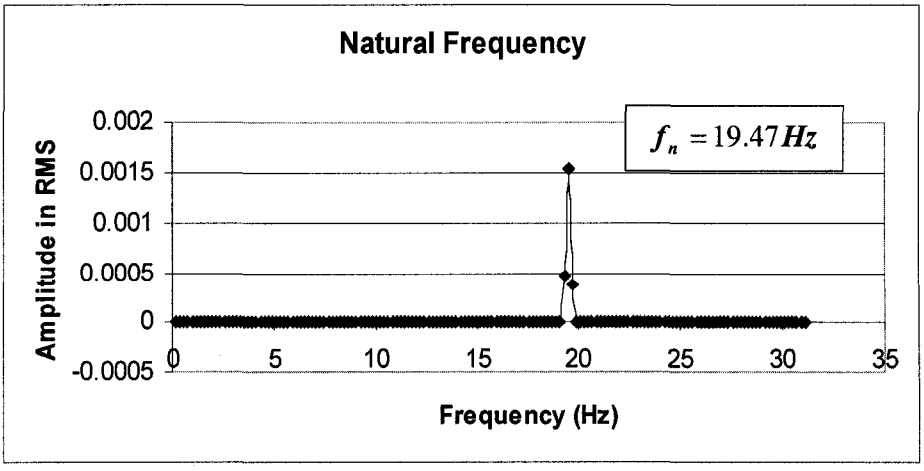
Natural Frequency
$f_n = 19.47 Hz$
Amplitude in RMS
Frequency (Hz)

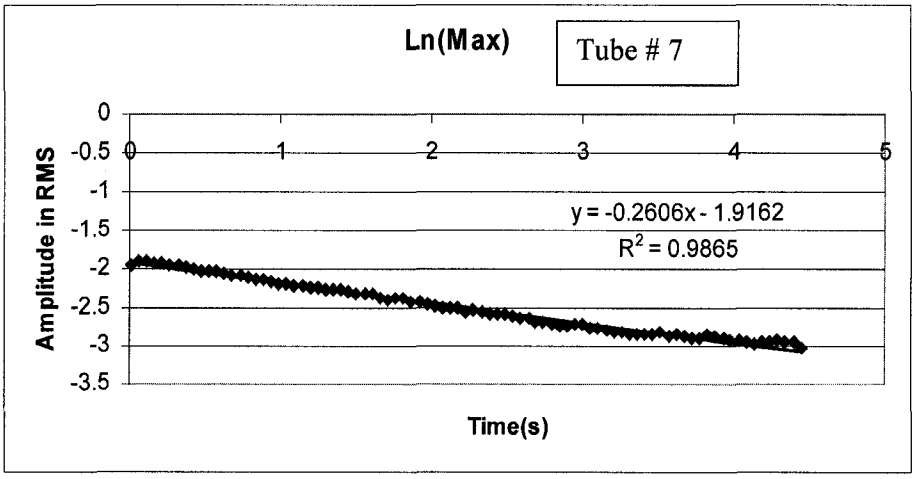
Ln(Max)
Tube # 7
Amplitude in RMS
0
-0.5
-1
-1.5
-2
-2.5
-3
-3.5
0
1
2
3
4
5
y = -0.2606x - 1.9162
R2 = 0.9865
Time(s)

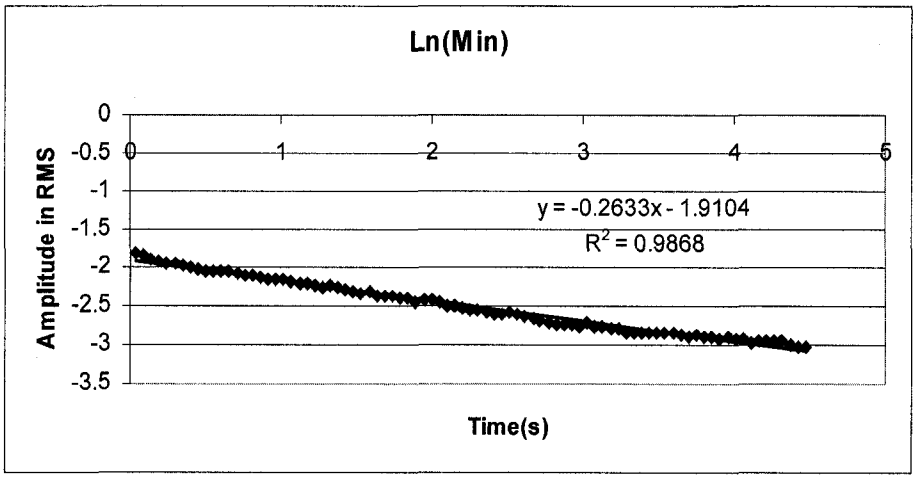
Ln(Min)
Amplitude in RMS
0
-0.5
-1
-1.5
-2
-2.5
-3
-3.5
0
1
2
3
4
5
y = -0.2633x - 1.9104
R2 = 0.9868
Time(s)

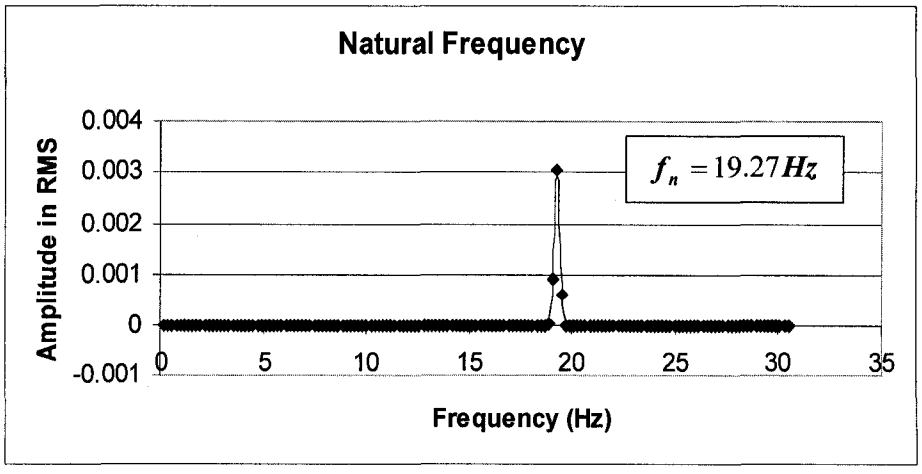
Natural Frequency
Amplitude in RMS
0.004
0.003
0.002
0.001
0
-0.001
0
5
10
15
20
25
30
35
$f_n = 19.27Hz$
Frequency (Hz)

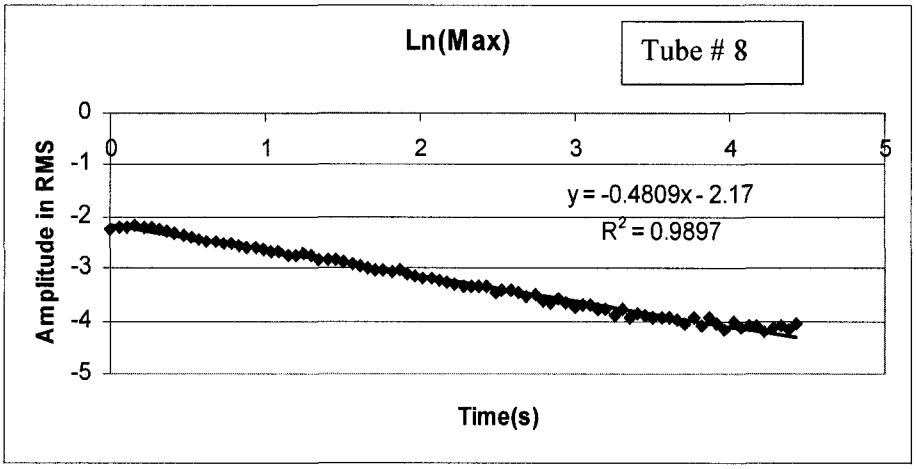
Ln(Max)
Tube # 8
Amplitude in RMS
0
-1
-2
-3
-4
-5
0
1
2
3
4
5
y = -0.4809x - 2.17
R2 = 0.9897
Time(s)

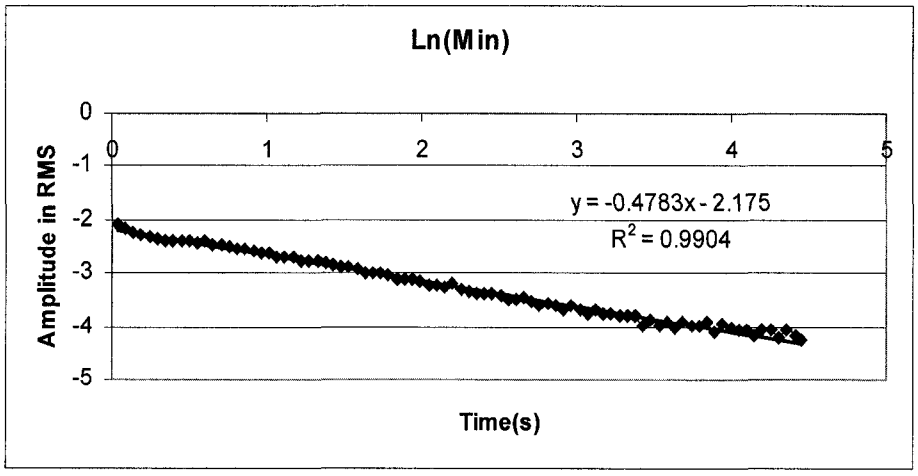
Ln(Min)
Amplitude in RMS
0
-1
-2
-3
-4
-5
0
1
2
3
4
5
y = -0.4783x - 2.175
R2 = 0.9904
Time(s)

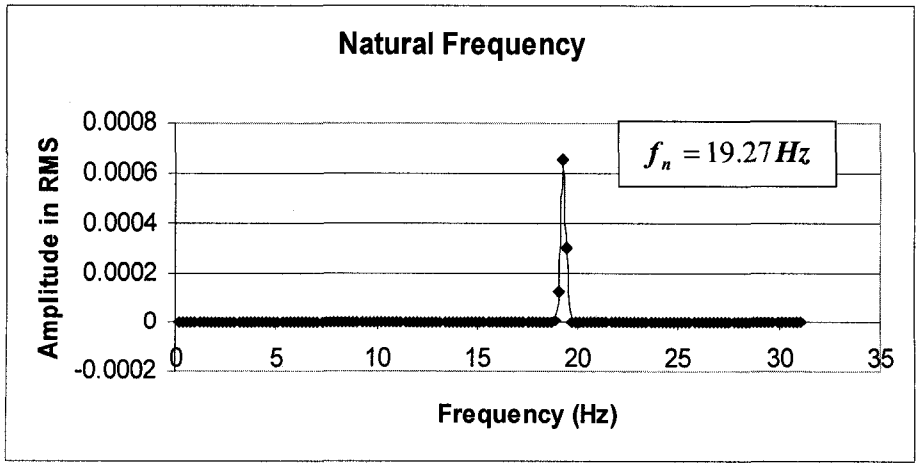
Natural Frequency
Amplitude in RMS
0.0008
0.0006
0.0004
0.0002
0
-0.0002
0
5
10
15
20
25
30
35
$f_n = 19.27 Hz$
Frequency (Hz)

Appendix C

Two-Phase Flow Test Section

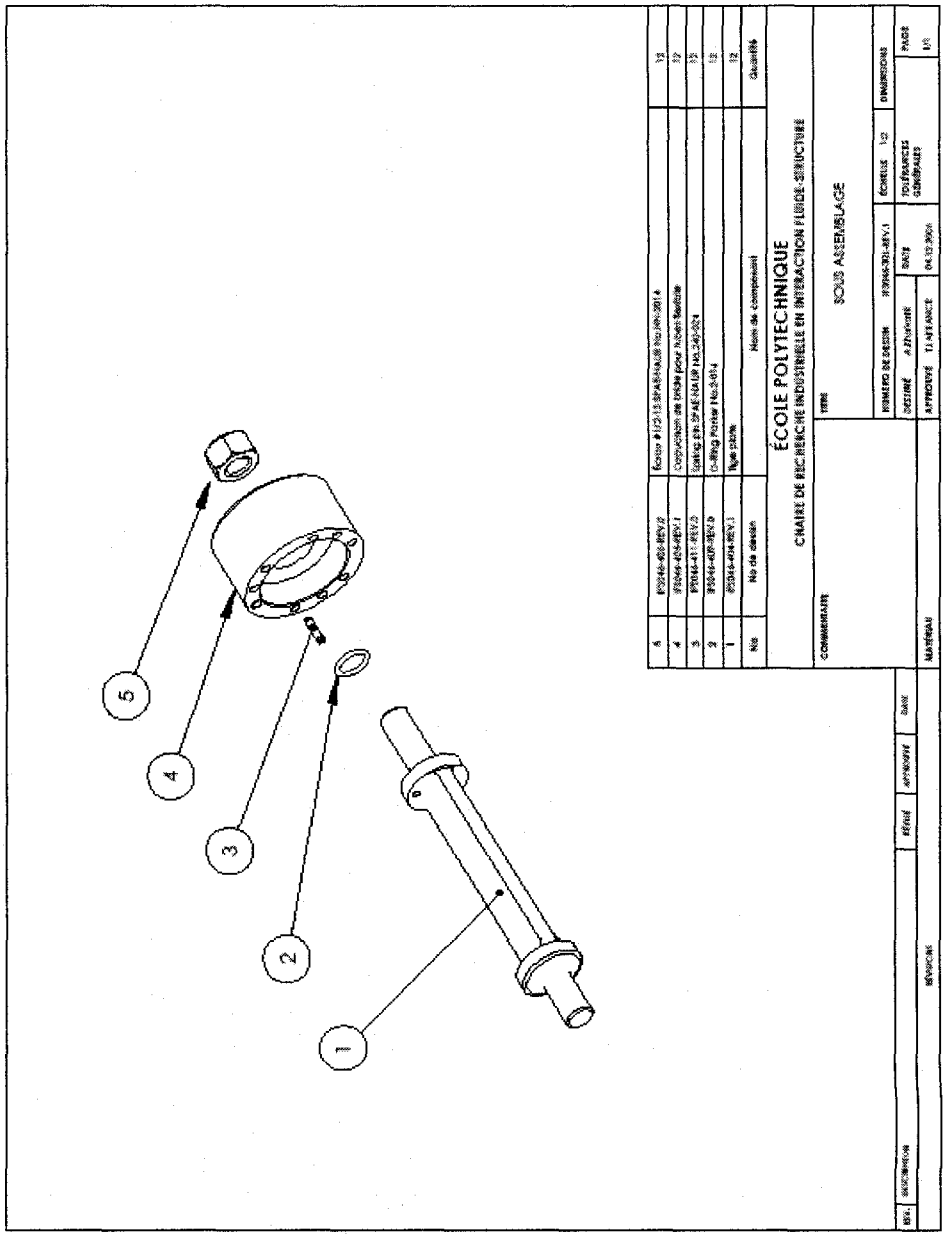

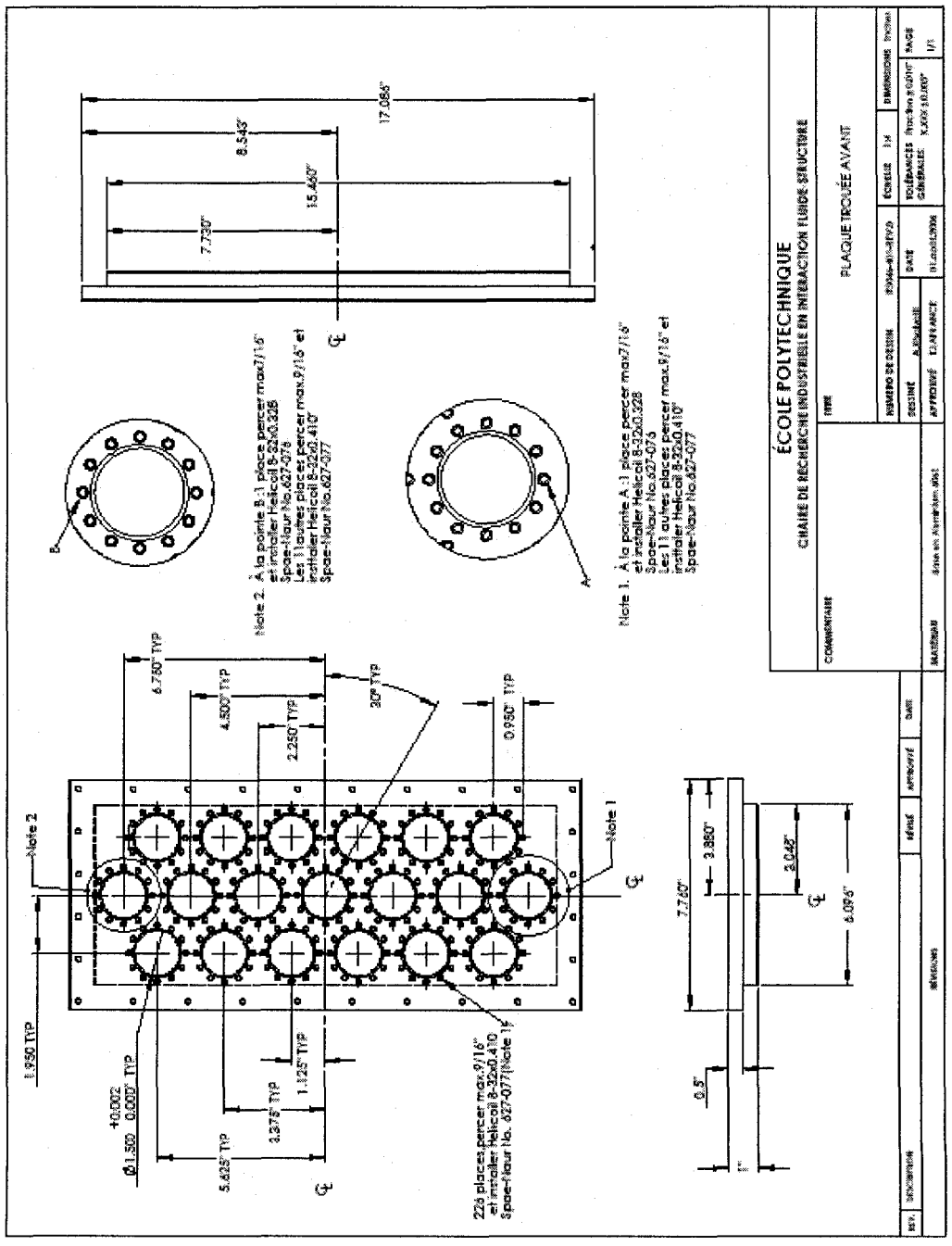
ÉCOLE POLYTECHNIQUE
CHAIRE DE RECHERCHE INDUSTRIELLE EN INTERACTION FLUIDE-STRUCTURE
PLAQUE TROUÉE AVANT
Note 1. À la pointe A : 1 place percer max7/16" et installer Helicoil 8-32x0.328 Spae-Naur No.627-076 Les 11 autres places percer max.9/16" et installer Helicoil 8-32x0.410" Spae-Naur No.627-077
Note 2. À la pointe B : 1 place percer max7/16" et installer Helicoil 8-32x0.328 Spae-Naur No.627-076 Les 11 autres places percer max.9/16" et installer Helicoil 8-32x0.410" Spae-Naur No.627-077
226 places percer max.9/16" et installer Helicoil 8-32x0.410 Spae-Naur No. 627-077 (Note 1)
Note 1
Note 2
17.086"
8.543"
15.460"
7.730"
6.750" TYP
4.500" TYP
2.250" TYP
30° TYP
0.950" TYP
1.950 TYP
+0.002
Ø1.500 0.000" TYP
5.625" TYP
3.375" TYP
1.125" TYP
7.760"
3.880"
3.048"
6.096"
0.5"
1"

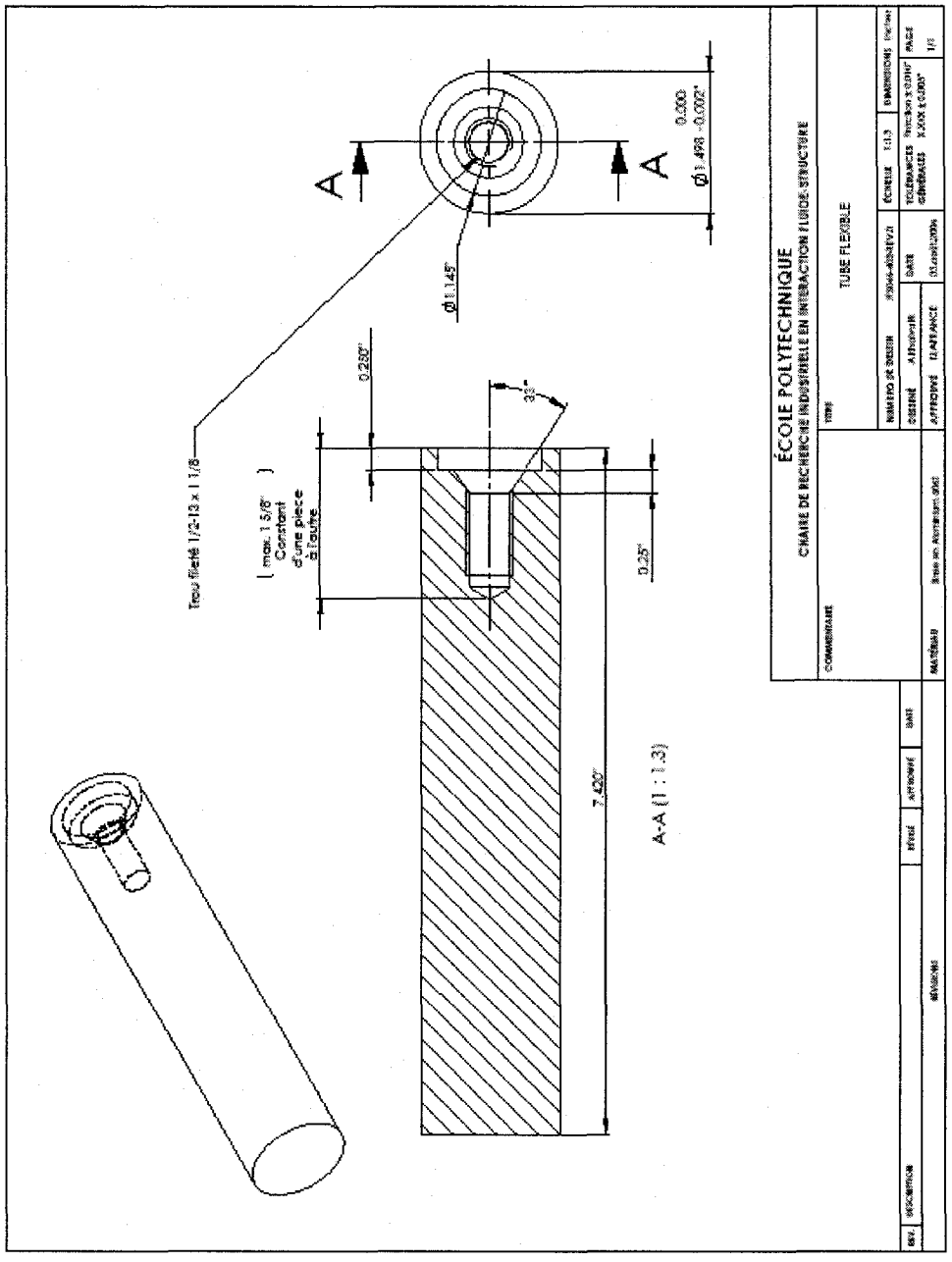
ÉCOLE POLYTECHNIQUE
CHAIRE DE RECHERCHE INDUSTRIELLE EN INTERACTION FLUIDE-STRUCTURE
TUBE FLEXIBLE
A
A
Trou fileté 1/2-13 x 1 1/8
(max. 1 5/8")
Constant
d'une pièce
à l'autre
0.250"
33°
0.25"
7.420"
A-A (1 : 1.3)
Ø1.145"
Ø1.498 -0.002"
0.000

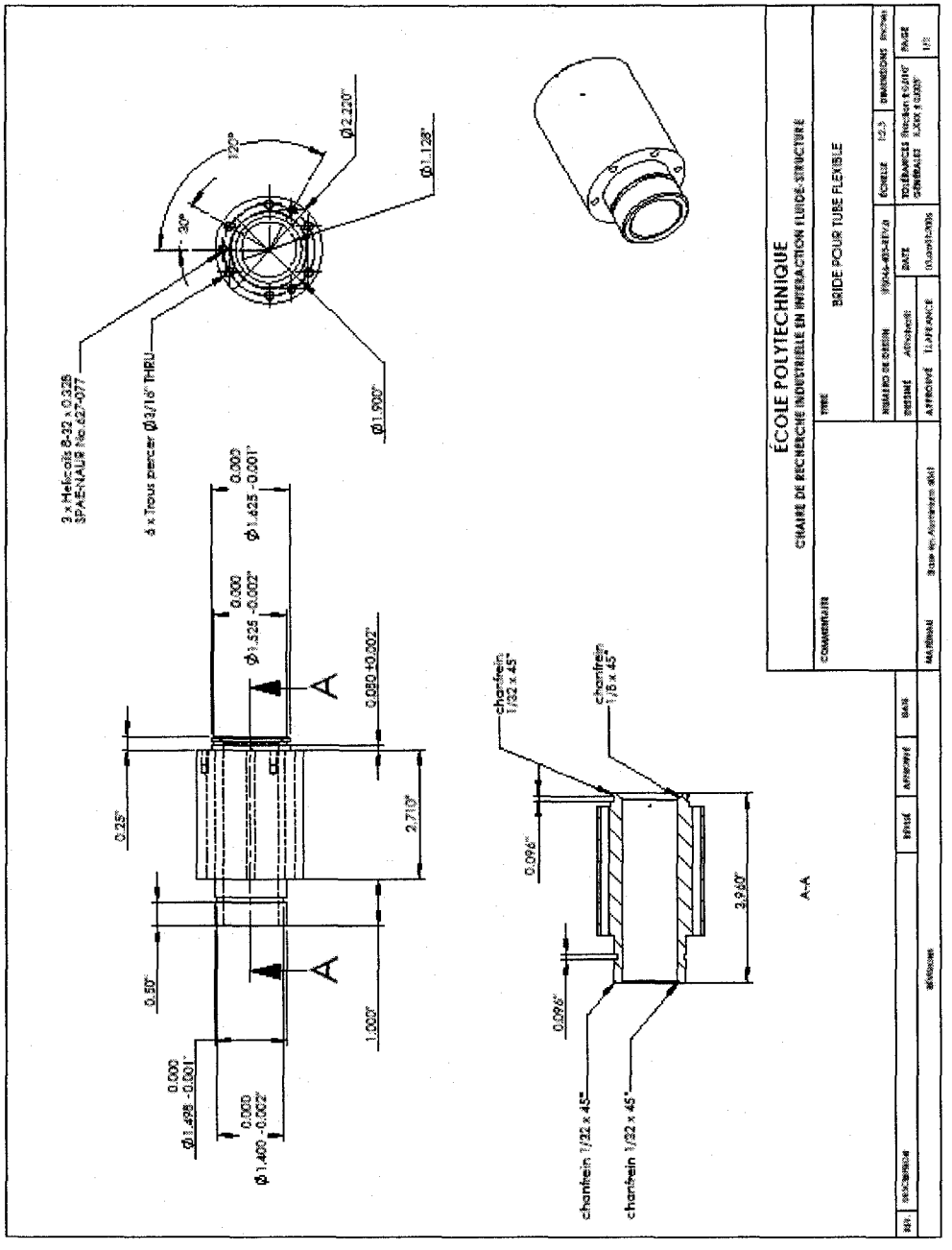
ÉCOLE POLYTECHNIQUE
CHAIRE DE RECHERCHE INDUSTRIELLE EN INTERACTION FLUIDE-STRUCTURE
BRIDE POUR TUBE FLEXIBLE
3 x Helicoils 8-32 x 0.325
SPAENAUR No.627-077
4 x Trous percer Ø3/16" THRU
Ø2.220"
Ø1.128"
Ø1.900"
120°
30°
Ø1.525 -0.002"
Ø1.625 -0.001"
0.050 +0.002"
2.710"
1.000"
0.25"
0.50"
Ø1.495 -0.001"
Ø1.400 -0.002"
A
A-A
chanfrein 1/32 x 45°
chanfrein 1/8 x 45°
0.096"
3.960"

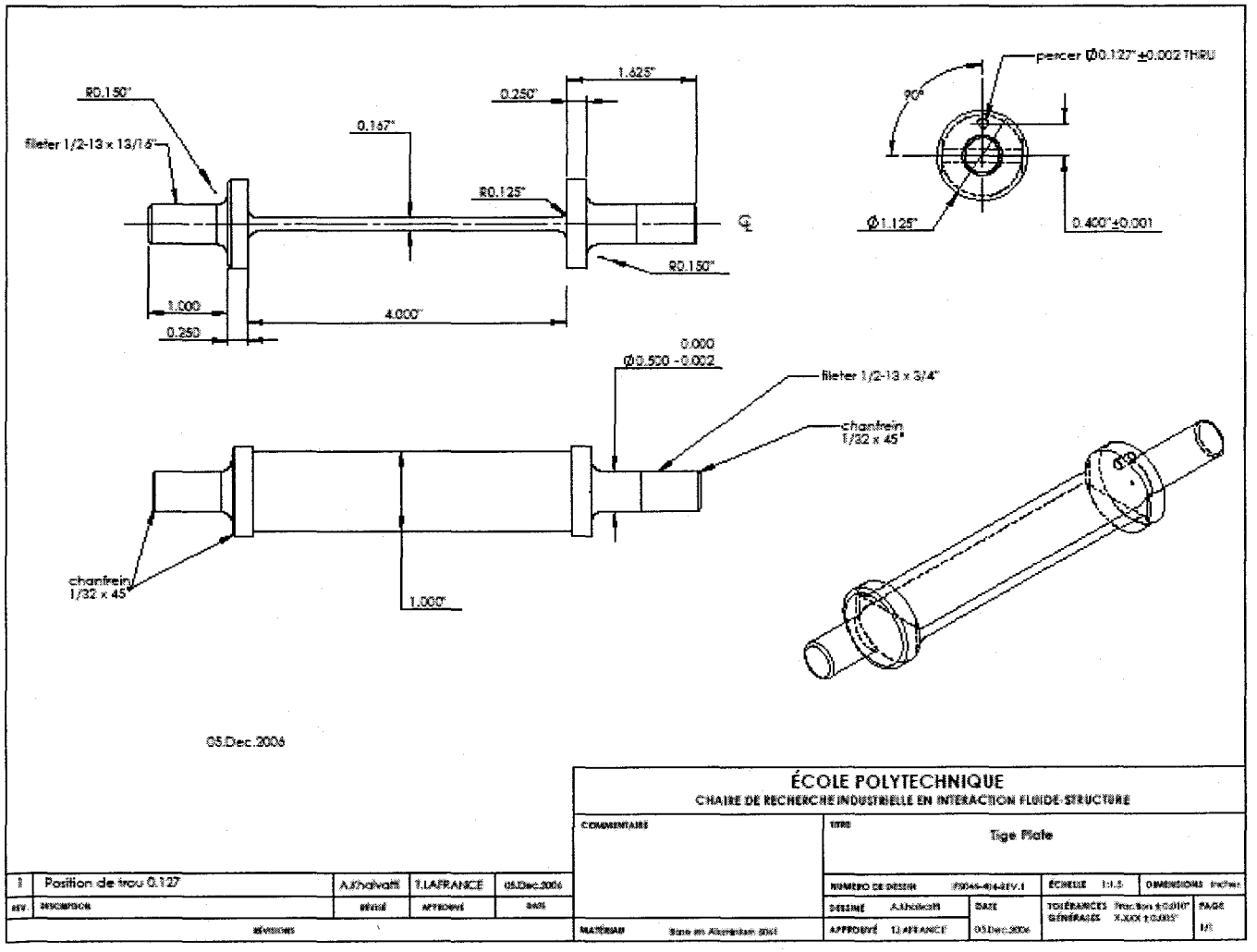
R0.150"
filetter 1/2-13 x 13/16"
0.167"
0.250"
1.625"
R0.125"
R0.150"
1.000
0.250
4.000"
percer Ø0.127"±0.002 THRU
90°
Ø1.125"
0.400"±0.001
0.000
Ø0.500 -0.002
filetter 1/2-13 x 3/4"
chanfrein 1/32 x 45°
chanfrein 1/32 x 45°
1.000"
05.Dec.2006
ÉCOLE POLYTECHNIQUE
CHAIRE DE RECHERCHE INDUSTRIELLE EN INTERACTION FLUIDE-STRUCTURE
COMMENTAIRE
TITRE
Tige Plate
1 Position de trou 0.127 A.Khalvati T.LAFRANCE 05.Dec.2006
REV. DESCRIPTION DESSINÉ APPROUVÉ DATE
RÉVISIONS
MATÉRIAU Barre en Aluminium 6061
NUMÉRO DE DESSIN
ÉCHELLE 1:1.5
DIMENSIONS Inches
DESSINÉ A.Khalvati
APPROUVÉ T.LAFRANCE
DATE 05.Dec.2006
TOLÉRANCES GÉNÉRALES Fraction ±0.0107" X.XXX ±0.005"
PAGE 1/1

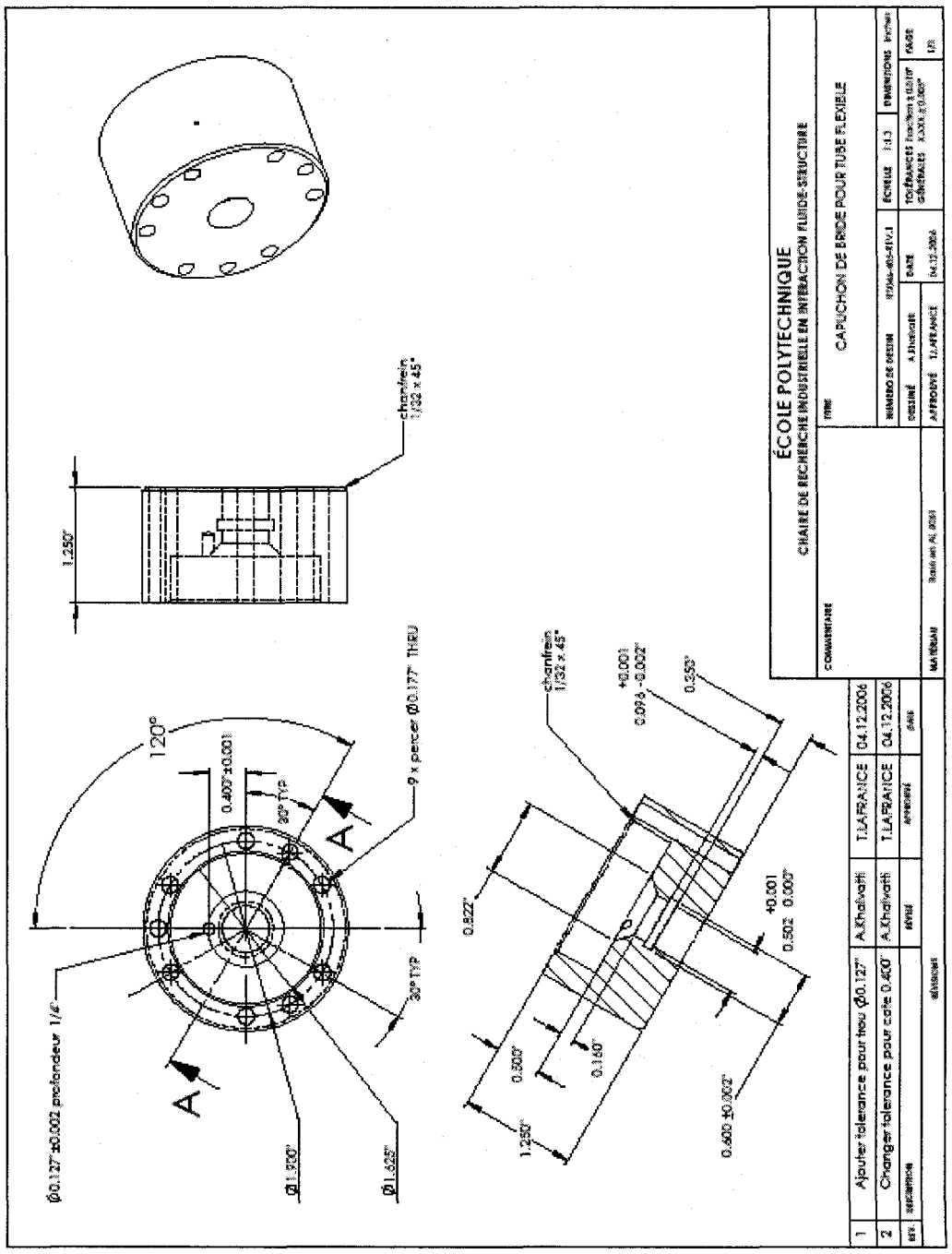
ÉCOLE POLYTECHNIQUE
CHAIRE DE RECHERCHE INDUSTRIELLE EN INTERACTION FLUIDE-STRUCTURE
CAPUCHON DE BRIDE POUR TUBE FLEXIBLE
1 Ajouter tolerance pour trou Ø0.127" A.Khalvatti T.LAFRANCE 04.12.2006
2 Changer tolerance pour cote 0.400" A.Khalvatti T.LAFRANCE 04.12.2006
Ø0.127" ±0.002 profondeur 1/4"
Ø1.900"
Ø1.625"
9 x percer Ø0.177" THRU
120°
0.400" ±0.001
30° TYP
A
1.250"
chanfrein 1/32 x 45°
0.822"
0.500"
0.160"
0.600 ±0.002"
0.350"
+0.001 0.096 -0.002"
+0.001 0.502 0.000"

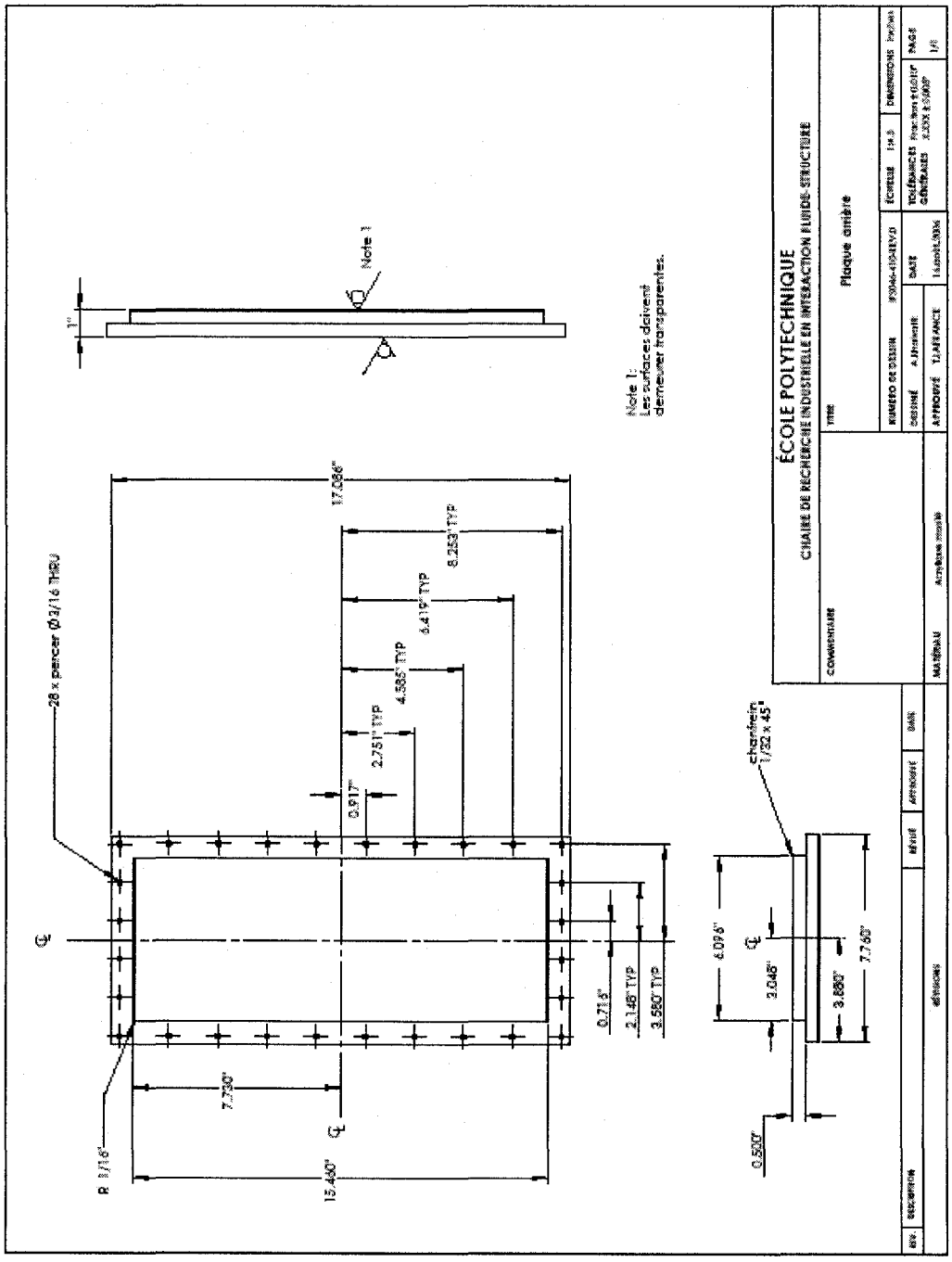
ÉCOLE POLYTECHNIQUE
CHAIRE DE RECHERCHE INDUSTRIELLE EN INTERACTION FLUIDE-STRUCTURE
Plaque arrière
Note 1
Note 1:
Les surfaces doivent
demeurer transparentes.
28 x percer Ø3/16 THRU
17.086"
8.253" TYP
6.419" TYP
4.585" TYP
2.751" TYP
0.917"
0.716"
2.148" TYP
3.580" TYP
7.730"
15.460"
R 1/16"
chanfrein
1/32 x 45°
6.096"
3.048"
3.880"
7.760"
0.500"
1"